IMPACT OF MUSCULAR FATIGUE AND ITS MODULATION USING TRANSCRANIAL PHOTOBIOMODULATION (tPBM) ON THE HUMAN BRAIN MEASURED BY FUNCTIONAL NEAR-INFRARED SPECTROSCOPY (fNIRS)

by

ELIZABETH LYDE URQUHART

DISSERTATION

Presented to the Faculty of the Graduate School of

The University of Texas at Arlington in Partial Fulfillment

of the Requirements

for the Degree of

DOCTOR OF PHILOSOPHY

THE UNIVERSITY OF TEXAS AT ARLINGTON
AUGUST 2020

ACKNOWLEDGMENTS

This research was supported by funding from the National Heart, Lung and Blood Institute with the award number NIH T32 HL134613 and NIH BRAIN Initiative (RF1MH114285).

I would like to thank my advisor, Dr. George Alexandrakis for his unrelenting guidance, mentorship, and support during the last 5 years. His mentorship and advise have proved to be invaluable and I will take it to heart for years to come.

Furthermore, I would like to thank my committee members, Dr. Hanli Liu, Dr. Paul Fadel, Dr. Matthew Brothers, and Dr. Jun Liao for their time and guidance on this work. In particular, Dr. Hanli Liu has also mentored my research and encouraged collaboration and discussion with her lab. I am thankful to Dr. Paul Fadel for inviting me to join his lab activities which provided new perspectives in research and further expanded my knowledge of exercise physiology.

I would like to extend my appreciation to Dr. Suvra Pal and Dr. Shan Sun-Mitchell of the University of Texas department of Math. Through their encouragement and guidance, I earned my Certificate of Applied Statistics, which directed my statistical analysis of this work.

Lastly, I would like to thank fellow doctoral, post-doctoral, and NIH-fellows colleagues for their assistant and support in my research including Dr. Xinlong Wang, Tyrell Pruitt, and Hashini Wanniarachchi.

DEDICATION

I dedicate this work to my husband for his unconditional love and support. I want to express my gratitude to my parents and brother, who have always encouraged me and led me to aspire to be as great as them. Thank you.

TABLE OF CONTENTS

ACKNOWLEDGMENTS iii
DEDICATION iv
List of Figures viii
List of Tables xii
ABSTRACT xiii
CHAPTER 1 1
INTRODUCTION 1
CHAPTER 2 4
Mapping cortical network effects of fatigue during a handgrip task by functional near-infrared spectroscopy in physically active and inactive subjects 4
2.1 INTRODUCTION 4
2.2 MATERIALS AND METHODS 6
2.2.1 Participants 6
2.2.2 Experimental Procedures 7
2.2.3 Mapping of Cerebral Hemodynamics 9
2.2.4 Functional Connectivity (FC) Analysis 11
2.3 RESULTS 12
2.3.1 Evolution of Maximal Handgrip Force over Time 12
2.3.2 Temporal Evolution of fNIRS Activation Patterns 13
2.3.3 Temporal Evolution of Functional Connectivity Patterns 17
2.3.3.1 FC maps with seed at lM1 17
2.3.3.2 FC maps with seed at lDLPFC 18
2.3.3.3 FC maps with seed at rDLPFC 19
2.3.3.4 Correlation between regional FC and grip strength 20
2.4 DISCUSSION 22
2.4.1 Changes in Handgrip Performance During the Task 23
2.4.2 Evolution of Hemodynamic Activation Patterns During the Handgrip Task 23
2.4.2.1 Evolution of Hemodynamic Activation Patterns at Primary and Secondary Sensory-Motor Cortices 24
2.4.2.2 Evolution of Hemodynamic Activation Patterns in the DLPFC 25
2.4.2.3 Evolution of Hemodynamic Activation Patterns at the Broca's Area 26
2.4.3 Evolution of FC Patterns During the Handgrip Task 26

2.4.3.1 Overall FC Pattern Differences between Inactive and Active Subjects 27
2.4.3.2 FC Pattern Comparisons with Seed at lM1 27
2.4.3.3 FC Pattern Comparisons with Seeds at lDLPFC and rDLPFC 28
2.4.3.4 Correlation between FC and Performance 30
2.5 LIMITATIONS 30
2.6 CONCLUSION 31
CHAPTER 3 37
Differences in net information flow and dynamic connectivity metrics between physically active and inactive subjects measured by functional near-infrared spectroscopy (fNIRS) during a fatiguing handgrip task 37
3.1 INTRODUCTION 37
3.2 MATERIALS AND METHODS 40
3.2.1 Participants 40
3.2.2 Experimental Procedures 40
3.2.3 Data Preprocessing 42
3.2.4 Phase Transfer Entropy (PTE) and Directed PTE (dPTE) Data Analysis 44
3.2.5 Data Processing Steps for dPTE 45
3.2.6 Directional Connectivity (DC) 46
3.2.7 Static FC (SFC) and FC Variability (FCV) Analysis 46
3.3 RESULTS 47
3.3.1 Relative Changes in MVC over time 47
3.3.2 Frequency Band Analysis with Information Flow and Directional Connectivity 48
3.3.2.1 Endogenic Frequency Band 49
3.3.2.2 Neurogenic Frequency Band 52
3.3.3 Correlations between SFC and FCV 57
3.4 DISCUSSION 60
3.4.1 Endogenic Frequency Band 61
3.4.2 Neurogenic Frequency Band 63
3.4.3 Myogenic Frequency Band 66
3.5 LIMITATIONS 68
3.6 CONCLUSION 69
CHAPTER 4 75

Transcranial photobiomodulation induced changes in functional connectivity and brain network topography mapped by functional near-infrared spectroscopy (fNIRS) 75
4.1. INTRODUCTION 75
4.2. MATERIALS AND METHODS 78
4.2.1 Participants 78
4.2.2 Experimental instruments and procedures 78
4.2.3 Data preprocessing 80
4.2.4 Cross correlation analysis to quantify functional connectivity 81
4.2.5 Graph theory analysis to determine topographical network metrics 82
4.3. RESULTS 85
4.3.1 Functional connectivity to the right prefrontal cortex derived with PCC 85
4.3.2 Graphical network metrics analyzed by GTA 88
4.4. DISCUSSION 90
4.4.1 Effects of tPBM on functional connectivity 90
4.4.2 Effects of tPBM on global topographical metrics 92
4.5. LIMITATIONS AND FUTURE WORK 94
4.6. CONCLUSION 95
CHAPTER 5 96
Conclusion and future work 96
5.1 Conclusion 96
5.2 Limitations 98
5.3 Future work 99
REFERENCES 101

List of Figures

Figure 2 - 1 Experimental set up and protocol timeline for the handgrip task. a) FNIRS multi-channel layout with 111 channels covering five regions of interest (ROI): M1/S1 (green), PMC (red), DLPFC (blue), and Broca's Area (yellow). All other channels, located over the temporal and occipital lobes, are shown in gray. b) Schematic of the experimental set-up of the fNIRS (LABNIRS) system and the BIOPAC handgrip force sensor system with one representative source-detector channel shown for simplicity. c) ΔHbO and ΔHbR hemodynamic responses at lM1/S1 for the first 10 blocks of the task. 9

Figure 2 - 2 Force produced during intermittent handgrip contractions at 100% MVC force level using the dominant hand for physically inactive (light gray) and active subjects (dark gray). Each data point represents an average of 60 consecutive trials, expressed as the Mean (bar height) + Standard Error to the Mean (SEM; error bar). Circles: individual performance. **p < 0.01, ***p < 0.001. 13

Figure 2 - 3 ROIs of statistically significant activity for inactive subject's at a) 0 – 100 s, b) 1 – 10 min, and c) 11 – 20 min, and for active subjects at d) 0 – 100 s, e) 1 – 10 min, f) 11 – 20 min of the handgrip task. Only ROIs with statistically significant (p < 0.05, FDR corrected) activation are shown with corresponding t-values next to it (red ovals – activation; blue ovals – deactivation). No significant group differences seen early in the handgrip task at g) 0 – 100 s, and greater activation in few regions was seen for active subjects (red ovals; negative t-values) over longer time intervals; h) 0 – 10 min, j) 11 – 20 min. With the exception of (h) and (i), all positive t-values corresponded to activation (red ovals) and all negative t-values corresponded to deactivation (blue ovals). 16

Figure 2 - 4 Evolution of FC patterns during the entire handgrip task with the seed region at lM1 for inactive subjects at a) baseline, b) 0 – 10 min, and c) 11 – 20 min and active subjects at d) baseline, e) 0 – 10 min, and f) 11 – 20 min. The black oval encircles the seed region channels and is only displayed at baseline for clarity. Only regions with statistically significant FC strength are shown (p < 0.05, Bonferroni corrected). 18

Figure 2 - 5 Evolution of FC patterns during the entire handgrip task with the seed region at lDLPFC for inactive subjects at a) baseline, b) 0 – 10 min, and c) 11 – 20 min and active subjects at d) baseline, e) 0 – 10 min, and f) 11 – 20 min. The black oval encircles the seed region channels and is only displayed at baseline for clarity. Only regions with statistically significant FC strength are shown (p < 0.05, Bonferroni corrected). 19

Figure 2 - 6 Evolution of FC patterns during the entire handgrip task with the seed region at rDLPFC for inactive subjects at a) baseline, b) 0 – 10 min, and c) 11 – 20 min and active subjects at d) baseline, e) 0 – 10 min, and f) 11 – 20 min. The black oval encircles the seed region channels and is only displayed at baseline for clarity. Only regions with statistically significant FC strength are shown (p < 0.05, Bonferroni corrected). 21

Figure 2 - S1 Exercise induced variance in ΔHbO and ΔHbR. a) representative time-series of HbO and HbR at lM1. Significant (p < 0.05) difference in variability, as determined by Levene's

test, between 0 – 10 min and 10 – 20 min periods are shown for inactive subjects for b) ΔHbO and c) Δ HbR and active subjects for d) ΔHbO and e) ΔHbR. 33

Figure 3 - 1 Experimental set up and protocol timeline for the handgrip task. A) FNIRS 111-channel layout with eleven regions of interest (ROIs) covered by the probe geometry: left and right frontopolar (lFP; rFP) (red) , left and right pre-frontal cortex (lDLPFC; rDLPFC) (yellow), Broca's area (green), left and right pre-motor cortex (lPMC; rPMC) (light blue), left and right primary motor and sensory cortical (lM1/S1; rM1/S1) areas (purple), and left and right sensory association cortex (lSAC; rSAC) (pink). B) Each circle shows the spatial average of the probe coordinates in each ROI, per brain hemisphere. These averaged probe locations served as reference points for plotting dPTE and DC between ROIs in this work. C) Schematic of the experimental set-up of the fNIRS (LABNIRS) system and the BIOPAC handgrip force sensor system with one representative source-detector channel shown for simplicity. D) The handgrip task protocol, starting with a 5-minute baseline. Subjects performed intermittent handgrip contractions for 3.5 s followed by 6.5 s of rest for 120 blocks at 100% MVC. 42

Figure 3 - 2 Force produced during intermittent handgrip contractions while physically inactive and active subjects attempted to attain 100% MVC. Each bar represents an average of 60 consecutive trials, expressed as the Mean (bar height) + Standard Error to the Mean (SEM; error bar). **p < 0.01, ***p < 0.001..... 48

..... 72

Figure 3 - S1 Significant dPTE and DC in the endogenic frequency band for inactive and active subjects during the handgrip task for ΔHb. Directed PTE t-values for each ROI as a color-coded map for inactive subjects (A-C) and active subjects (D-F). Hot (yellow-reds) and cold (light blue-dark blue) colors indicate information outflow and inflow, respectively. Arrows indicate statistically significant information flow between functional regions for inactive (G-I) and active subjects (J-L). Black arrows (p < 0.05); Red arrows (p < 0.01). Eleven regions of interest (ROIs) were mapped: left and right frontopolar (lFP; rFP) (red), left and right pre-frontal cortex (lDLPFC; rDLPFC) (yellow), Broca's area (green), left and right pre-motor cortex (lPMC; rPMC) (light blue), left and right primary motor and sensory cortical (lM1/S1; rM1/S1) areas (purple), and left and right sensory association cortex (lSAC; rSAC) (pink)..... 72

..... 73

Figure 3 - S2 Significant dPTE and DC in the neurogenic frequency band for inactive and active subjects during the handgrip task for ΔHb. Directed PTE t-values for each ROI as a color-coded map for inactive subjects (A-C) and active subjects (D-F). Hot (yellow-reds) and cold (light blue-dark blue) colors indicate information outflow and inflow, respectively. Arrows indicate statistically significant information flow between functional regions for inactive (G-I) and active subjects (J-L). Black arrows (p < 0.05); Red arrows (p < 0.01). Eleven regions of interest (ROIs) were mapped: left and right frontopolar (lFP; rFP) (red), left and right pre-frontal cortex (lDLPFC; rDLPFC) (yellow), Broca's area (green), left and right pre-motor cortex (lPMC; rPMC) (light blue), left and right primary motor and sensory cortical (lM1/S1; rM1/S1) areas (purple), and left and right sensory association cortex (lSAC; rSAC) (pink)..... 73

..... 74

Figure 3 - S3 Significant dPTE and DC in the myogenic frequency band for inactive and active subjects during the handgrip task for ΔHb. Directed PTE t-values for each ROI as a color-coded map for inactive subjects (A-C) and active subjects (D-F). Hot (yellow-reds) and cold (light blue-dark blue) colors indicate information outflow and inflow, respectively. Arrows indicate statistically significant information flow between functional regions for inactive (G-I) and active subjects (J-L). Black arrows ($p < 0.05$); Red arrows ($p < 0.01$). Eleven regions of interest (ROIs) were mapped: left and right frontopolar (lFP; rFP) (red), left and right pre-frontal cortex (lDLPFC; rDLPFC) (yellow), Broca's area (green), left and right pre-motor cortex (lPMC; rPMC) (light blue), left and right primary motor and sensory cortical (lM1/S1; rM1/S1) areas (purple), and left and right sensory association cortex (lSAC; rSAC) (pink). 74

Figure 4 - 1. Experimental set-up and protocol. A) 111-channel layout with twelve regions of interest covered by the optode geometry: frontopolar (FP) (red), dorsolateral prefrontal cortex (DLPFC) (yellow), Broca's area (green), premotor cortex (PMC) (light blue), primary motor and somatosensory cortical (M1/S1) areas (dark blue), somatosensory association cortex (SAC) (pink), and Wernicke's Area (gold). B) 1064-nm laser. C) The experimental protocol randomized placebo (PBO) and tPBM treatment for subjects. For the protocol, there was a period of at least one week between the two experiments to avoid any carry-over effect. 80

Figure 4 - 2. Group-level differences in FC between the right PFC and all other cortical regions compared between tPBM and placebo conditions at A) stimulation, and B) post-stimulation periods. Red lines indicate greater FC strength during tPBM than the placebo treatment. Blue lines indicate weaker FC strength during tPBM than the placebo treatment. Only significant ($p < 0.05$, FDR corrected) FC changes are shown. Black boxes enclose channels within the right PFC; Red circle marks the approximate location of tPBM. Different ROIs are denoted by color: frontopolar (FP) (red), dorsolateral prefrontal cortex (DLPFC) (yellow), Broca's area (green), premotor cortex (PMC) (light blue), primary motor and somatosensory cortical (M1/S1) areas (dark blue), somatosensory association cortex (SAC) (pink), and Wernicke's Area (gold). 86

Figure 4 - 3. Significant increases in FC strength from right PFC to other regions of the brain, compared between post-stimulation and the tPBM stimulation period. The black box encloses all the channels within the right PFC. The red circle near rPFC marks the location of tPBM stimulation. ROIs are denoted by color; frontopolar (FP) (red), dorsolateral prefrontal cortex (DLPFC) (yellow), Broca's area (green), premotor cortex (PMC) (light blue), primary motor and somatosensory cortical (M1/S1) areas (dark blue), somatosensory association cortex (SAC) (pink), and Wernicke's Area (gold). A) Red lines indicate greater FC strength during post-tPBM than the stimulation period. Only significant ($p < 0.05$, FDR corrected) FC strength changes are shown. B) The total number of significant connections between ROIs from right PFC to other regions of the cortex. Line thickness indicates the number of significant connections from 1 (thinnest) to 11 (thickest) connections. 87

Figure 4 - 4. Global network characteristics between tPBM and placebo treatment during the 2nd half of stimulation period (5-8 min) for A) global efficiency (E_g), B) local efficiency (E_{loc}), and C) averaged path length (L_p). Significant differences ($p < 0.05$) between the treatments are represented with black stars, *. Red lines indicate tPBM treatment while blue lines indicate placebo treatment. Mean + SEM. 89

Figure 4 - 5. Small-worldness differences between tPBM and placebo treatment during post-stimulation period. Significant differences ($p < 0.05$) between the two treatments are represented with black stars, *. Red lines indicate tPBM treatment. Blue lines indicate placebo treatment. Mean + SEM. 90

List of Tables

Table 2 - 1 Mann-Whitney U statistics results between force (%MVC) between active and inactive subjects. 13

Table 2 - 3 Pearson's correlation analysis summary between regional FC magnitude and time to 50% MVC (Pearson's correlation coefficient (r) and p-value). 22

Table 2 - 4 Correlation coefficients comparison summary between inactive and active subjects for regional FC magnitude and 50% MVC (z-value and p-value). 22

Table 2 - S1 Spatial registration of fNIRS channel positions on a standard brain fMRI atlas. MNI coordinates displayed as mean (SD); r-right contralateral brain hemisphere; l-left ipsilateral brain hemispheres. 34

Table 2 - S2 Pearson's correlation analysis summary between regional FC magnitude and time to 50% MVC (Pearson's correlation coefficient (r) and p-value). 36

Table 2 - S3 Correlation coefficients comparison summary between inactive and active subjects for regional FC magnitude and 50% MVC (z-value and p-value). 36

Table 3 - S1 Spatial registration of fNIRS channel positions on a standard brain fMRI atlas. MNI coordinates displayed as mean (SD); r-right contralateral brain hemisphere; l-left ipsilateral brain hemispheres. 70

Table 3 - S2 Preprocessing input parameters used in Homer2. 71

ABSTRACT

Impact of muscular fatigue and its modulation using transcranial photobiomodulation (tPBM) on the human brain measured by functional near-infrared spectroscopy (fNIRS)

Elizabeth Lyde Urquhart, Ph. D.

The University of Texas at Arlington, 2020

Supervising Professor: George Alexandrakis

When performing exercise, the brain must register and simultaneously integrate input from feedforward (i.e., central command) and feedback (e.g., exercise pressor reflex) neural mechanisms to make appropriate cardiovascular adjustments to meet metabolic demands. Muscle fatigue occurs during prolonged exercise and is characterized by a reduction in force-generating capability of the muscle. Fatigue comprises of two components: central and peripheral fatigue. Peripheral fatigue is produced at or distal to the neuromuscular junction whereas, central fatigue originates in the central nervous system. However, central fatigue's contribution to peripheral fatigue is less understood and functional neuroimaging is being investigated as a tool to elucidate the underlying mechanisms.

Photobiomodulation (PBM) is the use of red to near-infrared light to penetrate through tissue and stimulate mitochondrial respiration via enhanced cytochrome - c- oxidase activity. Transcranial PBM (tPBM) is when light is targeted at the cerebral cortex and has recently been used in tandem with functional neuroimaging to show enhanced cerebral oxygenation and cognitive function. Prior studies have demonstrated PBM ability to attenuate fatigue when administered to the muscle before or following

exercise. However, no studies have examined tPBM potential to delay fatigue onset. This collection of work addresses the knowledge gap of altered hemodynamic response and functional connectivity (FC) patterns induced by motor fatigue and tPBM, with the implication of eventually applying tPBM on the motor cortex during exercise in future work.

Specifically, Chapter 2 depicts the effects of physical fatigue on cerebral hemodynamics while considering how it is modulated during peripheral fatigue in subjects of differing physical activity levels and its temporal evolution as measured by functional near-infrared spectroscopy (fNIRS). Brain activation patterns and FC changes were mapped before and during the intermittent handgrip task. The hemodynamic metrics and concurrent force measurements of the intermittent handgrip task provided insight in the differences in cortical network adaptation patterns as fatigue sets in, which was dependent on subject physical activity.

Chapter 3 further expands on the effect of physical fatigue on cerebral hemodynamics by analyzing vasomotion-induced oscillations as measured by fNIRS at each hemodynamic frequency band: endothelial, neurogenic, and myogenic component. To help understand how these three neurovascular regulatory mechanisms relate to the fatiguing handgrip task performance, several dynamic fNIRS metrics were quantified including directional phase transfer entropy, directional connectivity, and the relationship between FC and FC variability (FCV) to understand their mutual dependence for each frequency band in the context of handgrip performance as fatigued increased. These findings imply that physical activity modulates neurovascular control mechanisms at the

endogenic, neurogenic, and myogenic frequency bands resulting in delayed fatigue onset and enhanced performance.

In Chapter 4, the effects of tPBM applied to the forehead on brain networks is investigated for the whole cortex as measured by fNIRS. FC and graph theory analysis (GTA) were quantified for the time series data before, during, and after tPBM was administered to the pre-frontal cortex. These results demonstrated that tPBM induced alterations in FC and GTA from the stimulated right pre-frontal cortex. Furthermore, this study suggests that tPBM has differing effects on FC and GTA during and after stimulation, signifying localized effects occurring during stimulation and global effects after stimulation. Our findings suggest the feasibility of expanding the use of fNIRS in the future as a means to map and identify cortical network alterations induced by tPBM in health and disease.

CHAPTER 1

INTRODUCTION

When performing physical exercise, the contracting muscles elicit demand for oxygen, which is supplied by increased blood flow. The brain must register and simultaneously integrate input from feedforward (i.e., central command) and feedback (e.g., exercise pressor reflex) neural mechanisms to make necessary cardiovascular adjustments to meet the metabolic demand of the exercise.[1, 2] During exercise using the forearm, peripheral fatigue sets in, as characterized by reduced force-generating capability of the muscles that subsequently evolves into central fatigue, resulting in decreased neural drive to the muscles, after prolonged physical activity.[1-7] Central fatigue's contribution to peripheral fatigue is less understood and functional brain imaging during exercises is being investigated as a tool to help elucidate the underlying mechanisms.[3-12]

Photobiomodulation (PBM) is the utilization of light to stimulate mitochondrial respiration and cellular function in many cell types, including neurons.[13] It utilizes light in the red to near-infrared (NIR) wavelengths (600 – 1200 nm) to penetrate through tissues to induce the mitochondrial and cellular changes.[14-17] The purported mechanism of PBM relies on photon absorption by cytochrome – c – oxidase (CCO), the terminal enzyme in mitochondrial respiration, and the dissociation of nitric oxide (NO), which inhibits CCO.[14, 15] As CCO activity and expression increases, the more oxygen consumption and simultaneous metabolic energy is produced via mitochondrial oxidative phosphorylation.[18, 19] Transcranial PBM (tPBM) is when the light is targeted for the human cerebral cortex and has recently been used therapeutically for various neurological and psychological disorders including ischemic stroke,[20, 21] chronic

traumatic brain injuries,[22, 23] and depression.[24, 25] Furthermore, it has been shown to enhance cerebral oxygenation and cognitive function in electroencephalography (EEG)[13] and functional near-infrared spectroscopy (fNIRS) studies.[18] Many studies have demonstrated PBM can be used to attenuate fatigue prior to or following strength and aerobic exercises when the muscle is exposed to the PBM therapy.[26-31] However, no studies have examined tPBM potential to delay fatigue onset.

As discussed, exercise and tPBM promote physiological changes in the brain. Noninvasive neuroimaging techniques like computerized tomography, electroencephalogram (EEG), functional magnetic resonance imaging (fMRI), and functional near-infrared spectroscopy (fNIRS) have been used to actively image and locate brain regions involved in motor functions,[8, 32] and neurophysiological effects of tPBM.[18, 33] Among them, fNIRS measures the concentration changes of oxyhemoglobin (ΔHbO) and deoxyhemoglobin (ΔHb) resulting from neurovascular coupling secondary to neuronal activation by utilizing NIR light wavelengths (650-1000 nm).[34] It is advantageous over other neuroimaging techniques due to its high temporal resolution compared to fMRI, robustness to motion, lower cost, and portability.[32, 35]

While several functional neuroimaging studies have examined the effects of physical fatigue,[3, 4, 6, 8, 9, 11, 12, 36-40] and tPBM[13, 18, 33] on brain activity, none have yet investigated how brain activity alters due to fatigue during the exercise nor explored tPBM as a means to ameliorate fatigue. The goal of this dissertation is to illustrate the use of fNIRS to (1) first discover how peripheral muscle fatigue effects brain activity in young, healthy adults of differing physical activity levels, (2) including how fatigue effects vasomotion-induced oscillations in the endogenic, neurogenic, and myogenic

frequencies in the human brain. (3) Then the impact of tPBM on young, healthy adults will then be explored to measure near-immediate hemodynamic responses and assure reliability. Our findings suggest the feasibility of expanding the use of fNIRS in tandem with tPBM interventions to further study brain network effects that could result in motor and cognitive enhancement in healthy subjects or those with brain injury and disorders in pre-clinical and clinical studies.[14, 15, 33] Possibilities for the latter include stroke, traumatic brain injury, Alzheimer's disease, Parkinson's disease, anxiety, and depression.[14, 15]

This dissertation comprises of 5 chapters which consists of two peer- reviewed publications (Chapter 2 and Chapter 3) and one manuscript that submitted (Chapter 4). Chapter 1 is a brief introduction on central and peripheral fatigue during exercise, tPBM, and functional neuroimaging using fNIRS. In Chapter 2, the temporal evolution of cortical activation and connectivity patterns during a fatiguing handgrip task were studied by fNIRS in physically active and inactive young adults. In Chapter 3, motor task fatigue effect on vasomotion-induced oscillations in ΔHbO, as measured by fNIRS, was explored at each hemodynamic frequency band: endothelial component (0.003- 0.02 Hz) associated to microvascular activity, neurogenic component (0.02-0.04 Hz) related to intrinsic neuronal activity, and myogenic component (0.04-0.15 Hz) linked to activity of smooth muscles of arterioles. In Chapter 4, the temporal evolution of functional connectivity and cortical network reorganization before tPBM, during tPBM, and after tPBM was evaluated in young adults as measured by fNIRS. Lastly, Chapter 5 concludes the dissertation and provides directions for future work.

CHAPTER 2

Mapping cortical network effects of fatigue during a handgrip task by functional near-infrared spectroscopy in physically active and inactive subjects

This chapter is a publication at the journal Neurophotonics, October 2019 (Neurophotonics 6(4): 045011)

Authorship: Elizabeth L. Urquhart, Hashini I. Wanniarachchi, Xinlong Wang, Hanli Liu, and George Alexandrakis

2.1 INTRODUCTION

When performing physical exercise, the contracting muscles elicit demand for oxygen, which is supplied by increased blood flow. The brain must register and simultaneously integrate input from feedforward (i.e., central command) and feedback (e.g., exercise pressor reflex) neural mechanisms to make necessary cardiovascular adjustments to meet the metabolic demand of the exercise.[1, 2] During exercise involving the arms, peripheral fatigue sets in, as characterized by reduced force-generating capability of the muscles that subsequently evolves into central fatigue, resulting in decreased neural drive to the muscles, after prolonged physical activity.[1-6] Central fatigue's contribution to peripheral fatigue is less understood and functional brain imaging during fatiguing exercises is being investigated as a tool to help elucidate the underlying mechanisms.[3-6, 8, 9, 11, 12, 40] Neural pathways gradually alter their connectivity (neuroplasticity), which affects regulation of the cardiovascular system both at rest and during exercise. Physically active individuals exhibit exercise-related neuroplasticity and have improved

cardiovascular health whereas inactive individuals may be predisposed to higher incidences of cardiovascular disease.[1, 5, 41]

Several modalities have been used for functional brain mapping during motor-fatigue exercise, such as electro-encephalography (EEG), functional magnetic resonance image (fMRI), and functional near infrared spectroscopy (fNIRS).[3-6, 8, 9] Among them, fNIRS measures noninvasively the concentration changes of oxyhemoglobin (ΔHbO) and deoxyhemoglobin (ΔHb) resulting from neurovascular coupling secondary to neuronal activation by utilizing near-infrared light (650-1000 nm wavelengths). FNIRS is advantageous because of its relatively lower cost, its safety, portability, robustness to motion artifacts, and higher sensitivity compared to fMRI.[35, 42]

While several functional neuroimaging studies have examined the effects of physical fatigue on brain activation and connectivity,[3, 4, 6, 8, 9, 11, 12, 36-40] none have as yet explored how brain activity is modulated during peripheral fatigue in subjects of differing physical activity levels, or shown the progressive effect of fatigue on brain activity. In healthy adult populations, fMRI has been used to show brain activation and connectivity continually during,[38, 39] or at the beginning and end of the exercise,[6, 8] to illustrate changing central motor command and strengthened functional connectivity (FC). In contrast, fNIRS optodes placed on the prefrontal cortex (PFC)[11, 12, 40] and primary motor cortex (M1)[11] in trained athletic adult populations illustrated hyperoxygenation in the PFC and deoxygenation in M1 as a result of prolonged fatiguing exercise. However, those studies were unable to provide further insight on brain activity patterns due to the limited number of optodes used. Only one fNIRS study to date has, to our knowledge, examined the differences in brain activity between athletes and non-athletes during

exhaustive sustained handgrip exercise but, again only two probes were used, thus limiting whole-brain interpretations of activation and network connectivity.[4] Therefore, prior functional neuroimaging studies have not provided a more global picture of the continuous temporal evolution of brain activity patterns, and their differences based on subject physical activity levels, during a fatiguing handgrip task.

To address this knowledge gap, the purpose of this study was to examine differences in cortical activity, as mapped by fNIRS, between physically inactive and active subjects during a maximal voluntary contraction (MVC) handgrip task. The temporal evolution of recorded hemodynamic activation and FC patterns was measured and compared. Analyzing brain network activation and connectivity allowed for detection of physical activity dependent network reorganization during a fatiguing motor task, which in the future could be explored as a novel means of evaluating exercise-induced functional changes in brain activation patterns in human health and disease.

2.2 MATERIALS AND METHODS

2.2.1 Participants

Twenty-three young adults were recruited (4 females, ages = 25.13 $\pm$ 3.72 years) for this study. All subjects were without any neurological or psychiatric disorders (self-reported). All but two subjects were right-handed, as determined by the Edinburgh handedness scale.[43] Subjects also self-reported as physically inactive (n=12, exercising less than twice a week for 30 minutes of moderately vigorous exercise), or active (n=11, exercising at least 4 times a week, for 30 minutes of moderately vigorous exercise).[44] All experimental procedures, including a written consent required prior to participation in

this study, were approved by the Institutional Review Board of the University of Texas at Arlington (IRB# 2018-0686).

2.2.2 Experimental Procedures

An fNIRS imaging system (LABNIRS, Shimadzu Corp., Kyoto, Japan) was used to measure cerebral hemodynamic responses in the ROIs: left and right dorsolateral prefrontal cortex (lDLPFC; rDLPFC), left and right pre-motor cortex (lPMC; rPMC), left and right primary motor and sensory cortical (lM1/S1; rM1/S1) areas, and Broca's area. The optode layout on the subject's head consisted of 32 source and 34 detector fibers that were arranged in a configuration resulting in a total of 111 channels with a source-detector distance of 3 cm for all that covered the aforementioned cortical areas, with no short-distance channel placement being available in that cap geometry (Fig. 2 - 1a). Each source fiber was connected to laser diodes at three wavelengths (780 nm, 805 nm, 830 nm). The back-reflected light collected by the detector optodes was converted to current by photomultiplier tubes and the resulting intensity data was sampled at a rate of 10.101 Hz. The anatomical location of the optodes in relation to the standard head landmarks, including inion, nasion, Cz, and left and right ears, were recorded for each subject using a 3D digitizer (FASTRAK, Polhemus VT, USA). Montreal Neurological Institute (MNI) coordinates for the channels were determined using the statistical parametric mapping NIRS_SPM software package, which provided the Brodmann area (BA) corresponding to each fNIRS channel as shown in Table 2 - S1.[45]

Subjects were seated at a table with their dominant upper arm at their side with their elbow flexed at 90^{o} relative to the plane of the table on which their lower arm was supported and were facing two screens: one displaying protocol commands and the

other displaying visual-feedback of performance (Fig. 2 - 1b). The fNIRS data acquisition began with a 5-minute baseline hemodynamics measurement, followed immediately by imaging of the aforementioned cortical areas while subjects performed the handgrip task. For the latter, subjects used their dominant hand to perform intermittent handgrip contractions for 3.5 s alternating with 6.5 s of rest for 120 blocks at 100% MVC as a means to induce fatigue in the forearm.[3, 4, 8, 9] Prior to the experiment, subjects performed three to five MVCs and their average was calculated as the pre-task MVC value for that subject. Handgrip force was measured by a hand dynamometer (BIOPAC, CA, United States) and displayed for visual feedback. Exerted force during the handgrip exercise was recorded using the hand dynamometer at 1 kHz sampling rate. The maximum force value for each trial was calculated for each data point and the resulting maximum force time-series data were low-pass filtered at 15 Hz.[9, 46]

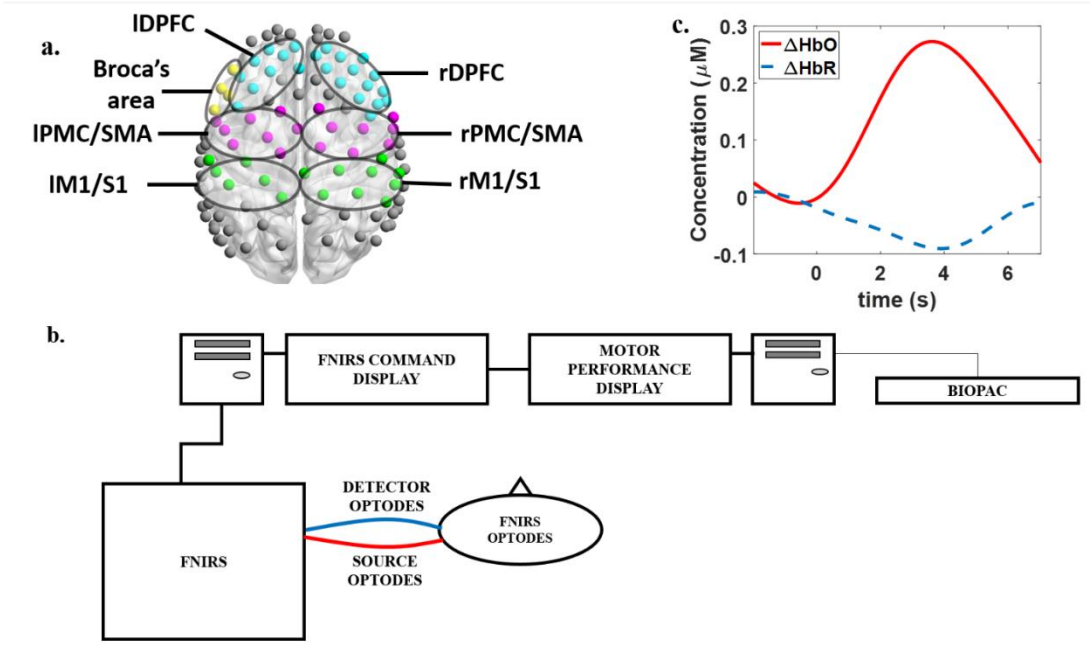

Figure 2 - 1 Experimental set up and protocol timeline for the handgrip task. a) FNIRS multi-channel layout with 111 channels covering five regions of interest (ROI): M1/S1 (green), PMC (red), DLPFC (blue), and Broca's Area (yellow). All other channels, located over the temporal and occipital lobes, are shown in gray. b) Schematic of the experimental set-up of the fNIRS (LABNIRS) system and the BIOPAC handgrip force sensor system with one representative source-detector channel shown for simplicity. c) ΔHbO and ΔHbR hemodynamic responses at lM1/S1 for the first 10 blocks of the task.

2.2.3 Mapping of Cerebral Hemodynamics

FNIRS data was preprocessed using Matlab 2012b (MathWorks, Natick, MA, USA) and the open-source package Homer 2.0 (Fig. 2 - 1c).[42] Detrending was implemented using the least-square fit of a line that was subtracted from the data.[47] The raw intensity data were then low-pass filtered using a 3rd order Butterworth filter at a cut-off frequency of 0.2 Hz to remove large portions of physiological noise, including heartbeat (1 – 1.5 Hz) and respiration (0.2 – 0.5 Hz).[35] The fNIRS data was also high-pass filtered using a 5th order Butterworth filter at a cut-off frequency of 0.01 Hz to remove any possible slow

baseline drift. In addition, data from left-handed subjects' data was flipped to its mirror image for group averaging purposes and the subsequent interpretation for all data was right (r) for contralateral and left (l) for ipsilateral brain hemispheres relative to the arm performing the task, as done in previous work.[48] Optical density data were converted into changes in hemoglobin concentration relative to baseline (ΔHbO) using the Modified Beer-Lambert Law with an estimated differential pathlength factor of 6.0 for each wavelength, an estimate used in Homer 2.0.[49] Lastly, a principal component analysis (PCA) filter was utilized to remove the first and second principal components, which are often associated with motion artifacts[42] and global hemodynamic flucations[35], which may overlap with the task-related hemodynamic response frequencies.

General linear model (GLM) analysis was used to quantify time-dependent ΔHbO patterns elicited during the handgrip task, by using a series of consecutive stimulation-specific boxcar functions convolved with a hemodynamic response function (HRF) as a regressor, as in prior studies.[50-52] Only ΔHbO values were analyzed and reported in this study because ΔHbR values were found to have similar and opposite qualitative trends, but with smaller amplitudes and lower signal-to-noise ratio as previously reported in other studies for other motor activation tasks and as seen in Fig. 2 - 1c.[52, 53] Subject group-level hemodynamic analyses were initially performed between baseline and during the task for each channel using a one-sample t-tests on β values obtained from GLM, with multiple comparison corrections (Bonferroni and False Discovery Rate (FDR)) . Subsequently, channels belonging to the same ROI on a group level, as determined by NIRS_SPM, were averaged together and tested using FDR.[54] Cortical activation images were visualized with the open-source network visualization tool

BrainNet Viewer,[55] using reference MNI coordinates that were not significantly ($p > 0.05$) different from the averaged MNI coordinates.

2.2.4 Functional Connectivity (FC) Analysis

FC was quantified using the open-source FC_NIRS software package.[47 23] Five-minute baseline data were converted to resting state connectivity maps. Connectivity maps were created for two contiguous 10-minute periods: 0-10 min and 10-20 min of the handgrip task. The raw optical density measurements were preprocessed the same as described in Sec. 2.2.3. Seed-based correlation analysis was performed by calculating the connectivity strength between the seed channel in cortical regions that showed significant activation during the task (rM1, lDLPFC, and rDLPFC) and every other channel via Pearson's correlation for every subject.[47] The seed channel was chosen based on highest percentage overlap to the desired BA, as determined by NIRS_SPM. For FC analysis, one-sample t-tests were performed on the Pearson correlation coefficient values of ΔHbO across subjects at $p < 0.05$ and were Bonferroni corrected for multiple comparisons of 111 channels. Topographic images for FC were generated using EasyTopo, an optical topography toolbox which projects data on a standard brain MRI atlas and implements 2D angular interpolation of the channel-wise data, for this study one-sample t-test t-values, in a spherical coordinate system.[56]

For statistical comparisons, 111 Pearson's correlation coefficient values (r) of ΔHbO were averaged into one value, designated as r_a, for each subject for each period. A two-sample t-test was performed at $p < 0.05$ on the averaged r-values between groups for each period. Paired t-tests were performed at $p < 0.05$ on the averaged r-values to compare FC across time within each group.

Lastly, the linear relationship between regional FC magnitude and grip strength was examined using Pearson's correlation analysis. This was done for each ROI at each time point per subject group. To calculate differences between the r-values, the follow formula was used:[57]

$$z_{observed} = \frac{z_1 - z_2}{\sqrt{\left(\frac{1}{N_1 - 3}\right)\left(\frac{1}{N_2 - 3}\right)}}, \quad (1)$$

where z_1 and z_2 are Fisher's r-to z transformed values and N_1 and N_2 are the number of pairwise comparisons.

2.3 RESULTS

2.3.1 Evolution of Maximal Handgrip Force over Time

The loss of handgrip force generated while intending to attain 100% of the MVC, recorded just prior to the beginning of the task, was quantified as a proxy measure of fatigue for inactive and active subjects. Force data were averaged over 60 blocks resulting in two time periods across the 120 contractions. The data blocks within each of the two time periods were tested for homogeneity of variances and normality, the assumptions for independent t-tests, which they did not pass. Therefore, data was analyzed using the nonparametric Mann-Whitney U test.[58] The relative decrease in MVC force between active and inactive subjects was comparable, but the absolute force produced by the active subjects was consistently higher at each period: 0 – 10 min and 10 – 20 min (Fig. 2 - 2, Table 2 - 1).

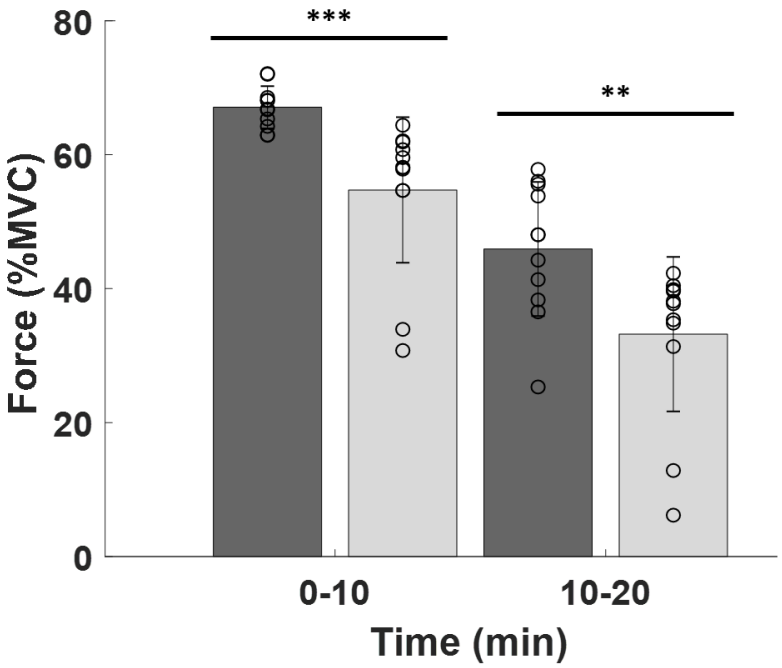

Figure 2 - 2 Force produced during intermittent handgrip contractions at 100% MVC force level using the dominant hand for physically inactive (light gray) and active subjects (dark gray). Each data point represents an average of 60 consecutive trials, expressed as the Mean (bar height) + Standard Error to the Mean (SEM; error bar). Circles: individual performance. **p < 0.01, ***p < 0.001.

Table 2 - 1 Mann-Whitney U statistics results between force (%MVC) between active and inactive subjects.

Time period (mins)	Mann-Whitney U	z-statistic	Effect size	p-value
0-10	195	3.85	0.80	0.0001
10-20	175	2.62	0.55	0.01

2.3.2 Temporal Evolution of fNIRS Activation Patterns

While activation results were intended to be displayed in ΔHbO activation maps, the high variability (Fig. 2 - S1) induced during the task did not allow for identification of

statistically significant changes in individual channels when Bonferroni multiple comparisons correction was applied in this work. As a result, channels were grouped by ROI and averaged so that significance could be obtained at the expense of spatial localization (Fig. 2 - 3). Following this analysis approach, significant activation was found in Broca's area for inactive subjects within the first 100 s of the task, as indicated by red oval (Fig. 2 - 3a). In contrast, active subjects showed significant activation in the lPMC and concurrent deactivation in the rDLPFC during the initial 100 s of the handgrip task (Fig. 2 - 3d). However, there were no significant differences between inactive and active subjects at these early times (Fig. 2 - 3g). In addition, while no statistical significance was found for any of the ROIs in the first half of the task (1 – 10 min; Fig. 2 - 3b) due to high hemodynamic signal variability and low ΔHbO amplitudes, in the second half of the task (11 – 20 min) inactive subjects showed statistically significantly deactivation in the rDLPFC and rPMC, as indicated by the blue ovals in Fig. 2 - 3c. Active subjects on the other hand, while they also had high hemodynamic signal variability in the first half of the task, also had higher ΔHbO magnitudes in certain cortical regions, which enabled detecting statistically significant activation in the lM1/S1 and Broca's area (Fig. 2 - 3e). Active subjects also showed significant deactivation in the rDLPFC during the first half of the task (Fig. 2 - 3e). Interestingly, in the second half of the task rDLPFC was not significant and instead activation was seen in the lDLPFC (Fig. 2 - 3f), opposite to what was seen for inactive subjects (Fig. 2 - 3e). In addition, the rPMC became significantly deactivated in the second half of the task (Fig. 2 - 3f), similar to what was observed for the inactive subjects (Fig. 2 - 3e). Lastly, active subjects were

significantly activated in Broca's area (Fig. 2 - 3h) in the first half of the task and in lDLPFC (Fig. 2 - 3i) in the second half of the task compared to inactive subjects.

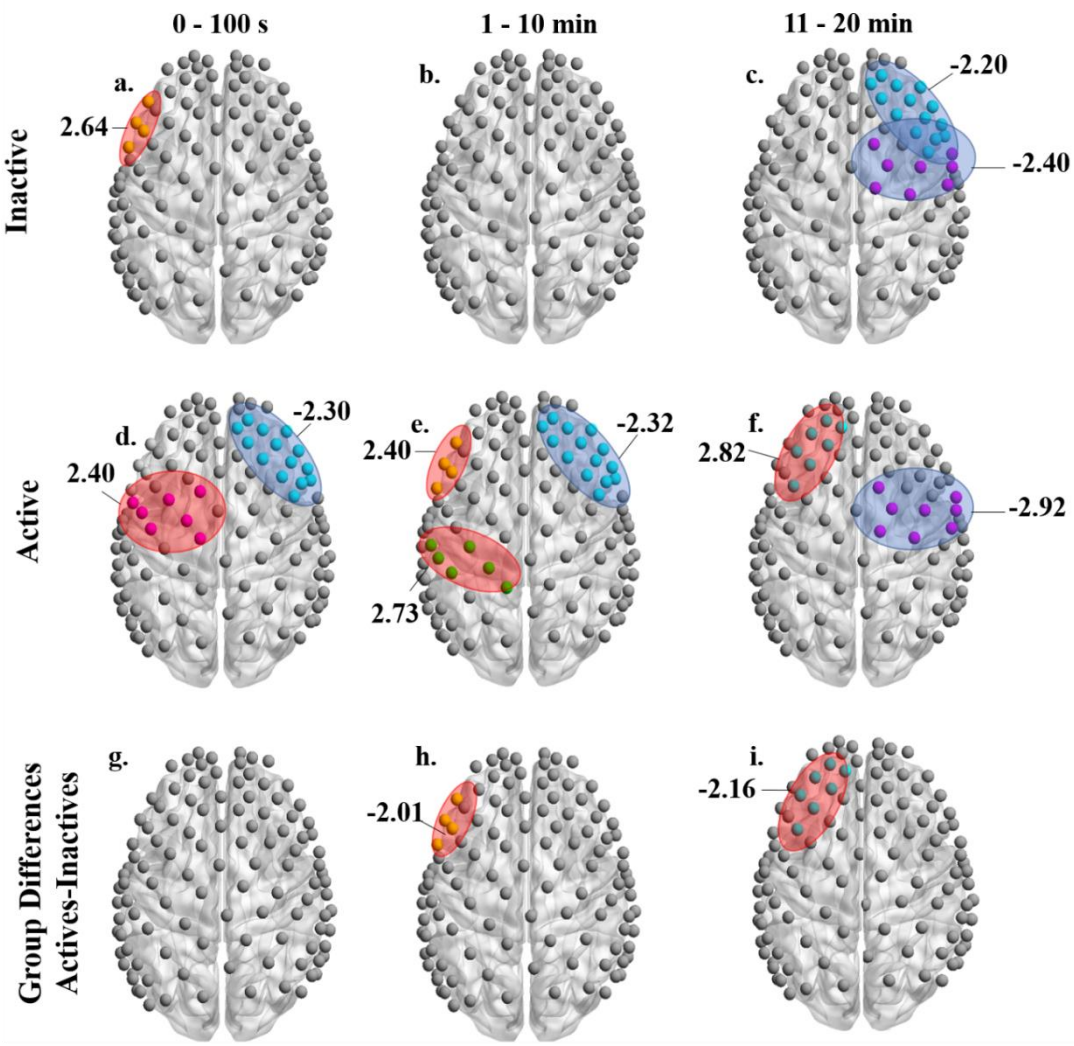

Figure 2 - 3 ROIs of statistically significant activity for inactive subject's at a) 0 – 100 s, b) 1 – 10 min, and c) 11 – 20 min, and for active subjects at d) 0 – 100 s, e) 1 – 10 min, f) 11 – 20 min of the handgrip task. Only ROIs with statistically significant ($p < 0.05$, FDR corrected) activation are shown with corresponding t-values next to it (red ovals – activation; blue ovals – deactivation). No significant group differences seen early in the handgrip task at g) 0 – 100 s, and greater activation in few regions was seen for active subjects (red ovals; negative t-values) over longer time intervals; h) 0 – 10 min, j) 11 – 20 min. With the exception of (h) and (i), all positive t-values corresponded to activation (red ovals) and all negative t-values corresponded to deactivation (blue ovals).

2.3.3 Temporal Evolution of Functional Connectivity Patterns

2.3.3.1 *FC maps with seed at lM1*

The lM1 seed location was placed based on activation seen in Fig. 2 - 3e and by channel location as determined by NIRS_SPM. The FC maps at rM1, contralateral to the hand performing the handgrip task, are shown in Fig. 2 - 4 for inactive (upper row) and active subjects (lower row). During the handgrip task, inactive subjects initially exhibited statistically significant FC between the lM1 and the DLPFC and rPMC (Fig. 2 - 4b). However, as the task progressed FC patterns became more localized to the lM1 with simultaneous loss of connectivity strength with the lDLPFC and receding connectivity strength in the rM1/S1 and the rDLPFC (Fig. 2 - 4c). Active subjects on the other hand, showed spatially broader FC patterns when performing the same task. In particular, active subjects exhibited significant FC with the DLPFC, the rM1/S1 and rPMC throughout the entire duration of the task (Figs. 2 - 4e and 2 - 4f). The r_a values were significantly greater in active subjects than inactive subjects at each time period: baseline ($p = 0.03$), 0 – 10 min ($p = 0.02$), and 10 – 20 min ($p = 0.02$). As well, r_a values within groups were significantly different from one another across time for inactive subjects at baseline and 0 – 10 min ($p = 0.003$) and 0 – 10 min and 10 – 20 min ($p = 0.02$) and active subjects at baseline and 0 – 10 min ($p = 0.05$) and 0 – 10 min and 10 – 20 min ($p = 0.01$).

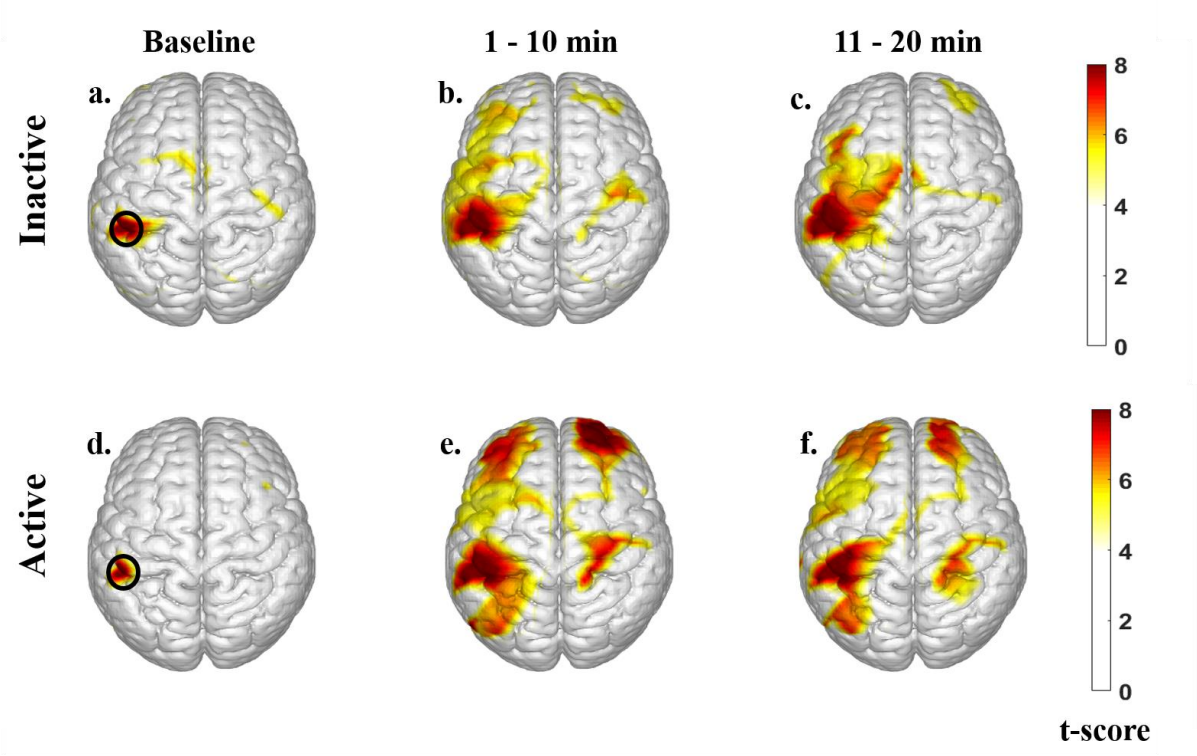

Figure 2 - 4 Evolution of FC patterns during the entire handgrip task with the seed region at lM1 for inactive subjects at a) baseline, b) 0 – 10 min, and c) 11 – 20 min and active subjects at d) baseline, e) 0 – 10 min, and f) 11 – 20 min. The black oval encircles the seed region channels and is only displayed at baseline for clarity. Only regions with statistically significant FC strength are shown ($p < 0.05$, Bonferroni corrected).

2.3.3.2 *FC maps with seed at lDLPFC*

When placing the seed at lDLPFC, the generated FC maps also showed major differences between the inactive and active subject groups (Fig. 2 - 5). Inactive and active subjects within the first 10 min of the task displayed statistically significant FC strength between the lDLPFC and the rDLPFC, PMC and M1/S1 (Fig. 2 - 5b and Fig. 2 - 5e). However, in the second half of the task the inactive subjects' FC pattern receded towards the DLPFC (Fig. 2 - 5c) while the active subjects' FC pattern broadened to the lPMC and somatosensory association cortex (Fig. 2 - 5f). The r_a values were

significantly greater in active subjects than inactive subjects at 0 – 10 min (p = 0.01) and 10 – 20 min (p = 0.02) but not at baseline (p = 0.06). The r_a values within groups were only significantly different across time at baseline and at 0 – 10 min for inactive (p = 0.002) and active subjects (p = 0.01).

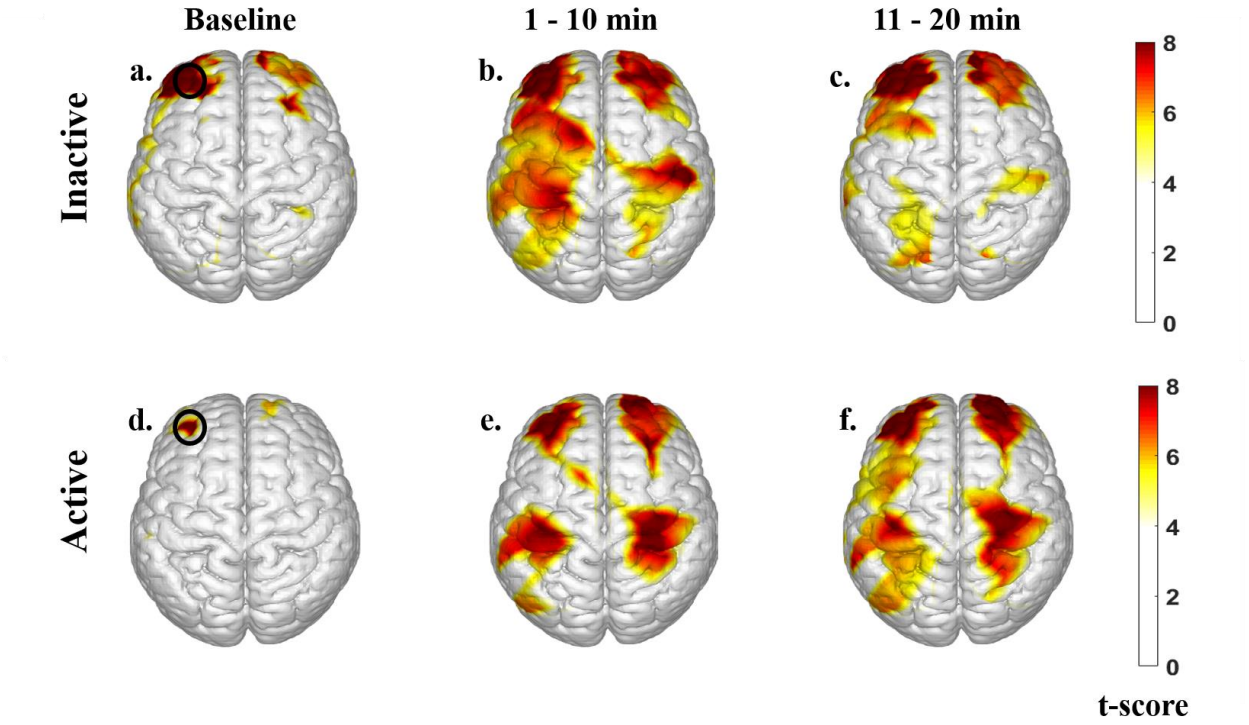

Figure 2 - 5 Evolution of FC patterns during the entire handgrip task with the seed region at lDLPFC for inactive subjects at a) baseline, b) 0 – 10 min, and c) 11 – 20 min and active subjects at d) baseline, e) 0 – 10 min, and f) 11 – 20 min. The black oval encircles the seed region channels and is only displayed at baseline for clarity. Only regions with statistically significant FC strength are shown (p < 0.05, Bonferroni corrected).

2.3.3.3 *FC maps with seed at rDLPFC*

The FC maps with the seed at rDLPFC, the symmetrically contralateral position to the lDLPFC seed considered above, are shown in Fig. 2 - 6. Within the first 10 min of the task, inactive subjects exhibited statistically significant but relatively weak FC strength to

the lDLPFC, rPMC, and lM1/S1 (Fig. 2 - 6b). In the subsequent 10 min of the task, there was loss of FC strength with the rPMC (Fig. 2 - 6c). In contrast, active subjects displayed significant FC strength with the lDLPFC, bilateral M1/S1 and some weaker but significant FC to bilateral PMC within the first 10 min (Fig. 2 - 6e), which weakened in the second 10 min of the task (Fig. 2 - 6f). The r_a values were significantly greater in active subjects than in inactive subjects at each time period: Baseline ($p = 0.02$), 0 – 10 min ($p = 0.01$), and 10 – 20 min ($p = 0.04$). The r_a values within groups were also significantly different from one another across time for inactive subjects at baseline and 0 – 10 min ($p = 0.003$) only and active subjects at baseline and 0 -10 min ($p = 0.03$) and 0 – 10 min and 10 – 20 min ($p = 0.01$).

2.3.3.4 *Correlation between regional FC and grip strength*

Pearson's correlation coefficient (r) values were quantified between regional FC magnitude and time to 50% MVC. This was performed for each group at each time point. Additionally, correlation coefficients were compared between active and inactive subjects at each time point. Active subjects had significant ($p < 0.05$), positive correlation between lM1, lDLPFC, and rDLPFC and 50%MVC at all time points, with the exception of rDLPFC at 0 – 10 min and 10 – 20 min whereas, inactive subjects had no significant correlation (Table 2 - 2). Active subjects' correlation was more significant than inactive subjects' at lM1 (baseline and 10 – 20 min), lDLPFC (all time periods), and at rDLPFC (baseline and 10 – 20 min) (Table 2 - 3).

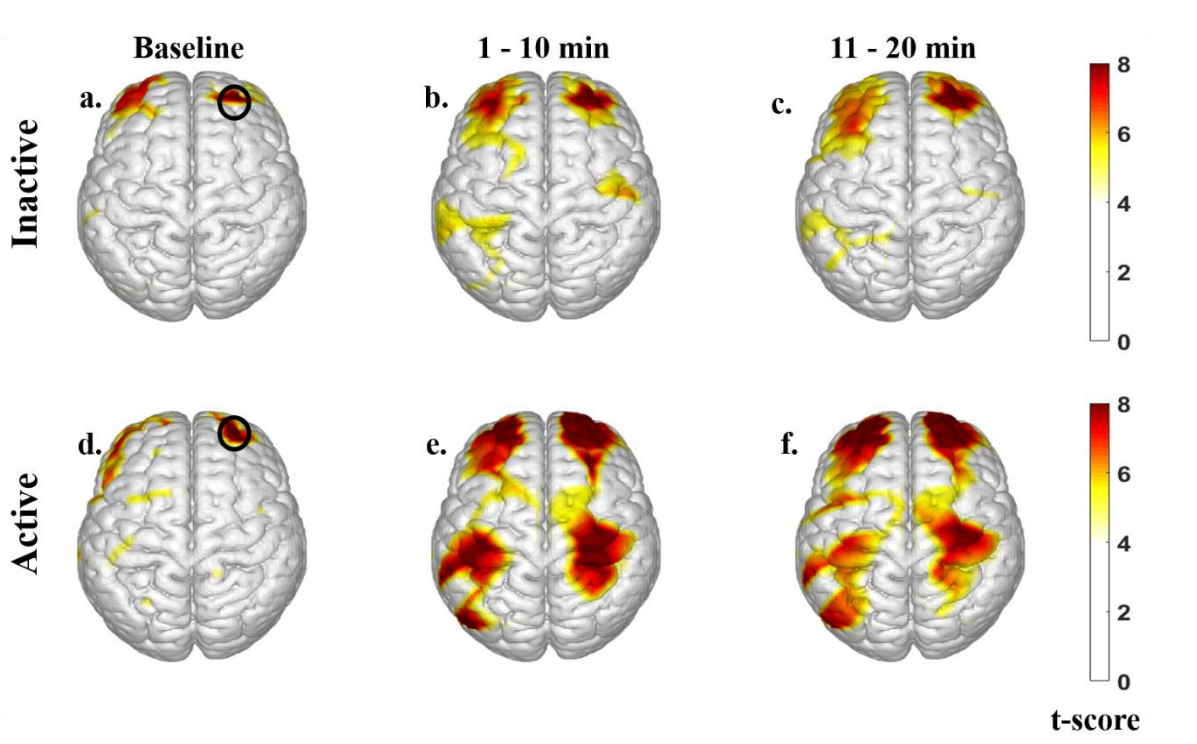

Figure 2 - 6 Evolution of FC patterns during the entire handgrip task with the seed region at rDLPFC for inactive subjects at a) baseline, b) 0 – 10 min, and c) 11 – 20 min and active subjects at d) baseline, e) 0 – 10 min, and f) 11 – 20 min. The black oval encircles the seed region channels and is only displayed at baseline for clarity. Only regions with statistically significant FC strength are shown ($p < 0.05$, Bonferroni corrected).

Table 2 - 3 Pearson's correlation analysis summary between regional FC magnitude and time to 50% MVC (Pearson's correlation coefficient (r) and p-value).

		lM1		lDLPFC		rDLPFC	
		r	**p**	**r**	**p**	**r**	**p**
Inactive	**Baseline**	-0.35	0.26	-0.56	0.06	-0.17	0.59
	0 – 10 min	-0.17	0.59	-0.5	0.10	-0.37	0.24
	10 – 20 min	-0.31	0.33	-0.45	0.15	-0.45	0.15
Active	**Baseline**	0.63	0.04	0.74	0.01	0.69	0.02
	0 – 10 min	0.69	0.02	0.65	0.03	0.49	0.13
	10 – 20 min	0.63	0.04	0.59	0.05	0.43	0.18

Table 2 - 4 Correlation coefficients comparison summary between inactive and active subjects for regional FC magnitude and 50% MVC (z-value and p-value).

	lM1		lDLPFC		rDLPFC	
	z	**p**	**z**	**p**	**z**	**p**
Baseline	-2.28	0.02	-3.26	0.001	-2.1	0.04
0 – 10 min	-1.88	0.06	-2.73	0.006	-1.9	0.06
10 – 20 min	-2.19	0.03	-2.39	0.02	-1.94	0.05

2.4 DISCUSSION

The present study aimed to map by fNIRS the temporal evolution in hemodynamic activation and FC patterns in physically inactive and active subjects performing a

fatiguing handgrip task. The observed differences in cortical activity patterns and concurrently acquired handgrip force data suggest physical activity dependent network reorganization across multiple cortical regions during this task.

2.4.1 Changes in Handgrip Performance During the Task

Physical fatigue induced by intermittent muscle contractions and its effect on force has been studied extensively in physiology[59, 60] and recent neuroimaging studies.[3, 6, 9, 38, 46, 61, 62] Fatigue has been defined as "any decline in muscle performance associated with muscle activity at the original intensity".[60] Both inactive and active subjects' muscle performance adhered to this definition *vis-á -vis* the gradual decline in MVC throughout the exercise. Moreover, our results are in agreement with a prior handgrip fatigue study showing that the rates of fatigue were similar between subjects with varying physical activity levels and initial strength, final strength, and absolute endurance were larger for the active subjects.[59]

2.4.2 Evolution of Hemodynamic Activation Patterns During the Handgrip Task

Previous functional neuroimaging studies concerning arm and hand movements have demonstrated activation in M1, PMC/SMA, and PFC.[6, 36, 38, 61, 63, 64] In this work, inactive and active subjects exhibit significant activity in these regions and in Broca's area as well. However, as the task progressed there were subsequent shifts in activity towards the DLPFC. In a prior fMRI study involving a handgrip task performed under non-fatiguing conditions (30% MVC), as verified by electromyography (EMG), increased activation was seen bilaterally in M1/S1 with concurrent EMG signal increased for several forearm muscles.[38] In contrast, during a fatiguing handgrip task (100% MVC) initial M1/S1 activation and concurrently acquired EMG signals declined, but

supplementary cortical regions such as the PFC maintained consistent activation.[39] While EMG measurements were not performed in this work, the above findings do support the notion that a stronger central command, via increased brain activation in the PFC, is needed to maintain task performance once fatigue sets in. However, prior studies do not discuss the temporal evolution of cortical activation and connectivity patterns during the handgrip task. These are discussed here in more detail with respect to the cortical areas involved.

2.4.2.1 *Evolution of Hemodynamic Activation Patterns at Primary and Secondary Sensory-Motor Cortices*

The primary sensory-motor cortex , or M1/S1, is responsible for motor control and execution[8, 65] and works in conjecture with the secondary sensory-motor cortex, or PMC, which is associated with movement planning and preparation.[65] Physically active individuals were able to elicit brain activation and deactivation in these regions, similar to a prior neuroimaging motor task study.[39] This work however differs from another prior study comparing athletes to non-athletes performing a sustained handgrip task, where athletes exhibited decreased M1 activation compared to non-athletes during a sustained handgrip task at 50% MVC.[4] As that study only used two fNIRS channels, it is possible that its results were affected by incomplete spatial coverage of the sensory-motor cortices, as the authors also suggested.[4] Also, in this work both athletes and non-athletes exhibited significant deactivation in the rPMC towards the end of the task, when subject fatigue was the highest.[4] We hypothesize that an increase in variability of activation as a result of exercise, hindered determination of activation significance in inactive subjects (Fig. 2 - S1), as also demonstrated in a prior fMRI fatiguing handgrip

study.[6] That study noted a positive correlation between exercise duration and increased hemodynamic signal variance, with high variance correlating to low pixel activation.[6]

This work demonstrates substantial location shifts of focal regions during the fatiguing handgrip task from contralateral to ipsilateral regions and from posterior to anterior regions of higher brain activity, in agreement with an EEG fatiguing handgrip study.[3] Moreover, brain activation changes in deeper subcortical structures participating in motor regulation (i.e. bilateral basal ganglia, cerebellum, and thalamus) are known to occur as a coordinated effort to optimize motor unit recruitment and activation level for prolonged fatiguing exercise.[62, 66] Although it would be reasonable to expect that these structures could also be activated as the handgrip task progressed, those regions were not accessible by fNIRS.

2.4.2.2 *Evolution of Hemodynamic Activation Patterns in the DLPFC*

In the context of motor tasks, the DLPFC is associated with motor preparation and planning over long periods of time, action selection and control,[65] and correlates with higher force output.[66, 67] In a prior study the DLPFC was activated predominantly on the side contralateral to the used hand,[66] which is consistent with the increased lDLPFC activation observed in physically active subjects in our work. Other fNIRS studies that measured PFC activation during near-maximal or exhaustive aerobic exercise found that as the near-exhaustion was reached DLPFC activation increased bilaterally.[12, 40] However, in these latter studies subjects were trained athletes performing a bilateral task such as cycling and not a unilateral task, like in our work.

The rDLPFC is associated with inhibition or avoidance behavior towards meeting a goal and has been suggested to be involved during prolonged exercise to purposefully inhibit

bodily afferences that arise with physical fatigue, and preserved mental effort during exercise maintenance.[40] In agreement with prior studies, the rDLPFC deactivation seen in our results correlated with a reduction in handgrip force.[11, 12, 40, 68] These prior studies suggest that subject stress due to the prolonged and physically challenging motor task may have contributed to the observed rDLPFC deactivation. The lDLPFC is associated with an approach reaction towards a goal and may suggest the willingness of the active subjects to challenge themselves and meet the task goal even in the presence of fatigue.[68] We hypothesize that as the task progressed, active subjects adopted a goal-oriented approach resulting in the dominance of lDLPFC activation, whereas inactive subjects adopted a goal-avoidance approach that resulted in the dominance of rDLPFC deactivation.

2.4.2.3 *Evolution of Hemodynamic Activation Patterns at the Broca's Area*

Inner speech refers to the activity of silent expression of conscious thought to oneself and results in activation in Broca's area in the left hemisphere.[69] Sports literature has further studied inner speech of positive, negative, motivational, and instructional context known as self-talk via questionnaires in athletes which found that athletes participate in self-talk more frequently in competition settings and when performing individually, as opposed to on a team.[70-72] While the active subjects were not athletes, they too had significantly more activation in Broca's area than inactive subjects.

2.4.3 Evolution of FC Patterns During the Handgrip Task

The application of FC analysis to the fNIRS data collected in this study provided detail of cortical area interconnectedness during the entire duration of the handgrip task than seen in prior neuroimaging studies using similar protocols, which only reported results

for the beginning and the end of the task period.[8, 9, 46, 62] In our work, seed regions were specifically placed at locations with significant hemodynamic activity namely, the lM1, the lDLPFC, and the rDLPFC. These seed regions are all known to be connected to the descending motor pathways that control hand and arm movements.[8, 11, 12, 40, 73]

2.4.3.1 *Overall FC Pattern Differences between Inactive and Active Subjects*

This study showed significant differences in FC patterns between inactive and active subjects when performing a fatiguing handgrip task. Active subjects exhibited more spatially extended FC patterns that persisted into the second half of the task, compared to inactive subjects that showed progressively diminished connectivity to areas distant to the seed region. Physical exercise is known to increase brain function throughout life and has been shown to enhance FC in the default mode network (DMN), frontoparietal network (FPN) , and motor network (MN) as well as increase gray brain volume in the prefrontal, and temporal cortex and the hippocampus.[74-77] Physically active subjects' expansive connectivity patterns highlight the greater availability of cortical network resources due to prior exercise. Overall, the findings of our work are consistent with the existing notion of exercise-related augmentation in FC at the resting state and during fatiguing tasks.[9]

2.4.3.2 *FC Pattern Comparisons with Seed at lM1*

The seed at lM1 indicated strengthened FC between bilateral DLPFC, bilateral PMC, and rM1/S1. However, the spatial extent, temporal persistence and hemispheric localization were different between inactive and active subjects. The M1 region is the primary neural output center of the brain to the working muscles because of its vital role in motor control and execution during exercise.[8, 65] FC strength between lM1 and

bilateral DLPFC, which is which is associated with executive behavior control[68, 78] and involved in motor planning and preparation,[11, 12, 40] was present throughout the task in both groups. However, only active subjects' FC strength towards bilateral DLPFC was consistent during the entire task, which is attributed as reinforcement of the top-down regulation to the primary and secondary motor cortices under fatiguing conditions.[8, 11] A prior neuroimaging study also reported enhanced connectivity in young adult endurance athletes compared to heathy controls, similar to the difference in FC strength to bilateral DLPFC seen between inactive and active subjects in this study.[77] The FC patterns between lM1 and rPMC and rM1/S1 regions illustrated the enhanced recruitment of cortical regions involved in motor planning and execution for active subjects compared to inactive subjects. Lastly, in prior fMRI work involving a similar protocol, the 1M1 connectivity to bilateral S1 in active subjects was suggested to be due to increased sensory feedback from the arm muscles to the central motor command.[8]

2.4.3.3 *FC Pattern Comparisons with Seeds at lDLPFC and rDLPFC*

The DLPFC is extensively connected with the sensory-motor cortex and is associated with regulating attention, goal-directed behavior, thought, and motor planning and preparation.[11, 12, 40, 68, 73, 79] However, the lDLPFC and rDLPFC are further involved in the role of approach and avoidance behaviors, respectively, which engenders differences in their connectivity with other cortical regions.[40, 68, 79] As a result, our data not only showed that FC patterns had significant differences between active and inactive subjects for both seed locations, but also showed slightly different FC patterns within each subject category depending on whether the seed location was at the lDLPFC, or the rDLPFC.

The lDLPFC has also shown high connectivity strength with cortical regions that associated with the pursuit of approach-related goals,[80]such as maintaining MVC. The lDLPFC also exhibits connectivity in cortical regions that are important for goal pursuit[80] – hence the lDLPFC FC to rDLPFC, bilateral PMC, and bilateral M1/S1 which are involved in motor planning an execution for this task. As the task progressed and handgrip force production decreased, the FC strength of the lDLPFC regions to other cortical areas diminished in inactive subjects but became more spatially extended in active subjects. Under fatigue conditions, noradrenaline and dopamine are released which impair the top-down or executive control of the DLPFC and strengthen the bottom-up control, driven by the salience of the stimulus, through the amygdala, which results in a more reflexive and habitual motor responses.[73] Prior FC studies have indicated that subcortical structures like the amygdala, basal ganglia, and anterior cingulate cortex, not accessible by fNIRS, reinforce the descending command under fatigue conditions which would contribute to maintaining task performance and possibly goal-pursuit.[8, 68, 79, 80] Lastly, FC between the lDLPFC and other motor planning and control cortical regions is also dependent on subject motivation, which suggests that active subjects are more motivated that inactive subjects during this task.[80]

The rDLPFC seed juxtaposes the difference in FC patterns between inactive and active subjects at each time period more clearly than the lDLPFC. This may be a result of the rDLPFC's specialized involvement in the maintenance of prolonged physical exercise due to its role in avoidance, or more specifically inhibition of impulse responses.[40] We propose that active subjects have stronger, persistent FC between rDLPFC and lDLPFC, bilateral PMC, and bilateral M1/S1 because they were able to inhibit bodily

afferences that arise with fatigue more successfully than their inactive counterparts.[40] In addition, the rDLPFC strongest connection was to lDLPFC (Table S2), especially in active subjects at baseline (Table S3), possibly because inhibition was needed to maintain task performance that required stronger, longer-lasting FC to other higher-order DLPFC areas, as suggested in a prior functional neuroimaging study.[11, 12, 40]

2.4.3.4 *Correlation between FC and Performance*

Correlation between regional FC and performance (i.e. time to 50% MVC) further exemplified the difference in FC strength between inactive and active subjects. Exercise has been suggested to improve neuronal activity and promote angiogenesis and vascular function to cortical brain regions including the motor cortex.[32] In addition, resistance exercise increases torque- and power- generating capacity in the muscle, and also positively impacts functional plasticity in older subjects.[81] This study further demonstrated that active subjects had a positive relationship between performance and FC strength in lM1, lDLPFC, and rDLPFC at nearly every time point. In contrast, inactive subjects had no significant correlation between performance and FC strength possibly due to limited exercise-related structural and functional changes.

2.5 LIMITATIONS

This study has some limitations that should be considered. Firstly, individuals were grouped based on a self-reported physical activity questionnaire which neglected to specify type of exercise (i.e. endurance or resistance) performed by the subject. This information could have better defined the active populations. In addition, fNIRS is limited in only measuring cortical brain areas and has lower spatial resolution compared to fMRI.[35, 42] Also, short-distance channels (< 1 cm) were not employed in this study as

they were not available in the commercial optode holder cap used. Signals measured by short-distance channels are dominated by systemic interferences from superficial scalp layers such as cardiac activity and respiration, and can be regressed out.[82] Short-distance channels could also provide blood flow changes in the extracerebral layer of the head due to the task.[83] Additionally, it is unknown which other method(s) would be the best approach in removing physiological noise. There exist several different ways to remove global interference due to the scalp and skull hemodynamics in addition to the PCA in our work. These methods include i) short-distance channels, as previously mentioned, ii) use of ICA, iii) adaptive filtering, iv) calculating the mean signal over all channels and using the mean as a superficial regressor, or v) a combination of these methods can be used for removal.[42, 84, 85] Thus, a quantitative comparison using different methods is warranted in future studies.

2.6 CONCLUSION

This is the first study, to our knowledge, that presents a direct comparison of differences in the temporal evolution of cortical hemodynamic activation and FC patterns between physically active and inactive subjects during a fatiguing handgrip task. The observed patterns suggest that physical activity modifies both baseline connectivity as well as the way that different cortical regions are recruited as subjects try to maintain maximum MVC for a prolonged time. Overall, hemodynamic activity moved from the sensory-motor areas early into the task, towards the PMC and DLPFC as the task progressed. However, the temporal evolution of activation patterns was different between active subjects (30 minutes of moderately vigorous exercise at least 4 times a week) and inactive subjects (exercised less than twice a week), consistent with approach (active)

versus avoidance (inactive) tendencies towards the task goal. At the same time active subjects exhibited longer-lasting and broader connectivity patterns, which likely contributed to the sustenance of higher handgrip force output, compared to inactive subjects, as fatigue set in. These results provide preliminary evidence for broad network pattern differences across multiple cortical regions during a fatiguing task that are specific to subjects' physical activity. We propose to use this protocol in future work as a novel means of evaluating exercise-induced functional changes in brain activation patterns in human health and disease.

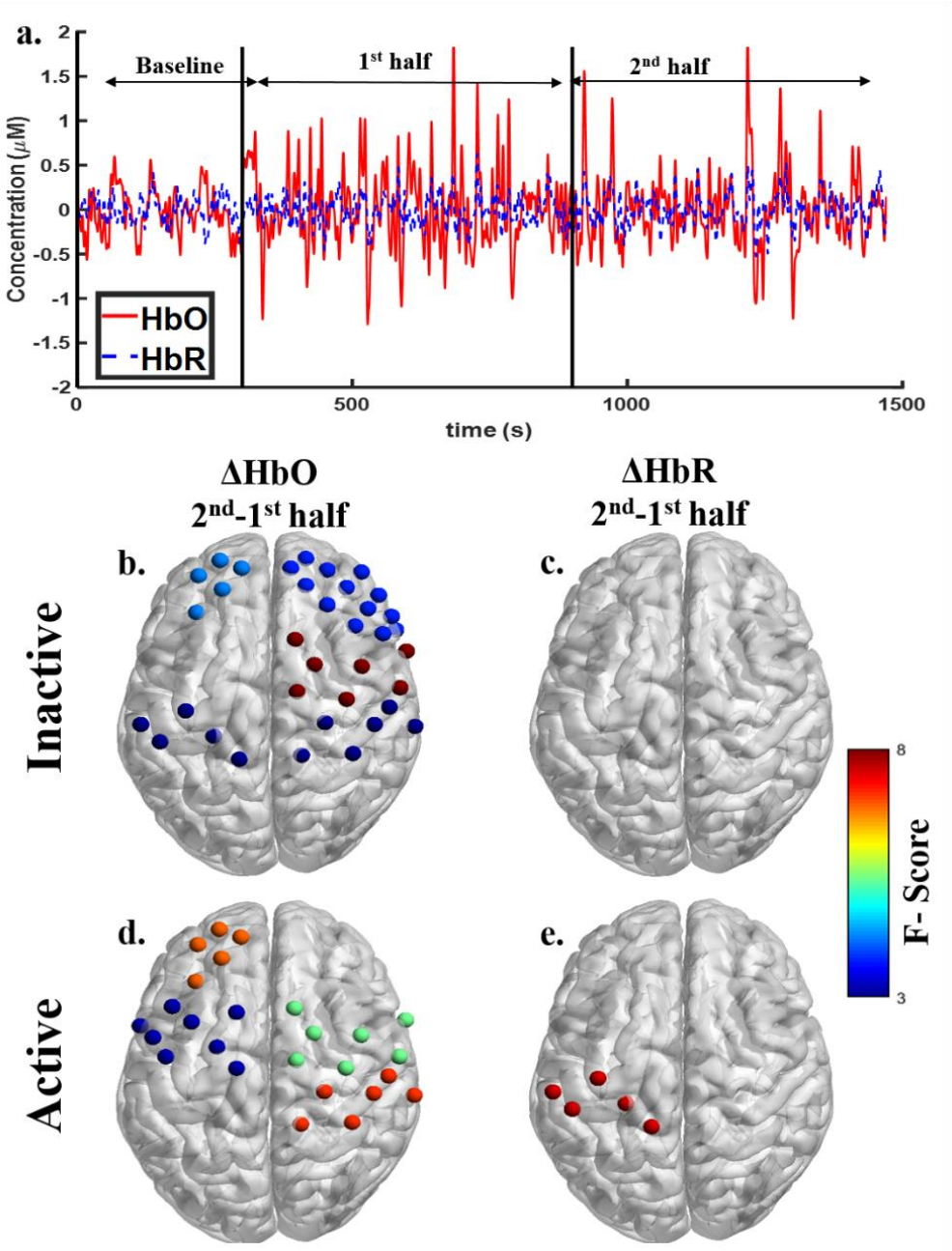

Figure 2 - S1 Exercise induced variance in ΔHbO and ΔHbR. a) representative time-series of HbO and HbR at IM1. Significant ($p < 0.05$) difference in variability, as determined by Levene's test, between 0 – 10 min and 10 – 20 min periods are shown for inactive subjects for b) ΔHbO and c) Δ HbR and active subjects for d) ΔHbO and e) ΔHbR.

Table 2 - S1 Spatial registration of fNIRS channel positions on a standard brain fMRI atlas. MNI coordinates displayed as mean (SD); r-right contralateral brain hemisphere; l- left ipsilateral brain hemispheres.

CHANNEL	MNI			ROI	BA
	x	y	z		
10	-18.70(4.14)	58.42(6.75)	34.80(10.06)	lDLPFC	BA9
12	23.84(4.12)	57.20(7.52)	35.33(8.66)	rDLPFC	BA9
13	-44.86(4.27)	45.98(6.40)	22.55(9.36)	Broca's	BA44/45
14	-29.03(5.33)	49.56(8.06)	37.27(9.58)	lDLPFC	BA9
15	-9.38(2.74)	52.12(9.01)	46.03(8.77)	lDLPFC	BA9
16	14.47(2.39)	51.38(9.31)	46.27(8.47)	rDLPFC	BA9
17	33.59(4.55)	48.26(8.68)	37.98(7.90)	rDLPFC	BA9
18	48.38(3.69_	45.52(7.43)	22.92(8.17)	rDLPFC	BA9
19	-52.56(4.03)	33.44(7.80)	22.02(5.60)	Broca's	BA44/45
20	-39.89(4.55)	38.27(9.44)	39.21(9.17)	lDLPFC	BA9
21	-19.52(3.54)	40.94(10.90)	51.24(9.18)	lDLPFC	BA9
23	23.44(3.81)	40.15(10.54)	52.16(7.06)	rDLPFC	BA9
24	41.97(7.65)	(36.82(9.38)	40.21(7.67)	rDLPFC	BA9
25	54.21(7.13)	32.68(8.64)	23.36(7.57)	Broca's	BA44/45
27	-58.54(3.43)	19.56(9.53)	21.71(7.33)	Broca's	BA44/45
28	-48.61(4.40)	25.98(9.87)	39.86(7.89)	Broca's	BA44/45
29	-31.88(5.64)	28.91(11.57)	53.58(8.18)	lDLPFC	BA9
32	33.44(6.50)	28.23(11.01)	54.55(5.99)	rDLPFC	BA9
33	50.08(5.45)	24.61(10.67)	41.23(6.81)	rDLPFC	BA9
38	-56.91(4.65)	10.29(11.67)	37.30(6.35)	lPMC	BA6
39	-42.89(4.48)	16.08(12.82)	5427(5.84)	lDLPFC	BA9
43	44.30(5.84)	14.72(13.02)	54.74(5.04)	rDLPFC	BA9
45	66.92(2.55)	1.39(9.31)	18.61(7.65)	rPMC	BA6
49	-51.35(4.99)	1.94(14.33)	52.29(4.78)	lPMC	BA6
50	-33.21(8.22)	5.89(15.35)	65.29(4.91)	lPMC	BA6
51	-13.64(4.83)	7.74(15.97)	71.09(6.52)	lPMC	BA6
52	13.56(6.13)	6.86(16.50)	72.09(4.26)	rPMC	BA6
54	53.55(5.44)	-1.08(13.36)	52.15(4.31)	rDLPFC	BA9
55	66.23(3.48)	-7.32(10.61)	34.15(5.19)	rPMC	BA6
60	-44.47(3.17)	-8.64(15.74)	61.53(3.68)	lPMC	BA6
61	-22.38(3.13)	-8.42(17.48)	73.18(2.64)	lPMC	BA6
63	23.73(2.47)	-9.14(16.25)	73.74(8.32)	rPMC	BA6
64	47.03(3.30)	-12.36(14.16)	62.18(2.84)	rPMC	BA6
65	63.67(2.77)	-19.62(11.49)	46(4.08)	rPMC	BA6

70	-54.95(2.56)	-26.30(14.18)	55.56(3.49)	lS1	BA1/2/3
71	-35.54(2.76)	-23.18(16.20)	70.86(2.40)	lM1	BA4
72	-13.97(1.75)	-20.91(16.47)	77.76(1.37)	lM1	BA4
73	14.26(1.47)	-21.55(15.61)	77.77(0.88)	rPMC	BA6
74	36.65(3.68)	-23.80(17.56)	71.47(1.44)	rM1	BA4
75	56.12(457)	-29.95(12.78)	56.02(2.95)	rS1	BA1/2/3
76	67.41(3.16)	-49.94(63.79)	38.03(5.91)	lS1	BA1/2/3
81	-46.74(3.49)	-37.18(14.07)	63.06(4.34)	lS1	BA1/2/3
82	-23.38(5.10)	-36.33(15.76)	74.06(3.00)	lM1	BA4
84	24.74(3.07)	-37.65(14.31)	73.61(6.53)	rM1	BA4
85	47.24(5.01)	-39.26(13.27)	62.92(3.91)	rS1	BA1/2/3
95	34.62(4.74)	-53.02(11.79)	67.73(5.53)	rS1	BA1/2/3

Table 2 - S2 Pearson's correlation analysis summary between regional FC magnitude and time to 50% MVC (Pearson's correlation coefficient (r) and p-value).

		lM1 and lDLPFC		lDLPFC and rDLPFC		lDLPFC and rDLPFC	
		r	**p**	**r**	**p**	**r**	**p**
Inactive	**Baseline**	0.47	0.13	0.54	0.07	0.19	0.55
	0 – 10 min	0.65	0.02	0.85	0.0005	0.83	0.001
	10 – 20 min	0.69	0.01	0.59	0.04	0.77	0.003
Active	**Baseline**	0.81	0.003	0.57	0.07	0.79	0.004
	0 – 10 min	0.72	0.01	0.62	0.04	0.89	0.0003
	10 – 20 min	0.87	0.0005	0.66	0.03	0.85	0.001

Table 2 - S3 Correlation coefficients comparison summary between inactive and active subjects for regional FC magnitude and 50% MVC (z-value and p-value).

	lM1 and lDLPFC		lDLPFC and rDLPFC		lDLPFC and rDLPFC	
	z	**p**	**z**	**p**	**z**	**p**
Baseline	-1.27	0.20	-0.09	0.92	-1.81	0.07
0 – 10 min	-0.27	0.78	1.09	0.28	-0.48	0.63
10 – 20 min	-1	0.32	-0.24	0.81	-0.49	0.62

CHAPTER 3

Differences in net information flow and dynamic connectivity metrics between physically active and inactive subjects measured by functional near-infrared spectroscopy (fNIRS) during a fatiguing handgrip task

This chapter is a publication at the journal of Frontiers in Neuroscience on March 2020. (14: 10.3389/fnins.2020.00167)

Authors: Elizabeth L. Urquhart, Xinlong Wang, Hanli Liu, Paul J. Fadel, and George Alexandrakis

3.1 INTRODUCTION

Cerebral autoregulation helps maintain a relatively constant oxygen supply to the brain during changes in arterial blood pressure, by maintaining cerebral blood flow (CBF) relatively constant. This occurs via vasoconstriction in response to increased blood pressure and vasodilation in response to decreased blood pressure. Regional CBF (rCBF) is flow-mediated vasodilation from distal to proximal vessels that occurs in activated brain regions which protects downstream microvascular pressure.[32, 86-89] There are overlapping regulatory mechanisms of rCBF that have been classified into contiguous ranges of hemodynamic frequencies as endogenic (0.003 – 0.02 Hz), neurogenic (0.02 – 0.04 Hz), and myogenic (0.04 – 0.15 Hz).[90, 91] These frequency oscillations reflect the influence of endothelial-related metabolic activity, intrinsic neuronal activity, and myogenic activity of the vascular smooth muscle, respectively.[90-92] Exercise may also modulate the regulatory mechanisms in each frequency band. Exercise is known to improve cardiovascular health[93] and brain health.[1, 89] Regular exercise produces

beneficial alterations in the brain that maintain or improve cognition,[1, 94] and promote motor function,[32] known as exercise-dependent neuroplasticity.

The hemodynamic oscillations at these frequency bands can be measured using functional brain mapping using functional magnetic resonance image (fMRI),[95] or functional near-infrared spectroscopy (fNIRS).[85, 91, 94, 96] FNIRS measures noninvasively the change of oxyhemoglobin (ΔHbO) and deoxyhemoglobin (ΔHb) concentrations resulting from neurovascular coupling secondary to neuronal activation by utilizing light at near-infrared wavelengths (650-1000 nm). It is advantageous because of its relatively lower cost, portability, robustness to motion artifacts, and its higher temporal resolution compared to fMRI.[35, 42]

In recently completed work, we demonstrated interesting temporal evolution patterns for hemodynamic activation and static functional connectivity (SFC) changes that depended on the physical activity levels of subjects while they were trying to maintain maximal handgrip task performance.[97] That work identified that physically active subjects experienced delayed fatigue onset as evident by their greater ability to maintain maximum voluntary contraction (MVC) force accompanied by longer-lasting and more spatially extended activation and SFC patterns in the primary motor (M1), premotor and supplementary motor areas (PMC/SMA) and the prefrontal cortex (PFC).[97] In contrast to the static networks explored in our previous work, the purpose of this work was to examine changes in dynamic cortical network patterns and how they relate to handgrip task performance for each hemodynamic frequency band, as a function of a subjects' physical activity level.

In this work we first applied directional phase transfer entropy (dPTE) analysis, a computationally efficient and data-driven method previously used in electroencephalography (EEG) research,[98] to estimate changes in the direction of information flow during the fatiguing handgrip task. It has been applied recently to fNIRS in one study,[85] but dPTE analysis has not been employed, to our knowledge, as yet to explore the effect of fatigue on the brain's networks. The net direction of information flow, or directional connectivity (DC), was also quantified between regions to better understand motor control regulation under fatiguing conditions.[98] A simultaneous multimodal neuroimaging study using fNIRS, fMRI, and EEG has previously examined directionality via Wiener-Granger causality on finger movement tasks, but their results were confined to the contralateral (i.e. left) hemisphere only and not broader cortical networks.[99] We also explored the relationship between SFC and functional connectivity variability (FCV), which represents spontaneous dynamic fluctuations of connectivity over time.[100] This was motivated by the fact that SFC is known to increase with task performance,[8, 32, 97] while FCV reflects resource availability during demanding tasks.[100, 101] The aim of this work was to identify differences between subject groups across all of the aforementioned fNIRS metrics and hemodynamic frequency bands. In addition, we aimed to demonstrate the feasibility of using time-dependent fNIRS metrics to help understand how dynamic connectivity regulation of cortical networks relates to performance during a fatiguing motor task.

3.2 MATERIALS AND METHODS

3.2.1 Participants

Twenty-three young adults (4 females) between the ages 18-30 (mean age 25.13 ± 3.72) participated in this study. All subjects gave prior written informed consent for their participation in this study, which was approved by the Institutional Review Board of the University of Texas at Arlington (IRB# 2018-0686) and performed in accordance with the Declaration of Helsinki. All but two subjects were right-handed, as determined by the Edinburgh handedness scale.[43] All subjects were free of any neurological or psychiatric disorders (self-reported), and were non-smokers. Subjects self-reported as being physically inactive (n=12, exercising less than twice a week for 30 min of moderately vigorous exercise), or active (n=11, exercising at least 4 times a week for 30 min of moderately vigorous exercise).

3.2.2 Experimental Procedures

A continuous wave fNIRS imaging system (OMM-3000, Shimadzu Corp., Kyoto, Japan) was used in this experiment, which utilized near infrared light diode sources (780, 805, and 830 nm) and photomultiplier detectors at a sampling frequency of 10.101 Hz. The setup geometry consisted of 32 sources and 34 detectors with a separation of 3 cm, resulting in 111 source-detector channels (Fig. 3 - 1A). This probe geometry covered cortical areas of the following 11 regions of interest (ROIs) (Fig. 3 - 1B): left and right frontopolar prefrontal cortex (lFP; rFP), left and right dorsolateral prefrontal cortex (lDLPFC; rDLPFC), Broca's area, left and right premotor cortex (lPMC; rPMC), left and right primary motor and sensory cortical (lM1/S1; rM1/S1) areas, and left and right sensory association cortex (lSAC; rSAC). Anatomical cranial reference points (nasion,

inion, left and right preauricular points and vertex) and optode locations were recorded for each subject using a 3D digitizer (FASTRAK, Polhemus VT, USA). Montreal Neurological Institute (MNI) coordinates for each source and detector location were calculated using the statistical parametric mapping NIRS_SPM software, which provided the Brodmann area (BA) corresponding to each fNIRS channel as shown in Table 3 - S1.[45]

Subjects sat upright with their dominant arm at their side, elbow flexed at 90º and resting on a table. Subjects faced two screens that displayed protocol commands and visual feedback of handgrip performance (Fig. 3 - 1C). Prior to starting the handgrip task, subjects performed three to five isometric MVCs with their dominant hand. All MVCs were recorded at a 1 kHz sampling rate using a handgrip dynamometer (BIOPAC, CA, United States). The pre-task MVCs were averaged for each subject and set as their maximum target of 100% MVC to reach during the subsequent handgrip task. The fNIRS data acquisition began with a 5 min resting period where subjects were asked to refrain from any movement or specific thoughts, followed immediately by a fatiguing handgrip task. The task required subjects to perform intermittent handgrip contractions for 3.5 s alternating with 6.5 s of rest for 120 blocks (Fig. 3 - 1D) while attaining 100% MVC as closely as possible, as a means to induce fatigue in the forearm.[3, 4, 8, 9] The recorded force time-series data were low-pass filtered at 15 Hz and the maximum force for each block was calculated.[9, 46]

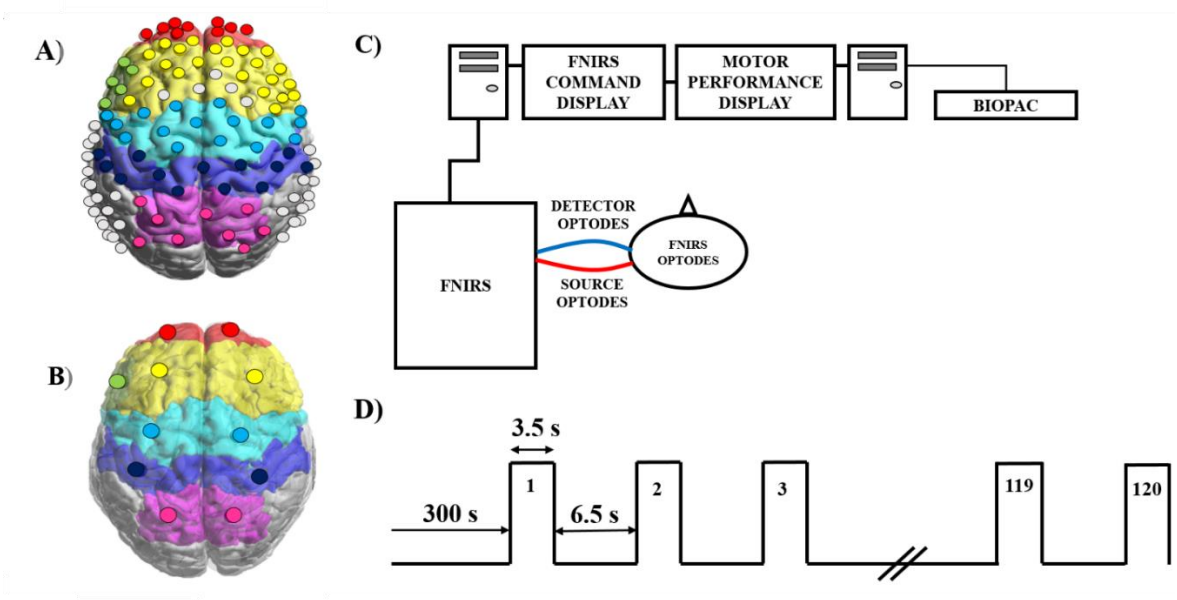

Figure 3 - 1 Experimental set up and protocol timeline for the handgrip task. A) FNIRS 111-channel layout with eleven regions of interest (ROIs) covered by the probe geometry: left and right frontopolar (lFP; rFP) (red) , left and right pre-frontal cortex (lDLPFC; rDLPFC) (yellow), Broca's area (green), left and right pre-motor cortex (lPMC; rPMC) (light blue), left and right primary motor and sensory cortical (lM1/S1; rM1/S1) areas (purple), and left and right sensory association cortex (lSAC; rSAC) (pink). B) Each circle shows the spatial average of the probe coordinates in each ROI, per brain hemisphere. These averaged probe locations served as reference points for plotting dPTE and DC between ROIs in this work. C) Schematic of the experimental set-up of the fNIRS (LABNIRS) system and the BIOPAC handgrip force sensor system with one representative source-detector channel shown for simplicity. D) The handgrip task protocol, starting with a 5-minute baseline. Subjects performed intermittent handgrip contractions for 3.5 s followed by 6.5 s of rest for 120 blocks at 100% MVC.

3.2.3 Data Preprocessing

This study used the open-source Homer2.0 to process (Table 3 - S2) the collected fNIRS data.[42] Detrending was implemented using the least-squares fit of a line that was subtracted from the data.[47] The data were then filtered for each respective frequency band. Following previously published work, frequency bands were defined as endogenic (0.003 – 0.02 Hz), neurogenic (0.02 – 0.04 Hz), and myogenic (0.04 – 0.15 Hz).[85, 102]

Data in each of these three hemodynamic frequency bands were low-pass filtered by a 3rd order and high-pass filtered by a 5th order Butterworth filter.[42] Channels were removed if signal standard deviations were greater than two times their mean signal amplitude.[85] Principal component analysis (PCA) was utilized to remove motion artifacts and global hemodynamic fluctuations that may overlap with the task-related hemodynamic response frequencies. The first two principal components were removed from all fNIRS channel data in order to remove these global artificats[35, 42] To avoid signal contamination especially by branches from the middle cerebral artery or the superficial temporal artery and temporal muscle, channels located near these structures were also removed from analysis.[103, 104] The resulting optical density data were then converted into changes in hemoglobin concentration relative to baseline (ΔHbO and ΔHb) using the Modified Beer-Lambert Law with an estimated differential pathlength factor of 6.0 for each wavelength, an estimate used in Homer 2.0.[49] Only ΔHbO values were presented in the Result section below because ΔHb values were found to have similar and opposite qualitative trends, but with smaller amplitudes and lower signal-to-noise ratio as previously reported in other neuroimaging studies observing motor activation tasks.[52, 53] Nevertheless, corresponding ΔHb results were included in the Supplementary Information section for completeness. Left-handed subjects' data was flipped to its mirror image on the brain for group averaging purposes and the subsequent interpretation for all data was right (r) for contralateral and left (l) for ipsilateral brain hemispheres relative to the arm performing the handgrip task.

3.2.4 Phase Transfer Entropy (PTE) and Directed PTE (dPTE) Data Analysis

The information flow between ROIs was estimated using phase transfer entropy (PTE) based on the same principle as Granger Causality.[85, 98, 105] It is calculated as the difference between the uncertainty of the target signal Y conditioned by its past and the uncertainty of the target signal conditioned on both its past and the source signal X:[85, 98]

$$\boldsymbol{PTE_{XY} = H(Y_{t+\delta}|Y_t) - H(Y_{t+\delta}|Y_t, X)} \quad (1)$$

where PTE_{XY} is the PTE from source X to target signal Y. Shannon Entropy (H) is defines as:

$$\boldsymbol{H(Y_{t+\delta}) = -\sum_{i=0}^{n} p(Y_{t+\delta_i}) log p(Y_{t+\delta_i})} \quad (2)$$

where the summation is performed for discrete time steps $t+\delta_i$ (i=0, n), where n signifies the total number of time bins, defined by the product of the time interval duration (rest, or task period) in seconds and the data sampling frequency of 10.101 Hz. The delay between signal Y_t and $Y_{t+\delta_i}$ is expressed as δ_i. For a more complete description of how Shannon entropy is computed the reader is referred to relevant prior literature.[98, 106, 107]

Due to PTE_{XY} lacking a meaningful upper boundary and to reduce bias, a normalizing process is used:[98]

$$\boldsymbol{dPTE_{XY} = \frac{PTE_{XY}}{PTE_{XY}+PTE_{YX}}}. \quad (3)$$

With a range between 0 and 1, if $0.5 < dPTE_{XY} < 1$ the information flow is preferentially from X to Y. But, if $0 < dPTE_{XY} < 0.5$, then the information flow is preferentially from Y to X. In the event that $dPTE_{XY} = 0.5$, there is no preferential direction of information flow.[85, 98]

3.2.5 Data Processing Steps for dPTE

Directed PTE analysis was applied to calculate information flow for the endogenic, neurogenic, and myogenic frequency bands at three periods: 5 min of resting state, 0-10 min, and 11-20 min of the handgrip task. Directed PTE for resting state requires a minimum of 5 min to attain stable computed values[98] and in this work 10 min periods were used to account for the higher amount of hemodynamic variation during the handgrip paradigm.[97] Firstly, PTE analysis was performed to quantify causality between every two channels among all 111 channels. Then PTE values were normalized into dPTE values, generating a 111 x 111 matrix. The value at Xth row and Yth column determined the scale of information flow from Y to X. If dPTE was between 0 and < 0.5 the net information flow was from Y to X, whereas if dPTE > 0.5 the net flow was from X to Y. If dPTE was equal to 0.5, within a rounding error of two decimals, no net information flow was assumed. Then the dPTE was averaged lengthwise by row, yielding a 1 x 111 matrix, which was the mean dPTE between each one channel and all other channels.[85] The two channels with the highest ROI percentage overlap relative to neighboring ROIs, as determined by NIRS_SPM, were averaged together and assigned to each ROI, yielding a 1 x 11 matrix. The high signal variability induced during the task, as demonstrated in our previous work,[97] did not allow for identification of statistically significant changes in individual channels. Therefore, the dPTE channels were averaged from up to 11 channels to 2 per ROI in order to allow for comparisons between dPTE at rest and during the task that could lead to statistically significant differences . A one-sample t-test was then performed across subjects for significant differences in dPTE across all possible pairs of ROIs ($p < 0.05$ and false discovery rate

(FDR) corrected).[54] This test was used to determine significant net information flow into or out of each ROI by testing against the null hypothesis of no net flow, where positive t-values indicated outgoing net information flow ('source') and negative t-values indicated incoming net information flow ('sink'). Significant net information flow values for each ROI were visualized using BrainNet Viewer, an open-source software package,[55] for each frequency band at each period per subject group. Dedicated software (G * Power v3.0.10, Franz Fual, Kiel University, Kiel Germany) was used to perform *post hoc* statistical power (1-β) analysis.[108]

3.2.6 Directional Connectivity (DC)

The dPTE values were first averaged to a single channel within each of the ROIs, generating an 11 x 11 matrix. A one-sample t-test was then performed across subjects for significant differences in dPTE across all possible pairs of ROIs ($p < 0.05$ and FDR corrected).[54] This test was used to determine directionality of significant information flow between each pair of ROIs by testing against the null hypothesis of no net flow ($dPTE_{XY} = 0.5$), where positive t-values indicated net information flow from ROI_1 to ROI_2 and conversely for negative t-values. Topographic images for DC were generated using BrainNet Viewer software[55] for each frequency band at each period per subject group.

3.2.7 Static FC (SFC) and FC Variability (FCV) Analysis

For each subject's data set, a static functional connectivity (SFC) matrix was generated by computing the Pearson's correlation coefficient (r) between the ROI-averaged channels per brain hemisphere.[100, 101] Subsequently, dynamic functional connectivity (DFC) between pairs of ROIs was calculated using a sliding-window correlation (SWC).[100, 101, 109] In this study, a 60 s time window was selected and shifted in 1 s

increments along the entire time course as described in prior fNIRS studies.[101, 110, 111] The FC within each time window was also calculated for each pair of ROIs via the Pearson's correlation coefficient. Then the functional connectivity variability (FCV) was calculated as the standard deviation of the correlation coefficient along time.[100] For group analysis, the FCV of each correlation coefficient for each ROI was averaged across subjects in each group.

3.3 RESULTS

3.3.1 Relative Changes in MVC over time

The loss of handgrip force, expressed as the relative reduction in %MVC compared to the pre-task maximum value, was quantified as a proxy measure of fatigue. Force data was first averaged over 12 blocks for the 0-2 min period. An independent t-test, satisfying normality and equal variance assumptions, determined that there was no significant ($p > 0.05$) difference between groups (not shown), indicating subjects did not fatigue within this initial period. Force data were then averaged over 60 blocks resulting in two periods (0-10 min and 11-20 min) across the 120 contractions. As these data periods did not meet assumptions for independent t-tests, data was analyzed using the nonparametric Mann-Whitney U test.[58] The absolute force produced by active subjects was significantly higher than inactive subjects at 0-10 min ($p < 0.01$) and 11-20 min ($p < 0.001$). Lastly, %MVC force decreased significantly between periods in both active ($p < 0.001$) and inactive ($p < 0.01$) subjects.

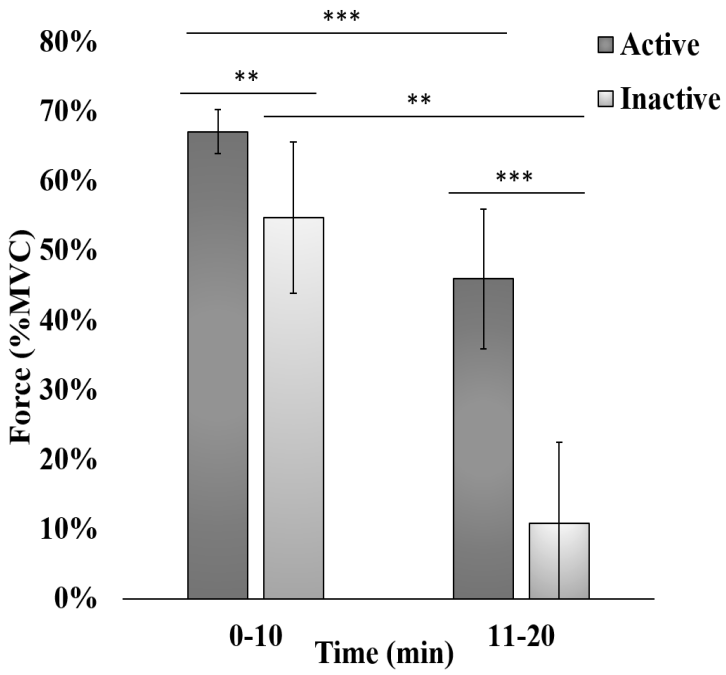

Figure 3 - 2 Force produced during intermittent handgrip contractions while physically inactive and active subjects attempted to attain 100% MVC. Each bar represents an average of 60 consecutive trials, expressed as the Mean (bar height) ± Standard Error to the Mean (SEM; error bar). **p < 0.01, ***p < 0.001.

3.3.2 Frequency Band Analysis with Information Flow and Directional Connectivity

The net information flow among the eleven ROIs (lPF, rFP, lDLPFC, rDLPFC, Broca's, lPMC, rPMC, lM1/S1, rM1/S1, lSAC, and rSAC) during the three task periods (rest, 0-10 min, and 11-20 min) was computed by dPTE analysis for the endogenic, neurogenic, and myogenic hemodynamic frequency bands and plotted in color-coded maps. In these maps, blue ROIs indicate net incoming information flow (the channels at those cortical locations are a 'sink') and red ROIs indicate net outgoing information flow (these channels are 'sources'). Green ROIs indicate no statistically significant net flow.

The directionality of information flow (DC) was averaged within each of the eleven ROIs, so as to enable averaged, region-specific dPTE values that were amenable to statistical comparisons. The latter yielded differing spatial DC patterns between inactive and active subjects that are presented here for each hemodynamic frequency band. The unidirectional arrows originate from a source ROI and end in a sink ROI. Black arrows correspond to a significance of $p < 0.05$ and red arrows denote a significance of $p < 0.01$.

All one-sample t-tests satisfied normality assumptions for dPTE and DC analyses. While physiological interferences were minimized using band-pass filters and PCA filter for each frequency band, global mean removal was also applied, and results were effectively indistinguishable between the methods. A *post hoc* power analysis with $\alpha = 0.05$ yielded a statistical power of 80% for both groups.

3.3.2.1 *Endogenic Frequency Band*

Maps of net information flow in the endogenic frequency band are shown in Figs. 3 - 3A - 3 - 3C (Figs. 3 - S1A - 3 - S1C for ΔHb) for inactive subjects and Figs. 3 - 3D -3 - 3F (Figs. 3 - S1D -3 - S1F for ΔHb) for active subjects. Outgoing information (sources) differed between the groups at all time periods. Inactive subjects had a statistically significant sink at lM1/S1, whereas active subjects had a dPTE sink at lFP at rest in the endogenic frequency band (Fig. 3 - 3A; Fig. 3 - 3D). For inactive subjects, rFP, lDLPFC, rDLPFC, and Broca's area were statistically significant sinks initially (Fig. 3 - 3B) that later became more strongly unilateral at rFP, rDLPFC, and rPMC as the task progressed (Fig. 3 - 3C). Additionally, inactive subjects had a statistically significant dPTE source at lPMC (Fig. 3 - 3C). In contrast, active subjects had a significant sink at

lDLPFC and rSAC initially (Fig. 3 - 3E) that changed to lFP, rFP, and rDLPFC as the task progressed(Fig. 3 - 3F).

In the endogenic frequency band, inactive subjects had notably more ROI pairs with significant DC than active subjects at rest (inactive: 6, active: 0), in the 0-10 min (inactive: 1, active: 0), and the 11-20 min intervals of the task (inactive: 8, active: 4) (Figs. 3 - 3G - 3 - 3L; Figs. 3 - S1G - 3 - S1L for ΔHb). During the task, inactive subjects initially had statistically significant DC form rPMC to Broca's area (Fig. 3 - 3H). However, as fatigue worsened in the second half of the task lM1/S1 became the primary functional area source connecting to bilateral FP, bilateral PFC, Broca's area, rPMC, and rSAC (Fig. 3 - 3I). Additionally, inactive subjects had two DC pairs in the 11-20 min period (lM1/S1 to rFP and lM1/S1 to rSAC) that had higher statistical significance ($p < 0.01$) (Fig. 3 - 3I).

In contrast, active subjects had an absence of significant net information flow between ROIs during rest and the 0-10 min periods (Fig. 3 - 3J -3 - 3K) and only exhibited significant net information flow between a few functional regions (from lPMC, rM1/S1, and rSAC to rDLPFC and rM1/S1 to lFP) in the 11-20 min period (Fig. 3 - 3L).

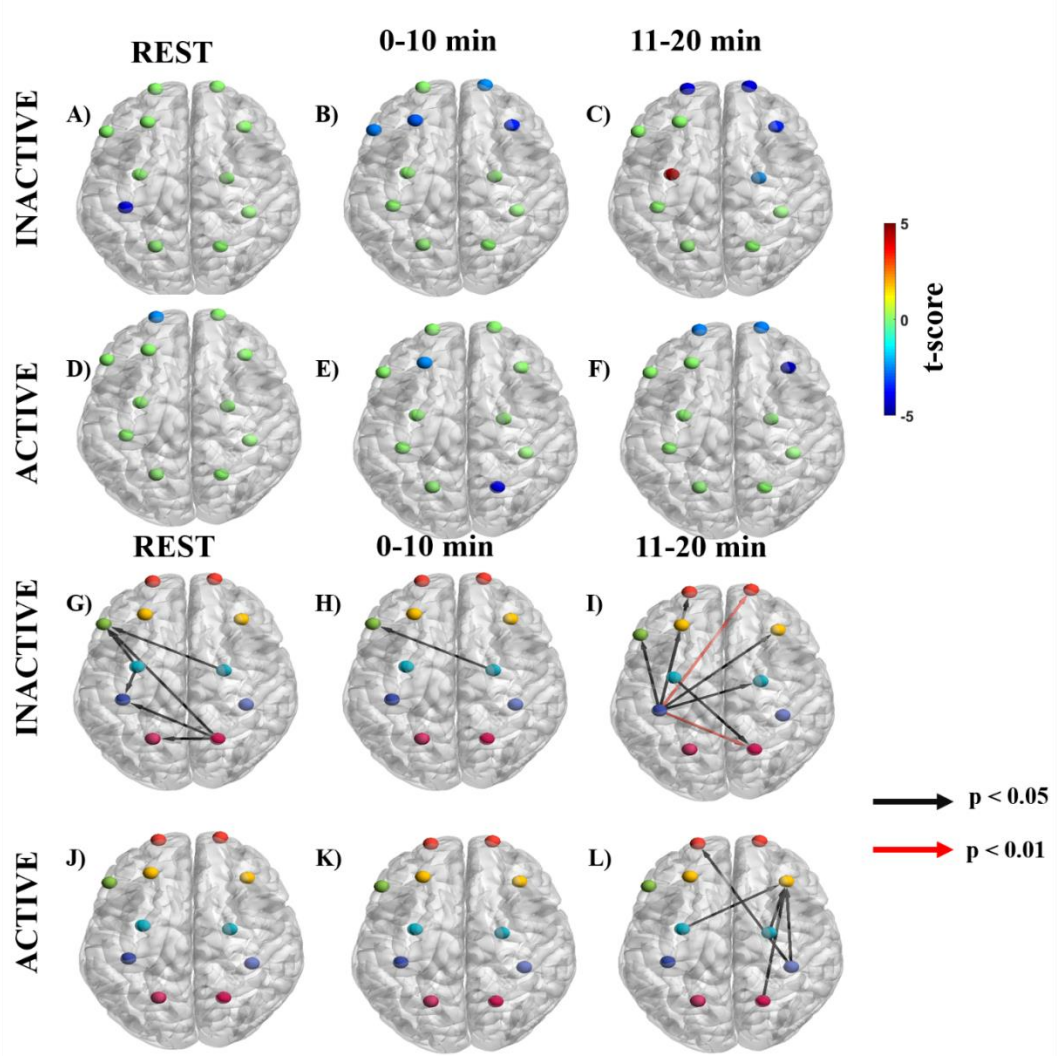

Figure 3 - 3 Significant dPTE and DC in the endogenic frequency band for inactive and active subjects during the handgrip task for ΔHbO. Directed PTE t-values for each ROI as a color-coded map for inactive subjects (A-C) and active subjects (D-F). Hot (yellow-reds) and cold (light blue-dark blue) colors indicate information outflow and inflow, respectively. Arrows indicate statistically significant information flow between functional regions for inactive (G-I) and active subjects (J-L). Black arrows ($p < 0.05$); Red arrows ($p < 0.01$). Eleven regions of interest (ROIs) were mapped: left and right frontopolar (lFP; rFP) (red), left and right pre-frontal cortex (lDLPFC; rDLPFC) (yellow), Broca's area (green), left and right pre-motor cortex (lPMC; rPMC) (light

blue), left and right primary motor and sensory cortical (lM1/S1; rM1/S1) areas (purple), and left and right sensory association cortex (lSAC; rSAC) (pink).

3.3.2.2 *Neurogenic Frequency Band*

Information flow in the neurogenic frequency band is shown in Figs. 3 - 4A - 3 - 4C (Figs. 3 - S2A -3 - S2C for ΔHb) for inactive subjects and Figs. 3 - 4D - 3 - 4F (Figs. 3 - S2D - 3 - S2F for ΔHb) for active subjects. At rest, inactive and active subject had dPTE sinks at the same ROIs, lFP and rFP (Fig. 3 - 4A; Fig. 3 - 4D). These dPTE sinks persisted during the handgrip task while the number of dPTE sources increased between the 0 -10 min and 11-20 min periods in both groups. In particular, inactive subjects had one dPTE source at rPMC in the first task period and none in the second period (Figs. 3 - 4B - 3 - 4C). For active subjects, there were two sources at rPMC and lM1/S1in the first period with two additional sources, at rDLPFC and lPMC, presenting in the second period (Figs. 3 - 4E -3 - 4F).

At the neurogenic frequency band, inactive subjects had more regions with significant net information flow than active subjects at resting state (inactive: 23, active: 10). However, active subjects had more significant regions with net information flow during the task at 0-10 min (inactive: 17, active: 25), and 11-20 min (inactive: 20, active: 26) (Figs. 3 - 4G - 3 - 4L; Figs. 3 - S2G - 3 - S2L ΔHb). Additionally, both groups had several directed connections with higher statistical significance ($p < 0.01$) at the first half (inactive: 7, active: 3) and the second half (inactive: 7, active: 5) of the task. All but one of these connections were directed to the FP regions bilaterally (Figs. 3 - 4G - 3 - 4L). At rest, inactive subjects had most ROIs connected to the FP regions bilateral (Fig. 3 - 4G) whereas, active subjects' statistically significant ROIs primarily connected to the lFP

(Fig. 3 - 4J). During the task, inactive subjects' significant directional connections were more unilateral, favoring the contralateral hemisphere and primarily directed to the FP regions bilaterally (Figs. 3 - 4H -3 - 4I). In contrast, active subjects had more bilateral connections which were largely directed to the rFP, lFP, lDLPFC, and Broca's area (Figs. 3 - 4K - 3 - 4L).

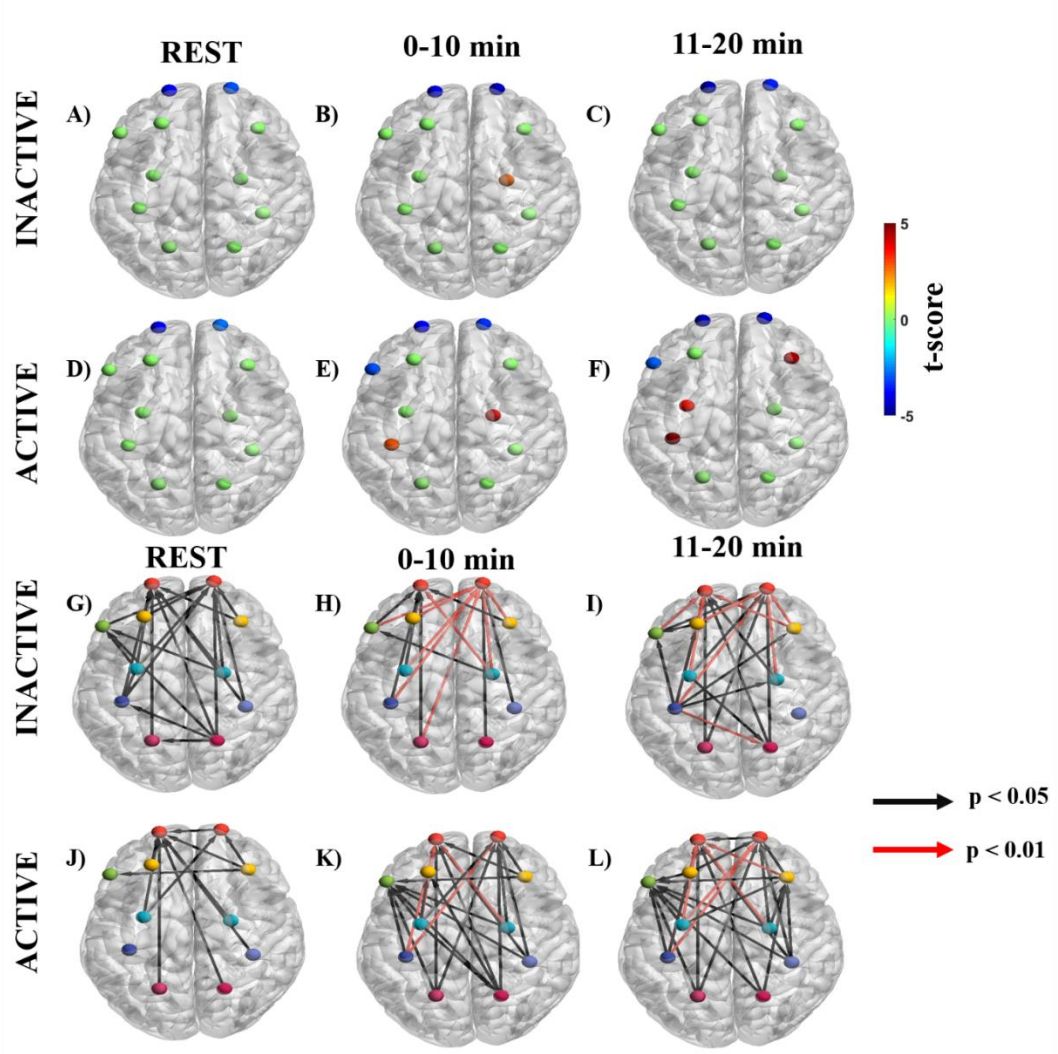

Figure 3 - 4 Significant dPTE and DC in the neurogenic frequency band for inactive and active subjects during the handgrip task for ΔHbO. Directed PTE t-values for each ROI as a color-coded map for inactive subjects (A-C) and active subjects (D-F). Hot (yellow-reds) and cold (light blue-dark blue) colors indicate information outflow and inflow, respectively. Arrows indicate statistically significant information flow between functional regions for inactive (G-I) and active subjects (J-L). Black arrows ($p < 0.05$); Red arrows ($p < 0.01$). Eleven regions of interest (ROIs) were mapped: left and right frontopolar (lFP; rFP) (red), left and right pre-frontal cortex (lDLPFC; rDLPFC) (yellow), Broca's area (green), left and right pre-motor cortex (lPMC; rPMC) (light blue), left and right primary motor and sensory cortical (lM1/S1; rM1/S1) areas (purple), and left and right sensory association cortex (lSAC; rSAC) (pink).

3.3.2.3 *Myogenic Frequency Band*

Information flow in the myogenic frequency band is shown in Figs. 3 - 5A -3 - 5C (Figs. 3 - S3A - 3 - S3C for ΔHb) for inactive subjects and Figs. 3 - 5D - 3 - 5F (Figs. 3 - S3D - 3 - 3F for ΔHb) for active subjects for each task period. Notably, the myogenic frequency had no significant sources for both groups (Fig. 3 - 5A -3 - 5F). At rest, both groups had significant sinks at lFP, rFP, and lM1/S1 (Fig. 3 - 5A; Fig. 3 - 5D). During the task, the number of ROIs with sinks increased from 9 to 10 in inactive subjects (Figs. 3 - 5B - 3 - 5C) and from 8 to 10 in active subjects (Figs. 3 - 5E - 3 - 5F).

At the myogenic frequency band, inactive subjects had more regions with significant net information flow than active subjects during the resting state (inactive: 21, active: 11), the 0-10 min (inactive: 5, active: 1), and the 11-20 min (inactive: 7, active: 1) task intervals (Figs. 3 - 5G -3 - 5L; Figs. 3 - S3G -3 - S3L for ΔHb) . During resting state, inactive subjects had five very significant ($p < 0.01$) directed connections originating from the rDLPFC, Broca's area, and rSAC, all ending at the FP regions bilaterally (Fig. 3 - 5G). In contrast, active subjects had only one very significant directed connection from rM1/S1 to lM1/S1 (Fig. 3 - 5J). During the task, inactive subjects initially had net information outflow from M1/S1 bilaterally (Fig. 3 - 5H); however, as the task progressed surrounding ROIs such as rDLPFC, and lSAC became information outflow sources directed at the lPMC and lM1/S1 (Fig. 3 - 5I). In contrast, active subjects demonstrated lM1/S1 as a net information outflow to lPMC during the first half of the task (Fig. 3 - 5K) but later transitioned as a net informational inflow from lSAC at the second half of the task (Fig. 3 - 5L).

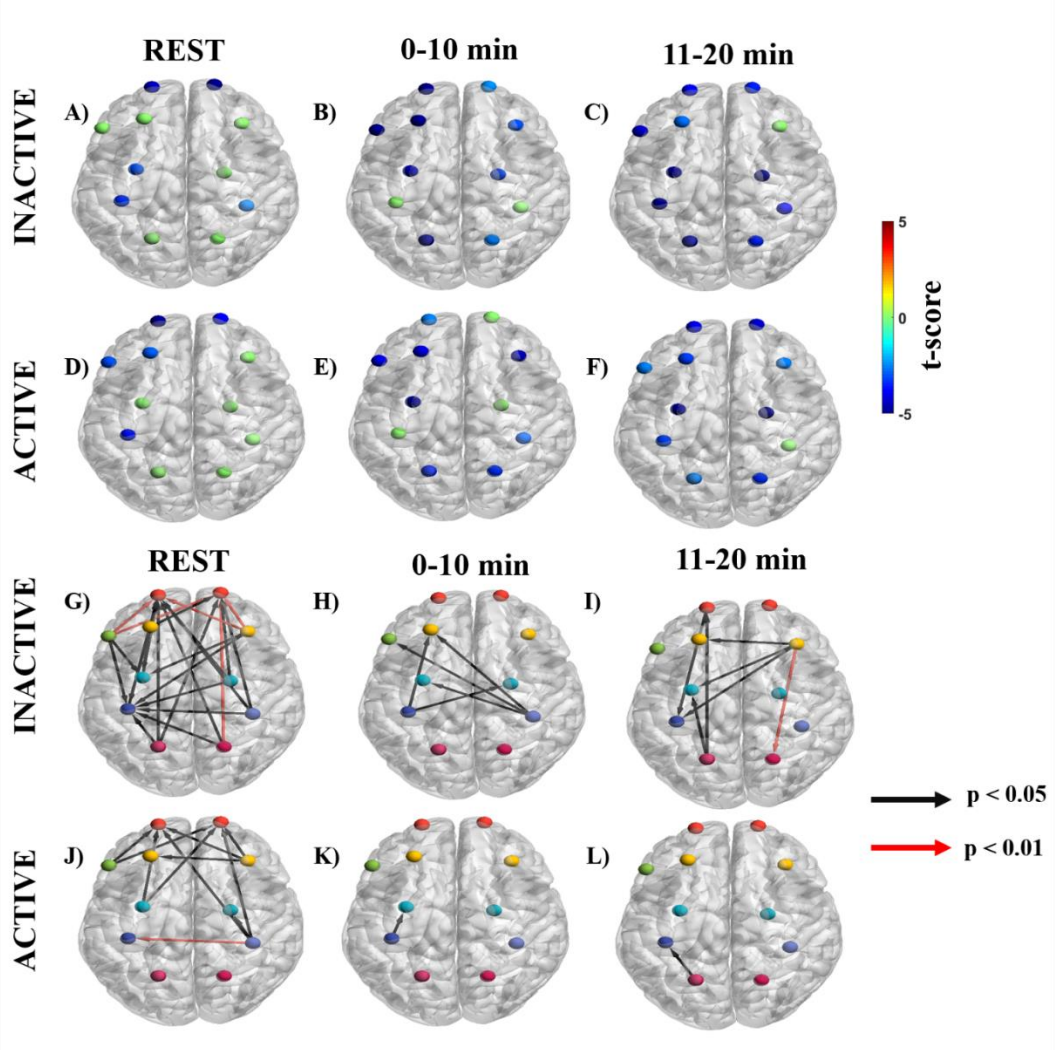

Figure 3 - 5 Significant dPTE and DC in the myogenic frequency band for inactive and active subjects during the handgrip task for ΔHbO. Directed PTE t-values for each ROI as a color-coded map for inactive subjects (A-C) and active subjects (D-F). Hot (yellow-reds) and cold (light blue-dark blue) colors indicate information outflow and inflow, respectively. Arrows indicate statistically significant information flow between functional regions for inactive (G-I) and active subjects (J-L). Black arrows ($p < 0.05$); Red arrows ($p < 0.01$). Eleven regions of interest (ROIs) were mapped: left and right frontopolar (lFP; rFP) (red), left and right pre-frontal cortex (lDLPFC; rDLPFC) (yellow), Broca's area (green), left and right pre-motor cortex (lPMC; rPMC) (light

blue), left and right primary motor and sensory cortical (lM1/S1; rM1/S1) areas (purple), and left and right sensory association cortex (lSAC; rSAC) (pink).

3.3.3 Correlations between SFC and FCV

Correlation patterns between SFC and FCV were also explored for each frequency band and subject group, before and during the handgrip task (Fig. 3 - 6). A representative pattern comparison between group-level SFC and FCV matrices and the resulting linear correlation plot are shown in Fig. 3 - 6A as an example of how the subsequent correlation plots were generated. Correlation plots for endogenic (top), neurogenic (middle), and myogenic (bottom) frequency bands are shown for inactive subjects in Fig. 3 - 6B and active subjects in Fig. 3 - 6C.

In the endogenic frequency band, quantitative correlation analysis revealed a strongly significant ($p < 0.001$) negative correlation between SFC and FCV at resting state and for the 11-20 min task interval for inactive subjects (Fig. 3 - 6B, top row). Similarly, strong negative correlations were found for all task periods for active subjects (Fig. 3 - 6C, top row). The correlation between SFC and FCV at 0-10 mins for inactive subjects was not significant but was marginally close to the significance criterion of $p = 0.05$ ($p = 0.07$).

Correlation analysis was significant ($p < 0.001$) in the neurogenic frequency band both for inactive (Fig. 3 - 6B, middle row) and active subjects at 0-10 min period only (Fig. 3 - 6C, middle row). Pearson's coefficient (r) values mostly indicated positive correlations, except for active subjects at resting state. Generally, the correlation trends were positive in contrast to the endogenic frequency band.

Quantitative correlation analysis at the myogenic frequency revealed significant ($p < 0.01$) negative correlation between SFC and FCV at 1-10 min and 11-20 min for inactive subjects (Fig. 3 - 6B, bottom row) and at the 1-10 min period for active subjects (Fig. 3 - 6C, bottom row). The correlation at the rest period for inactive subjects missed significance marginally ($p = 0.06$). The negative correlation trend in the myogenic frequency band was similar to that in the endogenic frequency band.

Overall, these plots illustrate a negative correlation trend in the endogenic and myogenic frequency bands and a positive correlation in the neurogenic frequency band, regardless of the physical activity levels of subjects. However, absolute z-values for inactive subjects were greater than active subjects for each frequency band, for both the positive and the negative trends, except for the 0-10 min and 11-20 min period in the endogenic frequency band.

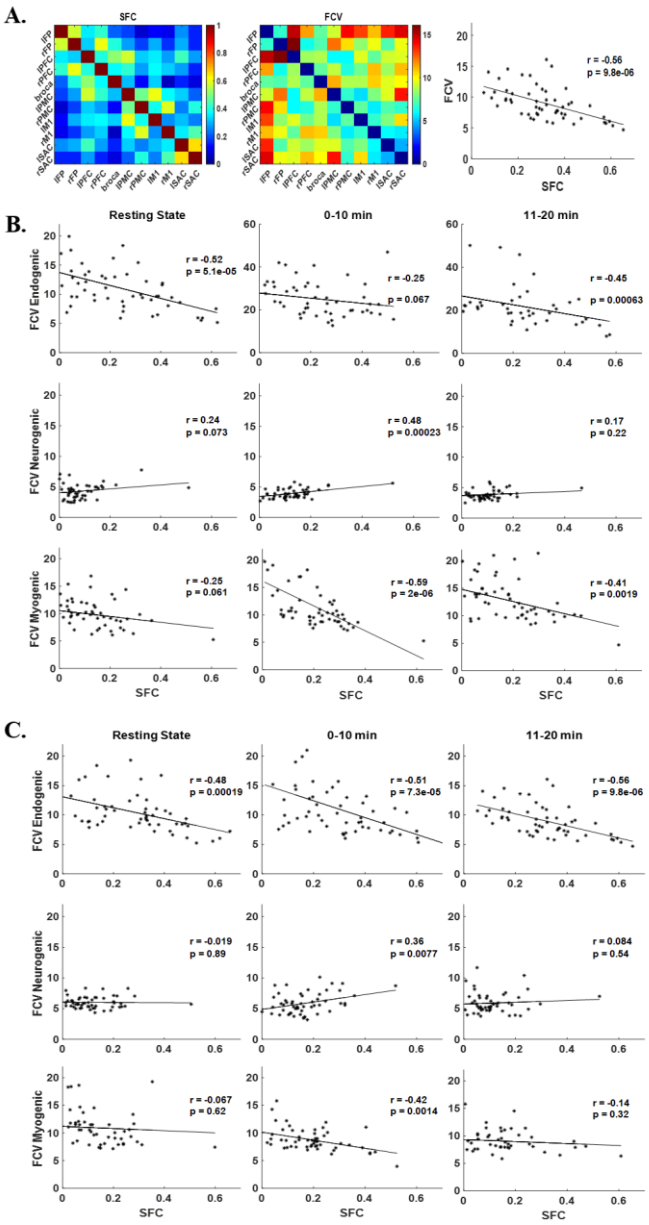

Figure 3 - 6 Pattern comparison between static functional connectivity (SFC) and functional connectivity variability (FCV) at endogenic, neurogenic, and myogenic frequencies for inactive and active subjects during the handgrip task. A) A representative example of the group-averaged SFC matrix (left), the FCV matrix (middle), and the linear relationship between them (right). B) Correlation plots between SFC and FCV for inactive subjects and C) active subjects at endogenic (top), neurogenic (middle), and myogenic (bottom) frequencies during resting state (left), 0-10 min (middle), and 11-20 mins (right) of the handgrip task.

3.4 DISCUSSION

Cerebral autoregulation is a multifactorial process of maintaining cerebral perfusion and brain tissue oxygenation against changes in arterial blood pressure that is challenged during exercise.[88] The brain maintains relatively constant regional CBF (rCBF) through coordinated effort of endogenic, neurogenic and myogenic mechanisms that are known to be active in different hemodynamic frequency bands.[86, 88-90] The correspondence of each of these physiological mechanisms to distinct hemodynamic frequency bands enabled us to examine in this work how different fNIRS metrics could provide information about the interplay of these neurovascular coupling mechanisms during a fatiguing handgrip task.

Firstly, patterns of net information flow quantified by total dPTE-per-ROI,[98] calculated as the sum of all pair-wise contributions to each ROI, revealed which ROIs contributed to regulation (information sources) versus which were being regulated (information sinks) during the handgrip task.[92] As the directionality of dominant contributions to net information flow is not evident in the total dPTE-per-ROI metric, the DC between ROIs was quantified also. The unidirectional connections indicate that one of the two ROIs serves as a functional source of coupling with a regulatory role over the connected sink region.[92] While results for ΔHbO only were discussed above in detail, the corresponding ΔHb results were examined as well (Supplementary Materials). In all, ΔHb signals yielded smaller dPTE values and fewer significant DC channel pairs due to smaller amplitudes and lower signal-to-noise ratio compared to ΔHbO signals, although the general trends were similar.

Furthermore, frequency band-based analyses were applied here to study the relationship between SFC, which measures coupling strength between ROIs and is known to increase with task performance,[8] and FCV, which reflects changes in spontaneous dynamic neural activity patterns between ROIs and relates to resource availability during demanding tasks.[100, 101] The relationship between SFC and FCV was studied here for each hemodynamic frequency band to help understand their interdependence in the context of maintaining handgrip performance in the presence of fatigue. The latter was evident in the decline in %MVC (Fig. 3 - 2) during a handgrip task. Our results showed differences between subject groups across all fNIRS metrics and hemodynamic frequency bands, suggesting that active subjects used different cortical activity strategies compared to inactive ones to maintain handgrip performance with increasing fatigue.

3.4.1 Endogenic Frequency Band

Subjects with different physical activity levels displayed different dPTE and DC patterns in the endogenic (0.003 - 0.02 Hz) frequency band (Fig. 3 - 3). Physical exercise increases CBF, as a result of elevated shear stress in the arterial walls which subsequently facilitates endogenic involvement in the regulation of rCBF.[112] The cerebrovascular endothelium releases vasoactive mediators, including nitric oxide (NO) and endothelium-derived hyperpolarizing factor, diffusing into vascular smooth muscle, which contribute to CBF regulation through vasodilation.[86, 90]

At rest, the dPTE and DC patterns together resemble the default mode network (DMN) for inactive subjects with either incoming (sinks) and outgoing (source) information flow at PMC, lM1/S1, Broca's area, and rSAC. The DMN is highly engaged during rest and is

involved in the emergence of spontaneous thought.[77, 113-115] The DMN has previously been observed in the endogenic frequency for dPTE analysis,[85] and endogenic frequency specific FC maps.[116] In this work active subjects did not exhibit any resting state dPTE network (indicating no net directional information flows) in the endogenic frequency band.

The handgrip task evoked significant dPTE and DC in the PFC and motor cortex in the endogenic frequency band, in particular for the inactive subjects. There was notable silencing of the ROIs associated with the DMN in dPTE and DC patterns once the task began, analogous to the DMN deactivation seen during tasks.[77] For inactive subjects, the initial connection was from lPMC to Broca's area. However, as fatigue increased the source became more unilateral in the left hemisphere at the motor cortex (lPMC and lM1/S1) and connected more to sinks in the PFC (FP and DLPFC). These observations suggest that motor regions (PMC and lM1/S1), which are involved in motor preparation and execution respectively,[65] regulated the DLPFC, which is associated with cognitive activity, planning, motivation during goal-driven tasks, and inhibiting/excitatory control during exercise.[65, 117, 118] Inactive subjects had notably more significant dPTE and DC than active subjects in the endogenic frequency band particularly during the first period. We speculate that active subjects had limited dPTE (lDLPFC and rSAC) and no significant DC until the second half of the task because regular exercise training enhances performance and the physically active subjects would presumably be more efficient earlier in the exercise task.

Strength of SFC is known to correlate with performance and increases with difficulty or effort in prior neuroimaging studies.[8, 9] On the other hand, FCV signifies a cortical region

that dynamically changes its connectivity strength with other regions so as to tap into more neuronal network resources while already established connections may fade in strength as fatigue sets in.[100] In the endogenic frequency, there is a negative correlation between SFC and FCV both for inactive (Fig. 3 - 6B, top row) and active subjects (Fig. 3 - 6C, top row). Several prior FCV studies have also found similarly negative correlations between these two metrics.[100, 101, 109] It has been suggested that task performance may depend on more stable (less variable) connectivity strength between regions involved in the regulation of the task.[100] The more significant r-value (which indicate less variable connectivity) and lower %MCV reduction seen in active subjects (higher performance) compared to inactive ones is consistent with this interpretation.

Overall, the endogenic frequency band may be related to fatigue levels, meaning that higher fatigue would result in more endogenic regulation. We speculate that active subjects likely did not experience as much fatigue as inactive ones, as suggested by Fig. 3 - 2, and supported by the difference in the amount of dPTE and DC between ROIs seen in Fig. 3 - 3F and Fig. 3 - 3L.

3.4.2 Neurogenic Frequency Band

Subjects with different physical activity levels displayed different dPTE and DC patterns in the neurogenic (0.02 - 0.04 Hz) frequency band. The neurogenic mechanism integrates the high metabolic demands of neuronal tissue during a task with the neurovascular unit (endothelial cells, perivascular nerves, and astrocytes abducted to cortical microvessels) to release vasoactive neurotransmitters as a means of regulating rCBF based on neuronal demands.[86, 90]

At rest, the dPTE and DC patterns together resemble the DMN and fronto-parietal network (FPN) for inactive and active subjects with either incoming (sinks) and outgoing (source) information flow at PMC and SAC, which integrates sensory information and forms connections between sensory and motor areas, for the DMN and FP and SAC for the FPN. The FPN is highly integrated with other brain networks, like the DMN and motor network (MN), and is involved in coordinating behavior in a rapid, accurate, and flexible goal-driven manner,[113, 115, 117] including planning of motor control.[77] Our FPN similarity findings are supported by a neuroimaging study indicating that endurance athletes had more significant FC in the FPN than non-athletes, although this fMRI study focused on a frequency range that mostly included the neurogenic frequency band.[77]

The handgrip task evoked significant dPTE and DC globally in the neurogenic frequency band for both active and inactive subjects. During the handgrip task, the FPN was still engaged as evident by dPTE and DC patterns. In FC studies, the FPN is known to activate during motor tasks, such as the fatiguing handgrip in this study,[97] to provide a functional back-bone for rapid and flexible modulation of other brain networks, such as the MN.[117] Inactive and active subjects also had similar, persistent dPTE and DC patterns during the handgrip task although, active subjects had more significant dPTE ROIs and DC connections. The neurogenic frequency band reflects the cortical resources available during the task, thus suggesting that active subjects have more cortical resources and exercise-altered neuroplasticity than inactive subjects.[1] Lastly, in the neurogenic frequency band, there were greater numbers of significant DC connections during the task than at rest, for all subjects, similar to prior neuroimaging studies.[3, 6, 9, 38, 46, 61, 62] During the handgrip task itself, the FP was a common functional

sink in all subjects, but active subjects also involved Broca's area. The FP region is associated with planning, cognitive branching, and monitoring importance of competing goal-driven tasks,[65, 117-119] and Broca's area is involved with producing language and inner speech.[69] The latter is likely related to the silent expression of conscious thought to oneself during handgrip task performance in our study. In our prior work, we demonstrated that active subjects reported utilizing self-talk to motivate themselves during the task.[97]

The neurogenic frequency band was the only frequency band to have a positive correlation between SFC and FCV for both inactive (Fig. 3 - 6B, middle row) and active (Fig. 3 - 6C, middle row) subjects. Prior neuroimaging studies also noted a positive correlation between exercise duration and increased hemodynamic signal variance,[6] and task performance and increasing neurogenic signal.[94] The non-significant r-value (which indicate more variable connectivity) and the %MCV reduction over time suggest that subjects were likely trying to tap into more cortical networks as they gradually fatigued. The significant r-values seen initially (0-10 min) in both groups support the notion that task performance may depend on more stable connectivity strength. As fatigue increased (11-20 min) both subject groups had more variable connectivity (i.e. non-significant r-value), possibly indicating an effort to recruit previously untapped cortical network resources.

Overall the neurogenic frequency band reflects the cortical resources available during the handgrip task.[120] Similar to FC, as physical effort for the task increased, the number of dPTE ROIs and DC connections increased as well before reducing again as fatigue increased. We hypothesize that active subjects had more dPTE ROIs and DC

connections than inactive ones because they could recruit more cortical network resources, as enabled by exercise-related neuroplasticity.

3.4.3 Myogenic Frequency Band

Subjects with different physical activity levels displayed different dPTE and DC patterns in the myogenic (0.04 – 0.15 Hz) frequency band. The myogenic regulatory mechanism plays an important role in stabilizing rCBF under differing physiological conditions, such as exercise.[90] Exercise causes increased blood pressure resulting in depolarization of smooth muscle cell membrane and calcium influx and initiating the myogenic response, resulting in smooth muscles constricting during increased pressure.[86, 90]

The resting state networks appeared to differ between inactive and active subjects in the myogenic frequency band based on dPTE and DC patterns. Inactive subjects' functional sinks at FP and most significant DC pair-wise connections (red arrows) resemble the FPN. As previously mentioned, the FPN is often interconnected with other resting state networks, such as the MN to facilitate motor task control.[117] In contrast, the active subjects' resting network was more reflective of the MN, with dPTE at M1/S1 and the most significant (red arrows) DC occurring between the M1/S1 areas as well as between the PMC areas bilaterally. The MN is a part of an extrinsic system of resting state networks that is typically driven by external sensory stimulation.[113] Active subjects appeared to have more active MN connectivity at rest than inactive subjects.

Inactive and active subjects also had different dPTE and DC patterns during the handgrip task in the myogenic frequency band. For inactive subjects, the lDLPFC was regulated by the M1/S1 during the first half (0-10 min). The M1/S1 sources are involved

in motor execution, in particular during hand movement, [8, 9, 46, 99, 121, 122] which we hypothesize is why the DC connections were directed towards these motor planning sink regions. The DC to lDLPFC is interesting due to its association with an approach reaction towards a goal,[68] such as maintaining task performance. As fatigued worsened for inactive subjects, the DC to lDLPFC was regulated by the rDLPFC instead that, especially during prolonged exercise, in known to purposely inhibit bodily afferences that arise with physical fatigue to preserve mental effort during exercise maintenance.[11, 40]

For active subjects, the lPMC was regulated by the lM1/S1 in the first half of the task. Like the inactive subjects, the lM1/S1 source is directed towards the motor planning associated PMC sink region. As fatigue worsened, the lM1/S1 became a net receiver of information by the lSAC source instead. Similarly, a prior EEG study demonstrated substantial location shifts of focal regions during a fatiguing handgrip task from anterior to posterior regions as a means to maintain task performance.[3]

Lastly, inactive subjects had nearly significant negative correlations between FCV and SFC at rest and significant negative correlations during the task (Fig. 3 - 6B, bottom row). Many FCV studies have found similarly negative correlations between these two metrics.[100, 101, 109] As previously mentioned, the significant r-values suggest that improved task performance requires less variable connectivity in the regulation of the task.[100] While active subjects also exhibited negative correlations between FCV and SFC, these were not significant except during 0-10 min. Active subjects likely experienced lower fatigue levels at 11-20 min, which could contribute to the non-

significant r-value (Fig. 3 - 6C, bottom row). Mayer waves could also possibly confound myogenic frequency band results due to their overlapping frequency at about 0.1 Hz.[123]

Overall the myogenic frequency band reflects the blood supply to the ROIs that is regulated by the arterioles.[90] We hypothesize that active subjects were able to dilate arterioles more efficiently,[124] and as a result they had improved blood supply to motor areas compared to inactive subjects. The increased availability of resources locally to the ROIs of active subjects controlling the motor task is a possible explanation for the lower number of DC pairs seen for this group relative to inactive subjects, whose ROIs had to recruit more resources from other locations while trying to maintain task performance.

3.5 LIMITATIONS

There are several limitations to this study that should be addressed. This study did not incorporate multimodal monitoring of systemic hemodynamics, such as heart rate, blood pressure, and respiration, which could be used as regressors to improve fNIRS signals as well as provide information of the systemic physiology itself.[84] An alternative method would be to employ short-distance channels (< 1 cm), which were not available in the commercial optode holder cap used, to remove by regression hemodynamic fluctuations that co-occur in the cortex as well as superficial scalp layers.[82, 84] Although we used bandpass filters and PCA to remove physiological inferences and global hemodynamic fluctuations, there exists several other different computational methods including i) independent component analysis, ii) singular value decomposition (SVD) and Gaussian kernel smoothing, iii) statistical correction methods, iv) wavelet-based methods, or v) a combination of these methods can be used for removal.[42, 84, 85, 125-127] Thus, a

quantitative comparison using different global component removal methods is warranted in future studies.

3.6 CONCLUSION

This study presents a direct comparison of differences in dynamic fNIRS metrics (dPTE, DC, SFC, FCV) between physically active and inactive subjects as they tried to maintain performance despite fatigue during a maximal effort task. The results of our study demonstrate how physical activity improves the neurovascular regulation mechanisms at the endogenic, neurogenic, and myogenic frequency bands. This modulation allowed for active subjects to maintain higher %MVC longer and delay fatigue onset. In future work we propose to expand these analyses to study subject populations of older age and impaired cardiovascular health.

Table 3 - S1 Spatial registration of fNIRS channel positions on a standard brain fMRI atlas. MNI coordinates displayed as mean (SD); r-right contralateral brain hemisphere; l- left ipsilateral brain hemispheres.

CHANNEL	***MNI***			***REGION OF INTEREST (ROI)***	**BRODMANN AREA (BA)**
	X	***Y***	***Z***		
1	-28.92(5.02)	66.44(1.93)	5.92(10.45)	lFP	BA10
2	-10.25(4.51)	71.27(2.29)	9.36(10.64)	lFP	BA10
3	15.74(2.76)	71.79(1.87)	9.95(11.07)	rFP	BA10
4	35.32(4.11)	64.89(2.91)	5.12(10.03)	rFP	BA10
5	-18.92(3.72)	68.30(2.73)	16.80(10.55)	lFP	BA10
7	24.85(3.94)	67.33(3.88)	17.24(9.80)	rFP	BA10
8	-10.14(3.90)	65.39(5.04)	28.02(10.45)	lFP	BA10
9	15.14(2.34)	65.50(5.42)	28.32(9.24)	rFP	BA10
10	-18.70(4.14)	58.42(6.75)	34.80(10.06)	lDLPFC	BA9
12	23.84(4.12)	57.20(7.52)	35.33(8.66)	rDLPFC	BA9
13	-44.86(4.27)	45.98(6.40)	22.55(9.36)	Broca's	BA44/45
14	-29.03(5.33)	49.56(8.06)	37.27(9.58)	lDLPFC	BA9
15	-9.38(2.74)	52.12(9.01)	46.03(8.77)	lDLPFC	BA9
16	14.47(2.39)	51.38(9.31)	46.27(8.47)	rDLPFC	BA9
17	33.59(4.55)	48.26(8.68)	37.98(7.90)	rDLPFC	BA9
18	48.38(3.69)	45.52(7.43)	22.92(8.17)	rDLPFC	BA9
19	-52.56(4.03)	33.44(7.80)	22.02(5.60)	Broca's	BA44/45
20	-39.89(4.55)	38.27(9.44)	39.21(9.17)	lDLPFC	BA9
21	-19.52(3.54)	40.94(10.90)	51.24(9.18)	lDLPFC	BA9
23	23.44(3.81)	40.15(10.54)	52.16(7.06)	rDLPFC	BA9
24	41.97(7.65)	36.82(9.38)	40.21(7.67)	rDLPFC	BA9
25	54.21(7.13)	32.68(8.64)	23.36(7.57)	Broca's	BA44/45
27	-58.54(3.43)	19.56(9.53)	21.71(7.33)	Broca's	BA44/45
28	-48.61(4.40)	25.98(9.87)	39.86(7.89)	Broca's	BA44/45
29	-31.88(5.64)	28.91(11.57)	53.58(8.18)	lDLPFC	BA9
32	33.44(6.50)	28.23(11.01)	54.55(5.99)	rDLPFC	BA9
33	50.08(5.45)	24.61(10.67)	41.23(6.81)	rDLPFC	BA9
38	-56.91(4.65)	10.29(11.67)	37.30(6.35)	lPMC	BA6
39	-42.89(4.48)	16.08(12.82)	5427(5.84)	lDLPFC	BA9
43	44.30(5.84)	14.72(13.02)	54.74(5.04)	rDLPFC	BA9
45	66.92(2.55)	1.39(9.31)	18.61(7.65)	rPMC	BA6
49	-51.35(4.99)	1.94(14.33)	52.29(4.78)	lPMC	BA6
50	-33.21(8.22)	5.89(15.35)	65.29(4.91)	lPMC	BA6
51	-13.64(4.83)	7.74(15.97)	71.09(6.52)	lPMC	BA6
52	13.56(6.13)	6.86(16.50)	72.09(4.26)	rPMC	BA6

54	53.55(5.44)	-1.08(13.36)	52.15(4.31)	rDLPFC	BA9
55	66.23(3.48)	-7.32(10.61)	34.15(5.19)	rPMC	BA6
60	-44.47(3.17)	-8.64(15.74)	61.53(3.68)	lPMC	BA6
61	-22.38(3.13)	-8.42(17.48)	73.18(2.64)	lPMC	BA6
63	23.73(2.47)	-9.14(16.25)	73.74(8.32)	rPMC	BA6
64	47.03(3.30)	-12.36(14.16)	62.18(2.84)	rPMC	BA6
65	63.67(2.77)	-19.62(11.49)	46(4.08)	rPMC	BA6
70	-54.95(2.56)	-26.30(14.18)	55.56(3.49)	lS1	BA1/2/3
71	-35.54(2.76)	-23.18(16.20)	70.86(2.40)	lM1	BA4
72	-13.97(1.75)	-20.91(16.47)	77.76(1.37)	lM1	BA4
73	14.26(1.47)	-21.55(15.61)	77.77(0.88)	rPMC	BA6
74	36.65(3.68)	-23.80(17.56)	71.47(1.44)	rM1	BA4
75	56.12(457)	-29.95(12.78)	56.02(2.95)	rS1	BA1/2/3
76	67.41(3.16)	-49.94(63.79)	38.03(5.91)	lS1	BA1/2/3
81	-46.74(3.49)	-37.18(14.07)	63.06(4.34)	lS1	BA1/2/3
82	-23.38(5.10)	-36.33(15.76)	74.06(3.00)	lM1	BA4
84	24.74(3.07)	-37.65(14.31)	73.61(6.53)	rM1	BA4
85	47.24(5.01)	-39.26(13.27)	62.92(3.91)	rS1	BA1/2/3
95	34.62(4.74)	-53.02(11.79)	67.73(5.53)	rS1	BA1/2/3
101	-24.77(3.71)	-63.60(10.99)	66.97(8.40)	lSAC	BA7
103	25.09(3.98)	-63.61(10.25)	65.98(11.02)	rSAC	BA7
107	-36.12(5.15)	-74.42(9.73)	51.08(10.61)	lSAC	BA7
108	-16.06(2.76)	-72.80(18.20)	60 (11.26)	lSAC	BA7
109	14.91(4.26)	-75.30(8.57)	60.33(11.14)	rSAC	BA7
110	33.50(5.72)	-72.80(17.21)	51.23(9.97)	rSAC	BA7

Table 3 - S2 Preprocessing input parameters used in Homer2.

Function	Input parameters	
hmrIntensity2OD		
enPCAFilter	nSV = 2	
hmrBandPassFilt	Endogenic	hpf = 0.003 lpf = 0.02
	Neurogenic	hpf = 0.02 lpf = 0.04
	Myogenic	hpf = 0.04 lpf = 0.15
hmrOD2Conc	6 6 6	

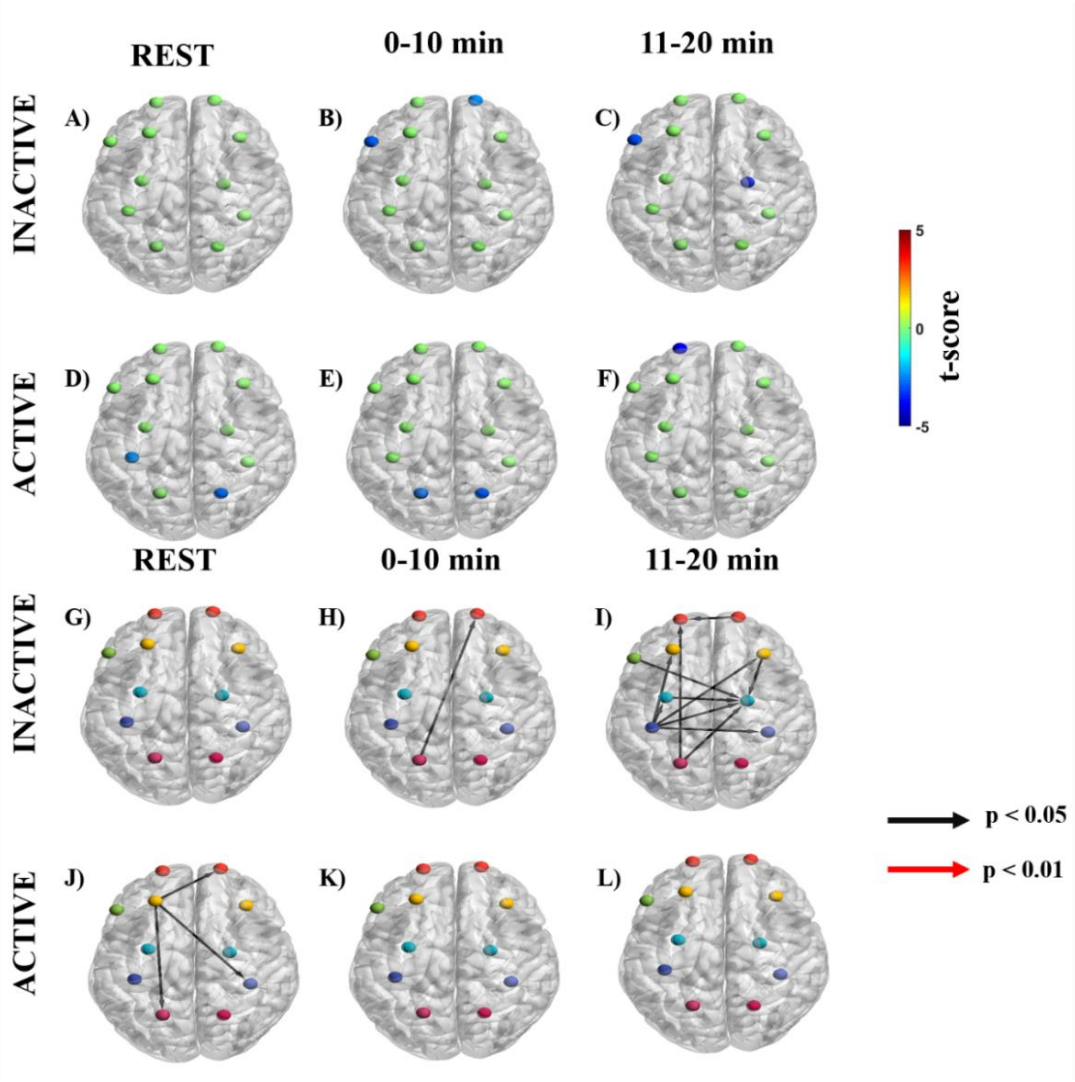

Figure 3 - S1 Significant dPTE and DC in the endogenic frequency band for inactive and active subjects during the handgrip task for ΔHb. Directed PTE t-values for each ROI as a color-coded map for inactive subjects (A-C) and active subjects (D-F). Hot (yellow-reds) and cold (light blue-dark blue) colors indicate information outflow and inflow, respectively. Arrows indicate statistically significant information flow between functional regions for inactive (G-I) and active subjects (J-L). Black arrows ($p < 0.05$); Red arrows ($p < 0.01$). Eleven regions of interest (ROIs) were mapped: left and right frontopolar (lFP; rFP) (red), left and right pre-frontal cortex (lDLPFC; rDLPFC) (yellow), Broca's area (green), left and right pre-motor cortex (lPMC; rPMC) (light blue), left and right primary motor and sensory cortical (lM1/S1; rM1/S1) areas (purple), and left and right sensory association cortex (lSAC; rSAC) (pink).

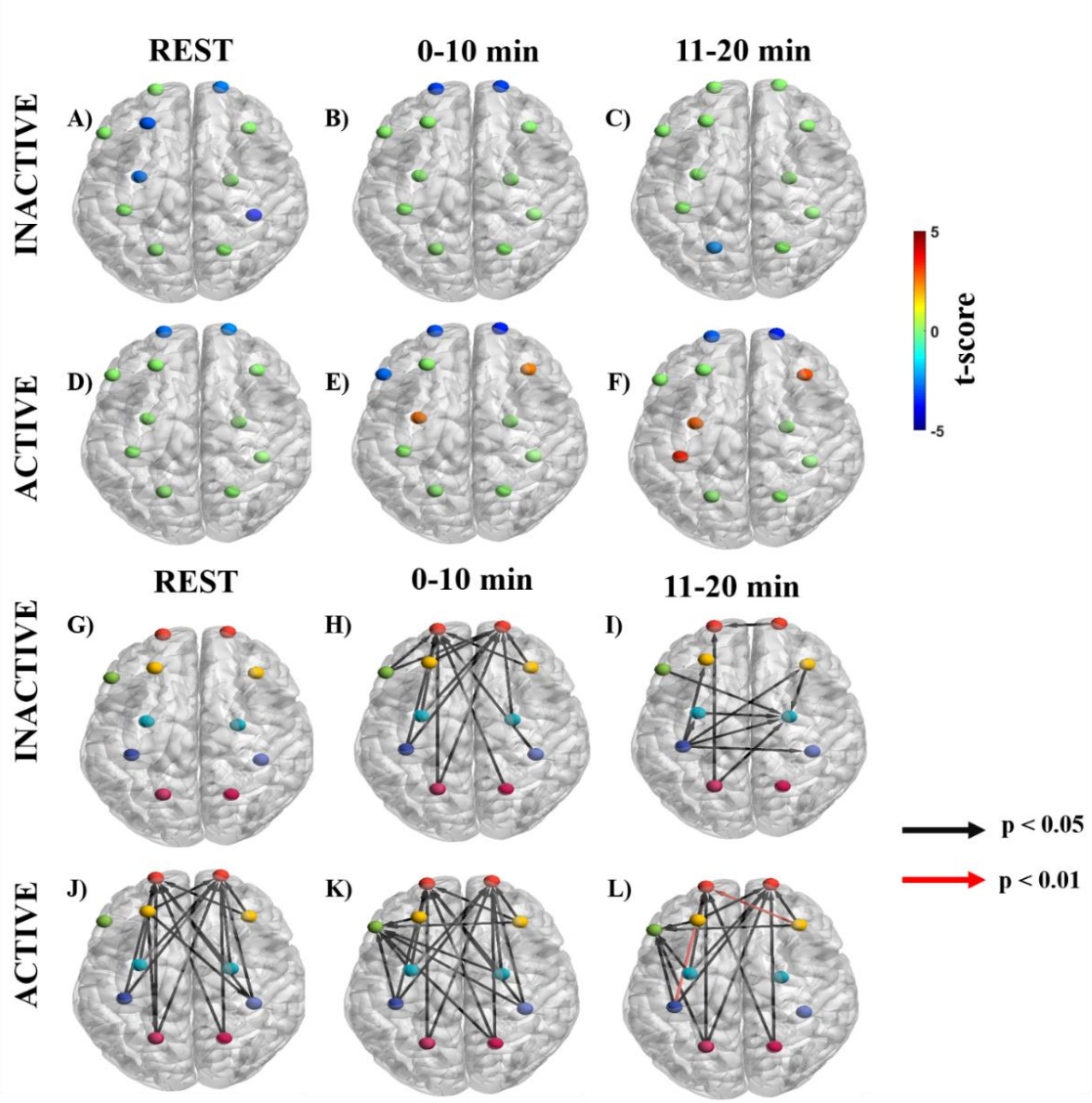

Figure 3 - S2 Significant dPTE and DC in the neurogenic frequency band for inactive and active subjects during the handgrip task for ΔHb. Directed PTE t-values for each ROI as a color-coded map for inactive subjects (A-C) and active subjects (D-F). Hot (yellow-reds) and cold (light blue-dark blue) colors indicate information outflow and inflow, respectively. Arrows indicate statistically significant information flow between functional regions for inactive (G-I) and active subjects (J-L). Black arrows ($p < 0.05$); Red arrows ($p < 0.01$). Eleven regions of interest (ROIs) were mapped: left and right frontopolar (lFP; rFP) (red), left and right pre-frontal cortex (lDLPFC; rDLPFC) (yellow), Broca's area (green), left and right pre-motor cortex (lPMC; rPMC) (light blue), left and right primary motor and sensory cortical (lM1/S1; rM1/S1) areas (purple), and left and right sensory association cortex (lSAC; rSAC) (pink).

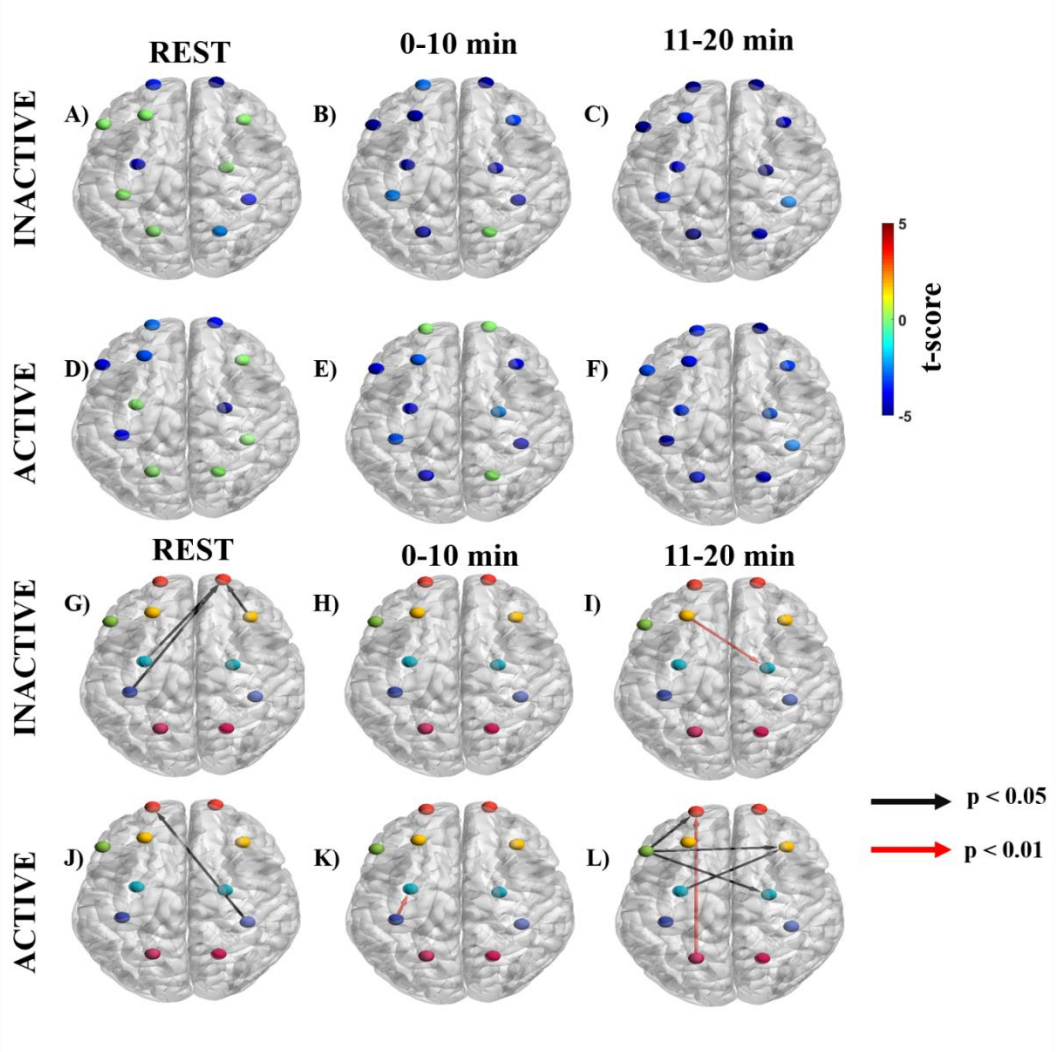

Figure 3 - S3 Significant dPTE and DC in the myogenic frequency band for inactive and active subjects during the handgrip task for ΔHb. Directed PTE t-values for each ROI as a color-coded map for inactive subjects (A-C) and active subjects (D-F). Hot (yellow-reds) and cold (light blue-dark blue) colors indicate information outflow and inflow, respectively. Arrows indicate statistically significant information flow between functional regions for inactive (G-I) and active subjects (J-L). Black arrows ($p < 0.05$); Red arrows ($p < 0.01$). Eleven regions of interest (ROIs) were mapped: left and right frontopolar (lFP; rFP) (red), left and right pre-frontal cortex (lDLPFC; rDLPFC) (yellow), Broca's area (green), left and right pre-motor cortex (lPMC; rPMC) (light blue), left and right primary motor and sensory cortical (lM1/S1; rM1/S1) areas (purple), and left and right sensory association cortex (lSAC; rSAC) (pink).

CHAPTER 4

Transcranial photobiomodulation induced changes in functional connectivity and brain network topography mapped by functional near-infrared spectroscopy (fNIRS)

This Chapter is a manuscript has been submitted

Authors: Elizabeth L. Urquhart, Hashini Wanniarachchi, Xinlong Wang, George Alexandrakis, Hanli Liu

4.1. INTRODUCTION

Photobiomodulation (PBM) entails the application of low-power, high-fluence light in the red to near-infrared (NIR) range (usually between 630-1100 nm) to modulate mitochondrial respiration in a non-destructive and non-thermal manner. Transcranial PBM (tPBM) refers to PBM directed at the cerebral cortex with the purpose of enhancing cerebral oxygenation and cognitive function.[128-133] Approximately 1-2% of NIR light between 660-940 nm penetrates through various layers of the human scalp and skull and reaches the cerebral cortex, several centimeters below the scalp's surface.[16, 17] The purported mechanism of PBM relies on photon absorption by cytochrome-c-oxidase (CCO), which is the terminal enzyme in the mitochondrial respiratory chain that is necessary in cerebral oxygen utilization for energy metabolism. As CCO activity increases, the more oxygen consumption and simultaneous metabolic energy are produced via mitochondrial oxidative phosphorylation.[130, 131, 133] The resulting increase in CCO activity leads to metabolic and hemodynamic alterations in the brain

that can facilitate neuroprotection and cognitive enhancements.[134] In several reviews by Hamblin,[14, 133] use of tPBM by various groups was reported as a possible intervention for acute and chronic stroke, traumatic brain injury, Alzheimer's disease, Parkinson's disease, depression, anxiety, and cognitive enhancement.

Several neuroimaging modalities have been used for functional brain mapping concurrently with tPBM administration such as electroencephalography (EEG), single photon emission computed tomography (SPECT), and functional near-infrared spectroscopy (fNIRS).[13, 18, 33, 135] Among them, fNIRS measures noninvasively concentration changes of oxyhemoglobin (ΔHbO) and deoxyhemoglobin (ΔHb) resulting from neurovascular coupling secondary to neuronal activation. Both fNIRS and the tPBM laser use light in the NIR range and thus share similar optical path trajectories through the tissue. Thus, fNIRS is a suitable tool for *in vivo* study of tPBM. Of the few fNIRS studies with concurrent tPBM administration reported to date, the number of fNIRS channels used was limited ($\leq$ 20) and only provided mapping of cerebral hemodynamics over the prefrontal cortex.[18, 33]

Prior fNIRS studies have demonstrated its reliability and popularity by researchers to investigate resting state functional connectivity (FC) based on Pearson's correlation coefficients (PCC) or graph theory analysis (GTA).[47, 111, 136-138] PCC quantifies temporal cross correlations between any available pair of spatially remote cortical/brain regions,[47, 114] while GTA presents the brain as a graphical networking system characterized with topological properties for global and local brain networks among brain regions. Neuroimaging studies under resting and/or task-based states have taken FC as an index to describe the relationship between hemodynamic activation patterns

of different brain regions and thus to reflect the level of functional communication between them.[8, 9, 77, 97, 114] On the other hand, GTA-derived graphical metrics can be used to compute alternate measures of statistically significant connectivity strength as another FC analysis approach.[7, 139] In particular, GTA features small-world networks that quantify the communication efficiency between nodes of the networks, where nodes can be defined as fNIRS channels or groups of channels clustered within functionally distinct brain regions.[140-142] GTA has been applied for the assessment of small-world properties in prior neuroimaging studies during resting state and task-based studies. However, no study to date has explored the effect of tPBM on small-world network properties although such analyses have been applied to other paradigms.[111, 136-138, 143, 144]

In this work, we utilized a 111-channel fNIRS system with a large field of view for the first-time to quantify changes in 1) FC pair-wise patterns and 2) brain network topographical metrics induced by tPBM on healthy adult subjects. The tPBM was directed to the right prefrontal cortex (rPFC), encompassing the right frontal polar (rFP) and right dorsolateral prefrontal cortex (rDLPFC). It is known from our prior studies that tPBM induces significant increases of ΔHbO in the PFC during and after tPBM delivery on the right forehead of human participants.[18, 33, 132] Moreover, a recent fNIRS study demonstrated that high-definition transcranial direct current stimulation (HD-tDCS) increases FC strength and small-world metrics during and after the stimulation using both PCC and GTA methods.[138] The focus of this study was to examine tPBM-evoked changes of FC pairwise and network patterns during and after tPBM based on 111-channel ΔHbO time series. Taking all aspects considered, we hypothesized that the

application of tPBM would increase cortex-wide FC strength relative to the stimulation site and enhance GTA-derived small-world metrics, despite different neuromodulation mechanisms between tPBM and HD-tDCS. If the hypothesis is proven true, this study will strongly support the possibility of using tPBM as an alternate neuromodulation intervention for future biomedical applications.

4.2. MATERIALS AND METHODS

4.2.1 Participants

Nineteen adults (5 females, age = 31.7 $\pm$ 9.5 years) were recruited for this study. All subjects were without any neurological or psychiatric disorders (self-reported). All experimental procedures, including a written consent required prior to participation in this study, were approved by the Institutional Review Board of the University of Texas at Arlington (IRB# 2017-0859).

4.2.2 Experimental instruments and procedures

A continuous wave (CW) fNIRS system (OMM-3000, Shimadzu Corp., Kyoto, Japan) was used in this study to measure cerebral hemodynamic responses with near infrared light diode sources (780, 805, and 830 nm) and photomultiplier detectors at a sampling frequency of 10.1 Hz. The optode geometry consisted of 32 sources and 34 detectors with a separation of 3 cm resulting in 111 source-detector channels (Fig. 4 - 1A). Anatomical cranial reference points (nasion, inion, left and right preauricular points and vertex) and optode locations were recorded for each subject using a 3D digitizer (FASTRAK, Polhemus VT, USA). Montreal Neurological Institute (MNI) coordinates for each source and detector location were calculated using the statistical parametric

mapping NIRS_SPM software, which provided the Brodmann area corresponding to each fNIRS channel.[45] All subjects' MNI coordinates were subsequently averaged together. Thus, the 111 channels covered cortical areas of the following 12 regions of interest (ROIs): left and right frontopolar prefrontal cortex (lFP; rFP), left and right dorsolateral prefrontal cortex (lDLPFC; rDLPFC), Broca's area, left and right premotor cortex (lPMC; rPMC), left and right primary motor and somatosensory cortical (lM1/S1; rM1/S1) areas, Wernicke's area, and left and right somatosensory association cortex (lSAC; rSAC). These 12 regions served as clusters for FC analyses in the following sections.

Transcranial PBM was administered using an FDA-cleared 1064-nm, CW laser (Model CG-5000 Laser, Cell Gen Therapeutics, Dallas, Texas) (Fig. 4 - 1B). The laser's aperture delivered a well-collimated beam with an area of 13.6 cm^2 at a maximum power of 3.5 W and a laser power density of 0.25 W/cm^2.[130, 132] The tPBM was applied by noncontact delivery to the right forehead of each subject at a frontal site (near Fp2 location of the international 10 – 10 EEG system). Subjects and experimental operators wore laser protection goggles through the duration of the experiment.

Subjects participated in two sessions that were randomized for tPBM or placebo treatments. If the tPBM session was first, there was a waiting period of at least one week for the placebo treatment to avoid any carry-over effect. During the stimulation period, the CW laser was administered on the right forehead with an output of 3.5 W, whereas placebo had negligible laser output by turning the laser on and then off immediately within 3 seconds. Subjects sat with their eyes closed for 8 minutes of pre-

placebo/tPBM period, 8 minutes during placebo/tPBM period, and 4 minutes of post-placebo/tPBM period (Fig. 4 - 1C).

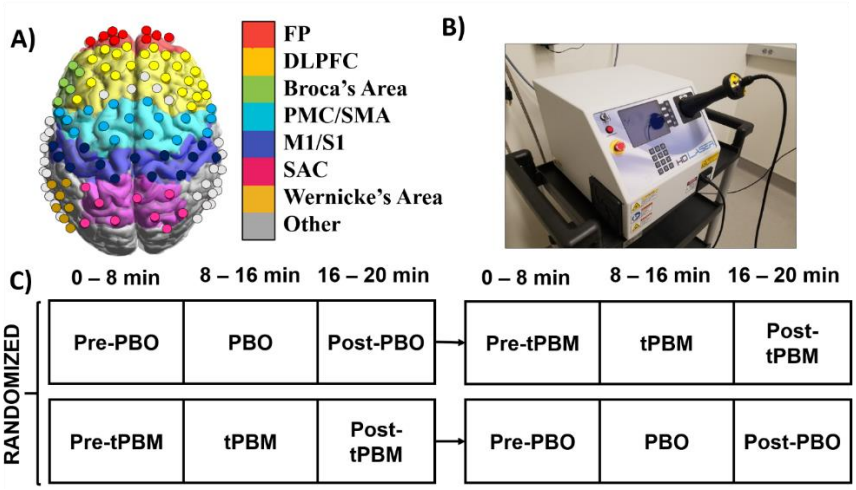

Figure 4 - 1. Experimental set-up and protocol. A) 111-channel layout with twelve regions of interest covered by the optode geometry: frontopolar (FP) (red), dorsolateral prefrontal cortex (DLPFC) (yellow), Broca's area (green), premotor cortex (PMC) (light blue), primary motor and somatosensory cortical (M1/S1) areas (dark blue), somatosensory association cortex (SAC) (pink), and Wernicke's Area (gold). B) 1064-nm laser. C) The experimental protocol randomized placebo (PBO) and tPBM treatment for subjects. For the protocol, there was a period of at least one week between the two experiments to avoid any carry-over effect.

4.2.3 Data preprocessing

FNIRS data were preprocessed using Matlab 2012b (MathWorks, Natick, MA, USA) and the open-source package Homer 2.0.[42] FNIRS data were detrended based on the baseline by a linear least-squares fit that was subtracted from the data.[47] The raw intensity data were then low-pass filtered using a 3rd order Butterworth filter at a cut-off frequency of 0.2 Hz to remove large portions of physiological noise, including heartbeat (1-1.5 Hz) and respiration (0.2-0.5 Hz).[35] Principal component analysis was utilized to

remove motion artifacts and global hemodynamic fluctuations that may overlap with hemodynamic response frequencies. The first two principal components were removed from all fNIRS channel data in order to remove these global artifacts.[35, 42] Channels located near the branches from the middle cerebral artery or the superficial temporal artery and temporal muscle were removed to avoid signal contamination. [103, 104] These removed channels are shown in gray in Fig. 4 - 1A. Optical density data were converted into changes in hemoglobin concentration relative to baseline (ΔHbO) using the Modified Beer-Lambert Law with an estimated differential pathlength factor of 6.0 for each wavelength, an estimate used in Homer 2.0.[49] Only ΔHbO values were presented in the Results section below because ΔHb values were found to have similar and opposite qualitative trends, but with smaller amplitudes and lower signal-to-noise ratio as previously reported in other neuroimaging studies.[9, 52, 53]

4.2.4 Cross correlation analysis to quantify functional connectivity

Functional connectivity (FC) was calculated for each period: pre-placebo/tPBM, placebo/tPBM, and post-placebo/tPBM. Whole-head PCC was performed by calculating the Pearson correlation values between each pair of all 111 channels, thus yielding an 111 x 111 matrix per period.[47] Pearson R values were then converted into Fisher's z-scores. Paired t-tests were performed on the z-transformed R values across subjects. False discovery rate (FDR) was employed for multiple comparisons correction with q = 0.05 and α = 0.05 with only significant results shown.[54] Only significant connections to the rPFC were displayed in topographic images that were generated using BrainNet Viewer, an open-source Matlab package.[55]

4.2.5 Graph theory analysis to determine topographical network metrics

Graph theory analysis (GTA) was applied to investigate tPBM-induced changes in global topological network organization derived from the fNIRS measurements of the whole head. In the analysis, channels were considered nodes and connections between channels were considered edges of the network. The FC matrix was then thresholded into a binary matrix in terms of sparsity (S), the number of current existing edges divided by the total possible number of edges in the current matrix.[136, 143, 145] In this study, we selected and quantified seven topological properties/metrics to study network patterns with a range of S level (S; 0.05 < S < 0.50; increment = 0.05). Five small-world property metrics were calculated including: clustering coefficient (C_p), characteristic path length (L_p), normalized clustering coefficient (γ), normalized characterized path length (λ), and small-worldness (σ).

C_p is the average of the clustering coefficients of all nodes. C_p is a measure of network segregation by signifying the likelihood that two nodes significantly connected to a third node are also significantly connected to each other, thus forming a connected triangular cluster. $C_p(i)$ of a certain node *i* is defined as the following:[142]

$$C_p(i) = \frac{2N_i}{k_{node}(i)[k_{node}(i) - 1]}$$

where N_i denotes the number of existing connections among the neighbors of node *i*, and k_{node} is the number of edges that are connected to node *i*.

Characteristic path length, L_p, is the average of the shortest pathlength between all pairs of nodes:[142]

$$L_p = \frac{1}{N(N-1)} \sum_{i \neq j \in G} d_{ij}$$

where N is the total node number, and d_{ij} is the shortest path length between node *i* and node *j*. Longer L_p values indicate weaker connections.[146]

Normalized clustering coefficient, γ, is the mean of all clustering coefficients over all nodes in a network:[140, 142]

$$\gamma = C_p^{real}/C_p^{random}$$

where C_p^{real} is the average of clustering coefficients over all nodes in a network, quantifying the extent of local group formation within a network. C_p^{random} is the mean cluster coefficient of matched random networks that preserve the same number of nodes, edges, and degree distribution as the real network.[147]

Normalized characteristic path length, λ, is the average of the shortest path lengths between any nodes of the networks and is defined as:[140, 142]

$$\lambda = L_p^{real}/L_p^{random}$$

where $L_p^{real}$is the average of the shortest path lengths between any pair of nodes in the network, quantifying the capability of parallel information propagation within a network. L_p^{random} is the mean characteristic path length of matched random networks that preserve the same number of nodes, edges, and degree distribution as the real network [147].

A small-world (σ) is defined as:[140, 142]

$$\sigma = \gamma/\lambda$$

Where a real network is considered small-world (σ) if $\lambda \approx 1, \gamma > 1$, and $\sigma > 1$. It is also characterized by a high C_p and low L_p.[136, 139, 146]

Two additional parameters were quantified to measure the efficiency of small-world networks, namely global efficiency (E_g) and local efficiency (E_{loc}). They are defined as:[140]

$$E_g = \frac{1}{N(N-1)} \sum_{i \neq j \in G} \frac{1}{d_{ij}} \quad (1)$$

$$E_{loc} = \frac{1}{N(N-1)} \sum_{i \in G} E(G_i) \quad (2)$$

where N is the total node number, d_{ij} is the shortest path length between node *i* and node *j*, and $E(G_i)$ is the global efficiency of the subgraph composed of the nearest neighbors of node *i*. E_g describes the efficiency of a parallel information transfer in the network, whereas E_{loc} describes how efficient the communication is between the first neighbors of *i* when *i* is removed.[140]

All global metrics were calculated for each subject at each period (i.e., pre-, during, and post-tPBM) for each stimulation type (placebo/tPBM) using GRETNA.[148] For the stimulation period, GTA metrics were only quantified for the last half period of tPBM (i.e., 5-8 min) to optimally observe its effects since tPBM has shown gradual alterations in cerebral hemodynamics and electrophysiology.[13, 132, 149] Paired t-tests were used to test statistical ($p < 0.05$) differences for each global metric between placebo and tPBM interventions for each period. Each global metric was compared at each S level, $0.05 < S < 0.50$ at 0.05 increments. All statistical assumptions were verified, including normality.

4.3. RESULTS

4.3.1 Functional connectivity to the right prefrontal cortex derived with PCC

Functional connectivity (FC) was quantified between all channels within the rPFC to every other channel on the cortex (Fig. 4 - 2), based on PCC. Channels within the rPFC were chosen due to its proximity to the stimulation site during tPBM exposure. Two types of comparisons were made to show difference effects in FC (1) between tPBM and placebo treatments (during all three periods) and (2) between tPBM and post-tPBM under the true stimulation.

For the 1st comparison, during the pre-stimulation period, there were no significant ($p > 0.05$) differences between tPBM and placebo. During the 8-min stimulation period, tPBM reduced FC with respect to the placebo treatment, as indicated by the blue lines in Fig. 4 - 2A. There were 5 significant ($p < 0.05$) connections in total to the rPFC: rFP to lFP (1 connection), rFP to rDLPFC (2), rDLPFC to lFP (1), and rDLPFC to l PMC/SMA (1). In contrast, during the 4-min post-stimulation period, there was greater FC strength across multiple cortical regions (or clusters) induced by tPBM treatment with respect to the placebo as marked by the red lines in Fig. 4 - 2B. There were 12 significant ($p < 0.05$) connections in total to the rPFC: rDLPFC to lDLPFC (2), rDLPFC to lPMC/SMA (1), rDLPFC to rPMC/SMA (1), rDLPFC to lM1/S1 (1), and 7 within the rDLPFC.

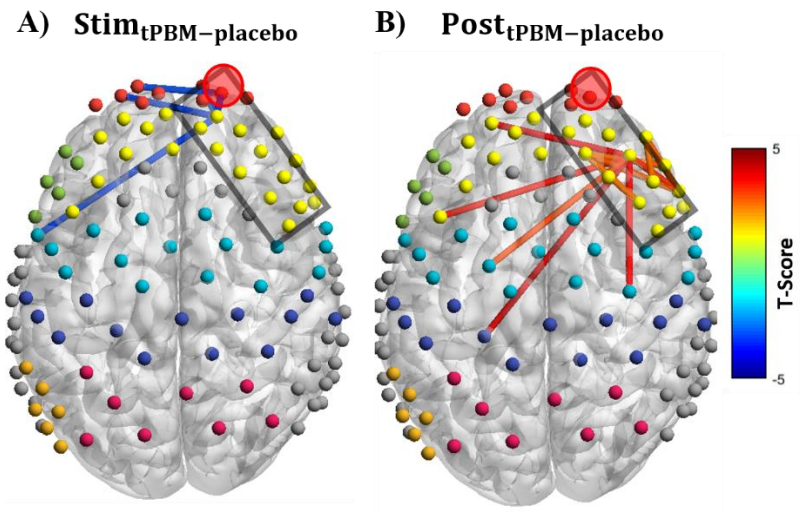

Figure 4 - 2. Group-level differences in FC between the right PFC and all other cortical regions compared between tPBM and placebo conditions at A) stimulation, and B) post-stimulation periods. Red lines indicate greater FC strength during tPBM than the placebo treatment. Blue lines indicate weaker FC strength during tPBM than the placebo treatment. Only significant ($p < 0.05$, FDR corrected) FC changes are shown. Black boxes enclose channels within the right PFC; Red circle marks the approximate location of tPBM. Different ROIs are denoted by color: frontopolar (FP) (red), dorsolateral prefrontal cortex (DLPFC) (yellow), Broca's area (green), premotor cortex (PMC) (light blue), primary motor and somatosensory cortical (M1/S1) areas (dark blue), somatosensory association cortex (SAC) (pink), and Wernicke's Area (gold).

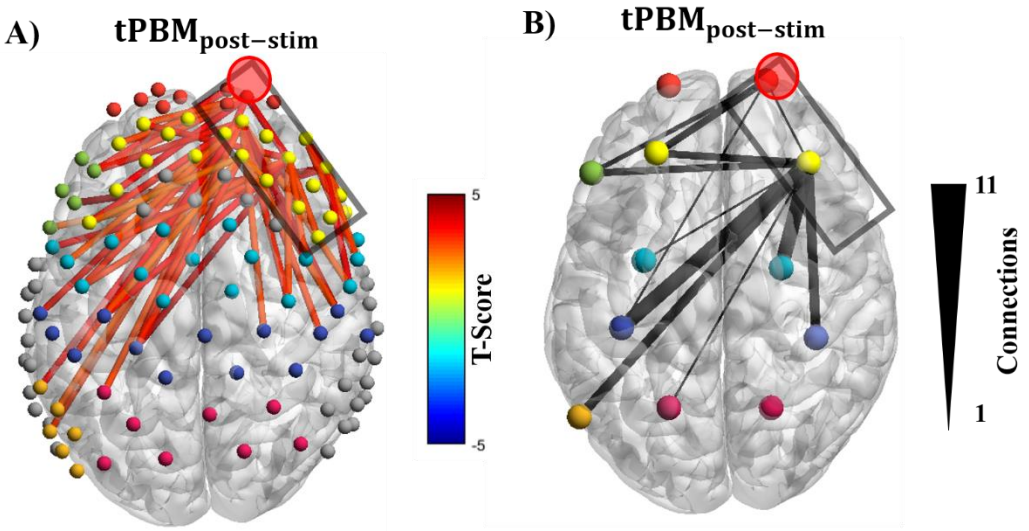

Figure 4 - 3. Significant increases in FC strength from right PFC to other regions of the brain, compared between post-stimulation and the tPBM stimulation period. The black box encloses all the channels within the right PFC. The red circle near rPFC marks the location of tPBM stimulation. ROIs are denoted by color; frontopolar (FP) (red), dorsolateral prefrontal cortex (DLPFC) (yellow), Broca's area (green), premotor cortex (PMC) (light blue), primary motor and somatosensory cortical (M1/S1) areas (dark blue), somatosensory association cortex (SAC) (pink), and Wernicke's Area (gold). A) Red lines indicate greater FC strength during post-tPBM than the stimulation period. Only significant ($p < 0.05$, FDR corrected) FC strength changes are shown. B) The total number of significant connections between ROIs from right PFC to other regions of the cortex. Line thickness indicates the number of significant connections from 1 (thinnest) to 11 (thickest) connections.

For the 2nd comparison, FC strength differences between the tPBM and post-tPBM periods were quantified. There was significantly ($p < 0.05$) greater FC strength during the post-stimulation period than the stimulation period as illustrated by the red lines in Fig. 4 - 3A. Specifically, there were 46 significant connections in total between channels

within the rPFC and all other channels in the brain. These connections were between the rFP and lPFC (3 connections), rFP and rPFC (1), rPF and Broca's (2), rPFC and lM1 (1), rPFC and lPFC (3), rPFC and rPFC (3), rPFC and Broca's (3), rPFC and lPMC/SMA (1), rPFC and rPMC/SMA (11), rPFC and lM1/S1 (9), rPFC and rM1/S1 (4), rPFC and lSAC (1), and rPFC and Wernicke's (4). To better overview the FC strength connecting right PFC to other cortical ROIs or clusters, we presented a topograph of number of connections for each pair among all 12 cortical ROIs (Fig. 4 - 3B).

4.3.2 Graphical network metrics analyzed by GTA

To show significant differences in global graphical network metrics between tPBM and placebo treatments, statistical paired t-tests were used, for each of the three periods, to investigate the effect of tPBM on seven global graphical metrics derived from GTA: C_p, L_p, λ, γ, σ, E_g, and E_{loc}. During the pre-stimulation period, the results showed no significant ($p > 0.05$) difference between tPBM and placebo treatments for any of the metrics at any S level. During the 2nd half of stimulation period (5-8 min), however, there were significant differences between tPBM and placebo treatments for efficiency and small-world metrics, namely, E_g, E_{loc}, and L_p (Fig. 4 - 4). Specifically, significant differences between the two treatments were: for E_g, at S = 0.05 ($p = 0.01$), S = 0.15 ($p = 0.05$), S = 0.3 ($p = 0.04$), S = 0.35 ($p = 0.02$), S = 0.4 ($p = 0.03$), and S = 0.45 ($p = 0.03$) (Fig. 4 - 4A); for E_{loc}, at S = 0.05 ($p = 0.02$), S = 0.10 ($p = 0.02$), S = 0.2 ($p = 0.05$), and S=0.3 ($p = 0.03$) (Fig. 4 - 4B); for L_p, at S = 0.05 ($p = 0.02$), S = 0.15 ($p = 0.04$), S = 0.3 ($p = 0.03$), S = 0.35 ($p = 0.01$), S = 0.4 ($p = 0.02$), and S = 0.45 ($p=0.03$) (Fig. 4 - 4C). During the post-stimulation period, the results showed that only σ had significant

differences between the two treatments, occurring at S = 0.1 (p = 0.05), S = 0.15 (p = 0.04), and S = 0.25 (p = 0.05) (Fig. 4 - 5).

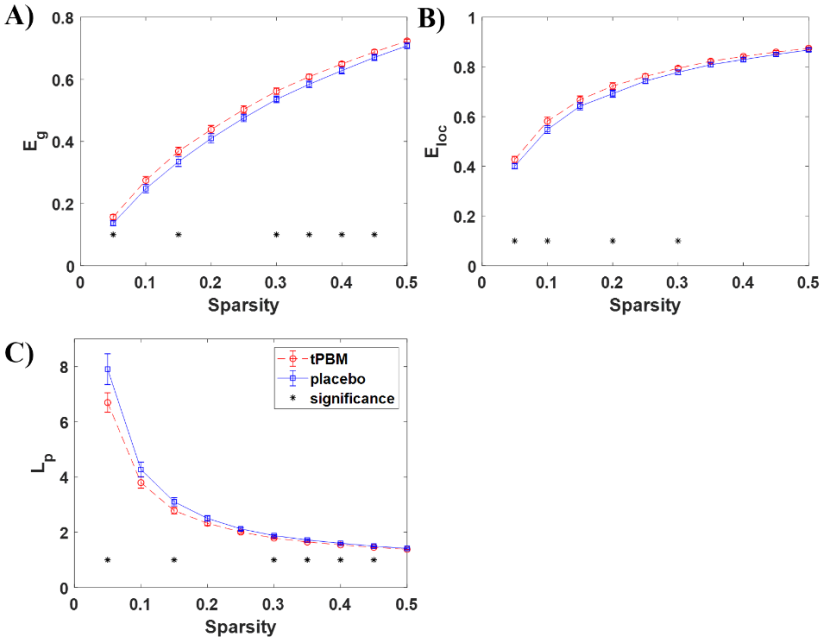

Figure 4 - 4. Global network characteristics between tPBM and placebo treatment during the 2nd half of stimulation period (5-8 min) for A) global efficiency (E_g), B) local efficiency (E_{loc}), and C) averaged path length (L_p). Significant differences ($p < 0.05$) between the treatments are represented with black stars, *. Red lines indicate tPBM treatment while blue lines indicate placebo treatment. Mean ± SEM.

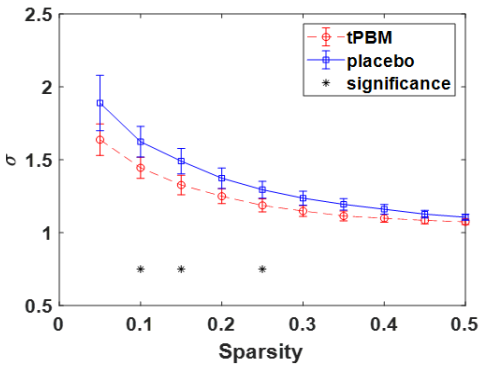

Figure 4 - 5. Small-worldness differences between tPBM and placebo treatment during post-stimulation period. Significant differences ($p < 0.05$) between the two treatments are represented with black stars, *. Red lines indicate tPBM treatment. Blue lines indicate placebo treatment. Mean + SEM.

4.4. DISCUSSION

4.4.1 Effects of tPBM on functional connectivity

To the best of our knowledge, this study is the first to evaluate the effects of tPBM on whole-head FC in humans using large field of view fNIRS and tPBM simultaneously. By examining the time dependence on FC for each period, this study shows that tPBM has two different effects on FC during and after stimulation. Seed-based PCC was performed to quantify and map FC between all channels within the rPFC, which encompasses the rFP and rDLPFC, and to all other ROIs due to rPFC's proximity to the location of tPBM administration.

During the stimulation period, the FC map exhibited decreased, localized connectivity between the rPFC and the lPFC and lPMC/SMA (Fig. 4 - 2A). Decreased FC from tPBM stimulation may be due to a regional increase in ΔHbO. Prior tPBM studies reported that tPBM increases ΔHbO during human brain stimulation,[18, 33, 132] and regional cerebral blood flow (rCBF) in animal and human studies.[15, 135, 150] Increased rCBF can be

attributed to tPBM's stimulation of the synthesis of nitric oxide (NO), an endogenous vasodilator.[151] In an animal study, tPBM at 808 nm increased NO concentration and rCBF in mice; however, the NO concentration and rCBF did not increase when NO synthase was blocked,[150] indicating that NO synthesis is integral in rCBF changes during tPBM stimulation. The decrease in localized FC during stimulation may therefore be partially attributed to the increase of rCBF in the rPFC region only, which caused differences or desynchronization in hemodynamic variability patterns relative to others in non-stimulated ROIs.

The post-stimulation FC maps exhibited enhanced global connectivity between the rPFC and all other ROIs (Fig. 4 - 2B; Fig. 4 - 3). These results suggest that post-tPBM hemodynamic recovery influences coactivation between the rPFC and ROIs that are involved in resting state networks (RSN), as also seen in tDCS studies.[138, 152] The rFP and rDLPFC are associated with high cognitive and executive functions; their direct connectivity in RSN and other ROIs is related to a top-down modulation of attention and working memory as seen in increased coactivation of frontal and parietal regions.[77, 114, 152-155] The default mode network (DMN), which comprises the rFP and rDLPFC, is a network that is highly active at rest and linked to human cognition, including the integration of cognitive and emotional processing.[77, 114, 154] The frontal-parietal network (FPN), also known as the central executive network, encompasses the FP, DLPFC, and SAC and is associated with executive functions, attention, and motor control. The FPN is highly integrated with other brain networks like the DMN, motor network, and language network.[77, 113, 114, 117, 154, 156] The FPN's integration with other networks is evident in this study with the extensive connection to the motor network, comprising of

PMC/SMA, M1/S1,[77, 114] and the language network anchored in Wernicke's and Broca's areas.[156, 157]

Overall, the most significant changes or increases of FC were found in the FPN and regions that belong to other brain networks and are highly integrated with the FPN. These findings are significant since it unambiguously demonstrates that tPBM modulates FC in distinct and remote functional brain networks of the human brain. The preferential involvement of the FPN is consistent with cognitive findings showing that tPBM improves executive function.[158]

4.4.2 Effects of tPBM on global topographical metrics

GTA was used to quantify network connectivity changes induced by tPBM across the entire cortical area mapped by fNIRS. TPBM induced significant changes during the 2nd half of stimulation period (5-8 min) (Fig. 4 - 4) and post-stimulation (Fig. 4 - 5) across the entire cortical network that can be characterized by the network's small-world features, including five small-world parameters: clustering coefficient (C_p), characteristic path length (L_p), normalized characteristic path length (λ), normalized clustering coefficient (γ), and small-worldness (σ).[139-141, 146] During 5-8 min tPBM stimulation, L_p was significantly lower than the placebo treatment at several S levels (Fig. 4 - 4C). L_p signifies the ability to rapidly combine pieces of specialized information from different brain regions or functional integration.[7, 146] Shortened L_p indicates that during 5-8 min tPBM, there is enhanced or faster information/integration processing.[159, 160] Economic small-worldness, σ, was exemplified (Fig. 4 - 5) after tPBM with $\sigma > 1$.[7] However, σ is significantly lower after tPBM stimulation compared to placebo. These results are similar

to an EEG study that showed brain networks being less evident of small-worldness after tDCS stimulation.[161]

Two additional parameters, global (E_g) and local efficiency (E_{loc}), were also calculated to determine how efficiently small-world networks exchange information. TPBM treatment resulted in significantly higher efficiency metrics for both E_g and E_{loc} during the stimulation. E_g was significantly higher than the placebo due to its susceptibility to shorter L_p, as also seen in this study. A high E_g assures effective functional integration of information between and across remote regions.[140, 146, 160] During the late 4-min tPBM stimulation, E_{loc} was also significantly higher than the placebo. E_{loc} measures the ability of fault tolerance of a network, or how efficient communication is between nodes when one node is removed.[140, 141, 146] Typically, a small-world network is characterized by high E_g and E_{loc},[140] but this is not seen after tPBM stimulation. This is in contrast with a prior fNIRS study that noted enhanced E_{loc} after anodal tDCS, but not during stimulation as seen in this study.[111] This difference could be due to different underlying mechanisms affecting neuroplasticity between tPBM and tDCS.

Overall, two different analysis methods (i.e., PCC and GTA) provided different aspects or views of tPBM-induced effects on human brain FC. During tPBM stimulation, tPBM resulted in desynchronization in hemodynamic oscillations between the intervention site and non-stimulated ROIs, while tPBM enabled faster functional integration/communication and improved efficiency of small-world brain networks. During the 4-min post-tPBM, while the brain gradually recovered to its RSN, FC in the FPN became significantly enhanced and connected to other distinct and remote cortical networks of the human brain.

4.5. LIMITATIONS AND FUTURE WORK

A few limitations should be noted for this study. First, fNIRS is limited to measuring only cortical brain areas and has a lower spatial resolution in comparison to fMRI.[35, 42] Second, this study would have improved FC and GTA metrics during the post-stimulation period if subjects were measured for at least 5 min after tPBM stimulation. The time was shortened in consideration of the subject's comfort while wearing the fNIRS optodes. However, an additional 1- 4 min would likely not have put undue burden onto the subject. Typically resting-state FC scans are most reliable when measured between 5 – 13 min.[162, 163] Third, the neuromodulation by tPBM involves a relatively slow hemodynamic process that is progressive,[13, 132] and thus could not be rigorously represented or quantified by either PCC or GRA, both of which are more appropriate for analyzing resting state FC without much external intervention during a period of 5 min or longer.

For future work, more advanced methods to analyze time-varying dynamic FC need to be explored to account for time-evolving features of neuromodulation by tPBM. Next, given the complex effects of tPBM on the brain, future studies may be better informed by multi-modal imaging. For example, since rCBF is expected to change with tPBM, concurrent fNIRS measurements with diffuse correlation spectroscopy or arterial spin labeling fMRI would be helpful to map the spatiotemporal extent of these changes.[164] Last, concurrent mapping of fNIRS with electrical activity from the neuronal networks with multi-channel EEG would be useful in deconvolving the tPBM-induced relative changes in hemodynamics versus cerebral electrophysiological activity.[13]

4.6. CONCLUSION

Our work demonstrates the feasibility of using fNIRS to study cortical network reorganization induced by tPBM. The analysis methods based on Pearson's correlation coefficients and graph theory were used to track changes in network connections and graphical metrics between the rPFC, where tPBM stimulation was administered, and other cortical regions. The PCC- and GTA-derived results revealed that during the later period of tPBM stimulation, local connections were enhanced, and faster information processing was observed. After stimulation, distant connections had increased FC strength, particularly for FPN, which supports cognitive findings showing that tPBM improves executive function.[158] These observations indicate that there was a time dependence in the change of FC and graphical network patterns during the administration of tPBM. Our findings demonstrated the excellent and novel applicability of wholehead fNIRS in tandem with the non-invasive tPBM intervention to investigate or characterize cortical network effects. These observed effects may shed light on the underlying large-scale network mechanism and potential application of tPBM for cognitive enhancement in healthy subjects and patients with brain injury and disorders, such as stroke, traumatic brain injury, Alzheimer's disease, Parkinson's disease, anxiety, and depression.[14, 15, 33]

CHAPTER 5

Conclusion and future work

5.1 Conclusion

The primary objective of this work was to evaluate the temporal evolution of cerebral hemodynamics and its patterns during task-related (i.e. fatiguing hand grip) and intervention- related (i.e. transcranial photobiomodulation (tPBM)) cortical responses. In all, the outcome of this work was the identification of functional near-infrared spectroscopy (fNIRS)-derived brain metrics including: activation, functional connectivity (FC), directional phase transfer entropy (dPTE), directional connectivity (DC), functional connectivity variability (FCV), and graph theory analysis (GTA) throughout the experimental paradigms.

Specifically, in the first study, as presented in Chapter 2, fNIRS was used to measure differences in young adults throughout the experimental paradigm to provide a more complete understanding of the differences in cortical activity due to physical activity, which is currently absent in current functional neuroimaging studies. Physically active subjects demonstrated delayed fatigue onset and significantly longer-lasting and more spatially extended functional connectivity (FC) patterns compared to inactive subjects. The observed differences in activation and FC suggested differences in cortical network adaptation patterns as fatigue set in, which were dependent on subject physical activity. The findings of this study suggest that physical activity increases FC with regions involved in motor task control and correlates to extended fatigue onset and enhanced performance.

The second study presented in this dissertation, in Chapter 3, further explored how motor fatigue affected the vasomotion-induced oscillations as measured by fNIRS at the endothelial, neurogenic, and myogenic hemodynamic frequency band. To help understand how these three neurovascular regulatory mechanisms relate to handgrip task performance, several dynamic fNIRS metrics were quantified including: dPTE, DC, and the relationship between FC and FCV was also explored to understand their mutual dependence for each frequency band in the context of handgrip performance as fatigued increased. These results imply that physical activity modulates neurovascular control mechanisms at the endogenic, neurogenic, and myogenic frequency bands resulting in delayed fatigue onset and enhanced performance.

After thorough investigation into the cortical response of motor fatigue, the final study, presented in Chapter 4, investigated the influence of tPBM on cerebral hemodynamics before, during, and after tPBM stimulation using fNIRS. Pearson's correlation coefficient- and graph theory- derived results revealed that during the later period of tPBM stimulation, local connections were enhanced, and faster information processing was observed. After stimulation, distant connections had increased FC strength, particularly for frontal-parietal network, which supports cognitive findings showing that tPBM improves executive function. These observations indicate that there was a time dependence in the change of FC and graphical network patterns during the administration of tPBM.

5.2 Limitations

In the future, this body of work could be improved upon overall adding multimodal monitoring of biometrics and adjusting experimental protocols. Firstly, the incorporation of electromyography (EMG) should be added to measure peripheral muscle response which can be used to identify motor fatigue and improve accuracy in the interpretation. Based on EMG measurements, the paradigm seen in Chapters 2 and 3 could have been adjusted to either 1) lower %MVC or 2) a shorter protocol (< 20 min) which would have improved subject comfort without sacrificing the objective of experiencing muscle fatigue. Other multimodal monitoring of hemodynamics such as heart rate and blood pressure could also have been used as regressors to improve fNIRS signals and provide systemic physiology information. As well, when considering static functional connectivity (SFC) and functional connectivity variability (FCV) in Chapter 3, it would be more informative to analyze the resulting r-values per subject and then average as oppose to a group average immediately per frequency band to test data consistency. Additionally, diffuse correlation spectroscopy (DCS) would be beneficial to map regional cerebral blood flow in motor fatigue and tPBM thus providing the spatiotemporal extent of the changes induced in these studies. In the tPBM study presented in Chapter 4, at least 5 min should have been recorded after tPBM stimulation, which is typically the minimum measurement time for reliable FC measurements. Lastly, while there have been several tPBM studies that have optimized wavelengths, daily doses, number of sessions, and power densities[165] there is a need to be further optimize the length of tPBM exposure.

5.3 Future work

The cumulation of this research may be used in future research towards mapping differences in cortical networks during fatiguing handgrip task in older type 2 diabetic population. This research has provided the foundation for cortical activation, connectivity, and other metrics during fatiguing handgrip task in young adults and can be extrapolated to an older population. Furthermore, more recent research has further supported the notion that strength training results in cortical adaptations, preceding motoneuronal adaptations. One study by Glover and Baker (2020) determined in non-human primates that strength training is associated more so with neural adaptations in the intracortical circuits than the corticospinal and motoneuronal adaptations.[166] In addition, Jorowitz et al. (2020) concluded that blood factor glycosylphosphatidylinositol - specific phospholipase D1 (GpId1) transferred to sedentary aged mice resulted in healthier and enlarged blood vessels in subcortical structures associated with motion control.[167] Ultimately, these studies and the work presented in this dissertation contribute to the idea that the brain could be used as an early indicator of vascular health issues.

Additionally, this research may attribute to the future testing of tPBM capability to attenuate muscle fatigue. A transcranial direct current stimulation (tDCS) study has previously explored the manipulation of motor cortex excitability during sub-maximal exercise and showed that it improve endurance time.[168] tPBM may have similar effects on brain networks during motor fatigue despite different neuromodulation mechanisms, as also seen in our third study presented in Chapter 4. Lastly, this work could be further

expanded upon by studying repeat tPBM treatments and correlating the results with improved physical performance, which would benefit current clinical studies.[169]

REFERENCES

1. P. J. Mueller et al., "Integration of Central and Peripheral Regulation of the Circulation during Exercise: Acute and Chronic Adaptations," *Compr Physiol* **8**(1), 103-151 (2017).
2. J. Gonzalez-Alonso et al., "Brain and central haemodynamics and oxygenation during maximal exercise in humans," *J Physiol* **557**(Pt 1), 331-342 (2004).
3. J. Z. Liu et al., "Shifting of activation center in the brain during muscle fatigue: an explanation of minimal central fatigue?," *Neuroimage* **35**(1), 299-307 (2007).
4. K. Shibuya, and N. Kuboyama, "Decreased activation in the primary motor cortex area during middle-intensity hand grip exercise to exhaustion in athlete and nonathlete participants," *Percept Mot Skills* **111**(1), 19-30 (2010).
5. S. W. Wong et al., "Sex differences in forebrain and cardiovagal responses at the onset of isometric handgrip exercise: a retrospective fMRI study," *J Appl Physiol (1985)* **103**(4), 1402-1411 (2007).
6. N. M. Benwell et al., "Primary sensorimotor cortex activation with task-performance after fatiguing hand exercise," *Exp Brain Res* **167**(2), 160-164 (2005).
7. J. Liu et al., "Complex Brain Network Analysis and Its Applications to Brain Disorders: A Survey," *Complexity* **2017**(8362741 (2017).
8. Z. Jiang et al., "Strengthened functional connectivity in the brain during muscle fatigue," *Neuroimage* **60**(1), 728-737 (2012).
9. J. Rhee, and R. K. Mehta, "Functional Connectivity During Handgrip Motor Fatigue in Older Adults Is Obesity and Sex-Specific," *Front Hum Neurosci* **12**(455 (2018).
10. T. Rupp et al., "Muscle, Prefrontal, and Motor Cortex Oxygenation Profiles During Prolonged Fatiguing Exercise," *Advances in experimental medicine and biology* **789**(149-155 (2013).
11. T. Rupp et al., "Muscle, prefrontal, and motor cortex oxygenation profiles during prolonged fatiguing exercise," *Adv Exp Med Biol* **789**(149-155 (2013).
12. T. Rupp, and S. Perrey, "Prefrontal cortex oxygenation and neuromuscular responses to exhaustive exercise," *Eur J Appl Physiol* **102**(2), 153-163 (2008).
13. X. Wang et al., "Transcranial photobiomodulation with infrared laser increases power of brain oscillations," *bioRxiv* 535757 (2019).
14. M. R. Hamblin, "Shining light on the head: Photobiomodulation for brain disorders," *BBA Clinical* **6**(113-124 (2016).
15. P. Askalsky, and D. V. Iosifescu, "Transcranial Photobiomodulation For The Management Of Depression: Current Perspectives," *Neuropsychiatr Dis Treat* **15**(3255-3272 (2019).
16. J. R. Jagdeo et al., "Transcranial Red and Near Infrared Light Transmission in a Cadaveric Model," *PLOS ONE* **7**(10), e47460 (2012).
17. C. E. Tedford et al., "Quantitative analysis of transcranial and intraparenchymal light penetration in human cadaver brain tissue," *Lasers Surg Med* **47**(4), 312-322 (2015).
18. F. Tian et al., "Transcranial laser stimulation improves human cerebral oxygenation," *Lasers Surg Med* **48**(4), 343-349 (2016).
19. X. Wang et al., "Interplay between up-regulation of cytochrome-c-oxidase and hemoglobin oxygenation induced by near-infrared laser," *Scientific reports* **6**(30540-30540 (2016).
20. Y. Lampl et al., "Infrared Laser Therapy for Ischemic Stroke: A New Treatment Strategy Results of the NeuroThera Effectiveness and Safety Trial-1 (NEST-1)," *Stroke; a journal of cerebral circulation* **38**(1843-1849 (2007).
21. J. Zivin et al., "Effectiveness and Safety of Transcranial Laser Therapy for Acute Ischemic Stroke," *Stroke; a journal of cerebral circulation* **40**(1359-1364 (2009).

22. M. A. Naeser et al., "Significant improvements in cognitive performance post-transcranial, red/near-infrared light-emitting diode treatments in chronic, mild traumatic brain injury: open-protocol study," *J Neurotrauma* **31**(11), 1008-1017 (2014).
23. M. Naeser et al., "Improved Cognitive Function After Transcranial, Light-Emitting Diode Treatments in Chronic, Traumatic Brain Injury: Two Case Reports," *Photomedicine and laser surgery* **29**(351-358 (2010).
24. F. Schiffer et al., "Psychological benefits 2 and 4 weeks after a single treatment with near infrared light to the forehead: a pilot study of 10 patients with major depression and anxiety," *Behav Brain Funct* **5**(46-46 (2009).
25. S. G. Disner, C. G. Beevers, and F. Gonzalez-Lima, "Transcranial Laser Stimulation as Neuroenhancement for Attention Bias Modification in Adults with Elevated Depression Symptoms," *Brain stimulation* **9**(5), 780-787 (2016).
26. K. Larkin Kaiser et al., "Photobiomodulation delays the onset of skeletal muscle fatigue in a dose-dependent manner," *Lasers in Medical Science* **31**((2016).
27. P. A. Borsa, K. A. Larkin, and J. M. True, "Does phototherapy enhance skeletal muscle contractile function and postexercise recovery? A systematic review," *J Athl Train* **48**(1), 57-67 (2013).
28. R. Dellagrana et al., "Photobiomodulation Therapy on Physiological and Performance Parameters During Running Tests: Dose-Response Effects," *The Journal of Strength and Conditioning Research* **32**(2807-2815 (2018).
29. C. Ferraresi, Y.-Y. Huang, and M. Hamblin, "Photobiomodulation in human muscle tissue: An advantage in sports performance?," *Journal of Biophotonics* **9**((2016).
30. E. C. Leal Junior et al., "Effect of phototherapy (low-level laser therapy and light-emitting diode therapy) on exercise performance and markers of exercise recovery: A systematic review with meta-analysis," *Lasers in medical science* **30**((2013).
31. A. Vanin et al., "Photobiomodulation therapy for the improvement of muscular performance and reduction of muscular fatigue associated with exercise in healthy people: a systematic review and meta-analysis," *Lasers in Medical Science* **33**((2017).
32. S. Perrey, "Promoting motor function by exercising the brain," *Brain sciences* **3**(1), 101-122 (2013).
33. E. Holmes et al., "Cognitive Enhancement by Transcranial Photobiomodulation Is Associated With Cerebrovascular Oxygenation of the Prefrontal Cortex," *Frontiers in Neuroscience* **13**(1129), (2019).
34. T. Hitoshi, Y. Kazuki, and I. Masako, "Measurement of Brain Function Using Near-Infrared Spectroscopy (NIRS)," (2012).
35. N. Naseer, and K.-S. Hong, "fNIRS-based brain-computer interfaces: a review," *Frontiers in human neuroscience* **9**(3-3 (2015).
36. N. S. Ward, and R. S. Frackowiak, "Age-related changes in the neural correlates of motor performance," *Brain* **126**(Pt 4), 873-888 (2003).
37. G. Derosiere, and S. Perrey, "Relationship Between Submaximal Handgrip Muscle Force and NIRS-Measured Motor Cortical Activation," *Advances in Experimental Medicine and Biology* **737**(269-274 (2012).
38. J. Z. Liu et al., "Human brain activation during sustained and intermittent submaximal fatigue muscle contractions: an FMRI study," *J Neurophysiol* **90**(1), 300-312 (2003).
39. J. Z. Liu et al., "Fatigue induced by intermittent maximal voluntary contractions is associated with significant losses in muscle output but limited reductions in functional MRI-measured brain activation level," **1040**(1), 44-54 (2005).

40. R. Radel, J. Brisswalter, and S. Perrey, "Saving mental effort to maintain physical effort: a shift of activity within the prefrontal cortex in anticipation of prolonged exercise," *Cogn Affect Behav Neurosci* **17**(2), 305-314 (2017).
41. J. Williamson, P. Fadel, and J. Mitchell, "New insights into central cardiovascular control during exercise in humans: A central command update," *Experimental physiology* **91**(51-58 (2006).
42. T. J. Huppert et al., "HomER: a review of time-series analysis methods for near-infrared spectroscopy of the brain," *Appl Opt* **48**(10), D280-298 (2009).
43. R. C. Oldfield, "The assessment and analysis of handedness: the Edinburgh inventory," *Neuropsychologia* **9**(1), 97-113 (1971).
44. K. M. McGregor et al., "Physical activity and neural correlates of aging: a combined TMS/fMRI study," *Behav Brain Res* **222**(1), 158-168 (2011).
45. A. K. Singh et al., "Spatial registration of multichannel multi-subject fNIRS data to MNI space without MRI," *NeuroImage* **27**(4), 842-851 (2005).
46. R. K. Mehta, and A. E. Shortz, "Obesity-related differences in neural correlates of force control," *Eur J Appl Physiol* **114**(1), 197-204 (2014).
47. J. Xu et al., "FC-NIRS: A Functional Connectivity Analysis Tool for Near-Infrared Spectroscopy Data," *Biomed Res Int* **2015**(248724 (2015).
48. J. Cao et al., "Evaluation of cortical plasticity in children with cerebral palsy undergoing constraint-induced movement therapy based on functional near-infrared spectroscopy," *Journal of biomedical optics* **20**(4), 046009-046009 (2015).
49. M. Kohl et al., "Determination of the wavelength dependence of the differential pathlength factor from near-infrared pulse signals," *Phys Med Biol* **43**(6), 1771-1782 (1998).
50. A. Yennu et al., "Prefrontal hemodynamic mapping by functional near-infrared spectroscopy in response to thermal stimulations over three body sites," *Neurophotonics* **3**(4), 045008 (2016).
51. A. Yennu et al., "Prefrontal responses to Stroop tasks in subjects with post-traumatic stress disorder assessed by functional near infrared spectroscopy," *Sci Rep* **6**(30157 (2016).
52. E. Visani et al., "Hemodynamic and EEG Time-Courses During Unilateral Hand Movement in Patients with Cortical Myoclonus. An EEG-fMRI and EEG-TD-fNIRS Study," *Brain Topogr* **28**(6), 915-925 (2015).
53. A. R. Anwar et al., "Comparison of causality analysis on simultaneously measured fMRI and NIRS signals during motor tasks," *Conf Proc IEEE Eng Med Biol Soc* **2013**(2628-2631 (2013).
54. A. K. Singh, and I. Dan, "Exploring the false discovery rate in multichannel NIRS," *NeuroImage* **33**(2), 542-549 (2006).
55. M. Xia, J. Wang, and Y. He, "BrainNet Viewer: a network visualization tool for human brain connectomics," *PloS one* **8**(7), e68910-e68910 (2013).
56. F. Tian, Z.-J. Lin, and H. Liu, "EasyTopo: A toolbox for rapid diffuse optical topography based on a standard template of brain atlas," *SPIE BiOS* 10 (2013).
57. D. E. Hinkle, W. Wiersma, and S. G. Jurs, *Applied Statistics for the Behavioral Sciences* 5th ed., Houghton Mifflin, Boston, MA (2002).
58. J. P. Marques, *Applied Statistics Using SPSS, STATISTICA, MATLAB and R*, Springer Publishing Company, Incorporated (2007).
59. D. H. Clarke, M. Q. Hunt, and C. O. Dotson, "Muscular strength and endurance as a function of age and activity level," *Res Q Exerc Sport* **63**(3), 302-310 (1992).
60. G. C. Bogdanis, "Effects of physical activity and inactivity on muscle fatigue," *Frontiers in physiology* **3**(142-142 (2012).
61. A. T. White et al., "Brain activation in multiple sclerosis: a BOLD fMRI study of the effects of fatiguing hand exercise," *Mult Scler* **15**(5), 580-586 (2009).

62. Zhiguo Jiang, Xiao-Feng Wang, and G. H. Yue, "Strengthened Corticosubcortical Functional Connectivity during Muscle Fatigue," *Neural Plasticity* **2016**((2016).
63. A. W. Subudhi et al., "Frontal and motor cortex oxygenation during maximal exercise in normoxia and hypoxia," *J Appl Physiol (1985)* **106**(4), 1153-1158 (2009).
64. N. H. Kashou et al., "Hand-grasping and finger tapping induced similar functional near-infrared spectroscopy cortical responses," *Neurophotonics* **3**(2), 025006 (2016).
65. R. S. Frackowiak, "Human Brain Function," (2004).
66. P. Wasson et al., "Predicting grip force amplitude involves circuits in the anterior basal ganglia," *Neuroimage* **49**(4), 3230-3238 (2010).
67. S. Badoud et al., "Effects of dorsolateral prefrontal cortex lesion on motor habit and performance assessed with manual grasping and control of force in macaque monkeys," *Brain Struct Funct* **222**(3), 1193-1206 (2017).
68. L. H. Ernst et al., "Prefrontal activation patterns of automatic and regulated approach–avoidance reactions – A functional near-infrared spectroscopy (fNIRS) study," *Cortex* **49**(1), 131-142 (2013).
69. M. Perrone-Bertolotti et al., "What is that little voice inside my head? Inner speech phenomenology, its role in cognitive performance, and its relation to self-monitoring," **261**(220-239 (2014).
70. M. Ypofanti et al., "Psychometric Properties of the International Personality Item Pool Big-Five Personality Questionnaire for the Greek population," *Health Psychol Res* **3**(2), 2206 (2015).
71. J. Hardy, C. R. Hall, and L. Hardy, "Quantifying athlete self-talk," *J Sports Sci* **23**(9), 905-917 (2005).
72. N. Zourbanos, Hatzigeorgiadis A , Chroni S, Theodorakis Y, and Papaioannou A, "Automatic Self-Talk Questionnaire for Sports (ASTQS): Development and Preliminary Validation of a Measure Identifying the Structure of Athletes' Self-Talk," *The Sports Psychologist* **23**(233-251 (2009).
73. A. F. T. Arnsten, "Stress signalling pathways that impair prefrontal cortex structure and function," *Nature Reviews Neuroscience* **10**(6), 410-422 (2009).
74. T.-W. Lin, S.-F. Tsai, and Y.-M. Kuo, "Physical Exercise Enhances Neuroplasticity and Delays Alzheimer's Disease," *Brain Plast* **4**(1), 95-110 (2018).
75. T. B. Weng et al., "The Acute Effects of Aerobic Exercise on the Functional Connectivity of Human Brain Networks," *Brain Plast* **2**(2), 171-190 (2017).
76. O. Seidel et al., "Motor learning in a complex balance task and associated neuroplasticity: a comparison between endurance athletes and nonathletes," *Journal of neurophysiology* **118**(3), 1849-1860 (2017).
77. D. A. Raichlen et al., "Differences in Resting State Functional Connectivity between Young Adult Endurance Athletes and Healthy Controls," *Frontiers in Human Neuroscience* **10**(610), (2016).
78. C. P. Kaller et al., "Dissociable Contributions of Left and Right Dorsolateral Prefrontal Cortex in Planning," *Cerebral Cortex* **21**(2), 307-317 (2010).
79. H. Doi, S. Nishitani, and K. Shinohara, "NIRS as a tool for assaying emotional function in the prefrontal cortex," *Frontiers in human neuroscience* **7**(770 (2013).
80. J. Spielberg et al., "A Brain Network Instantiating Approach and Avoidance Motivation," *Psychophysiology* **49**(1200-1214 (2012).
81. T. Liu-Ambrose et al., "Resistance training and functional plasticity of the aging brain: a 12-month randomized controlled trial," *Neurobiology of Aging* **33**(8), 1690-1698 (2012).
82. L. Gagnon et al., "Short separation channel location impacts the performance of short channel regression in NIRS," *NeuroImage* **59**(3), 2518-2528 (2012).
83. M. D. Pfeifer, F. Scholkmann, and R. Labruyere, "Signal Processing in Functional Near-Infrared Spectroscopy (fNIRS): Methodological Differences Lead to Different Statistical Results," *Front Hum Neurosci* **11**(641 (2017).

84. I. Tachtsidis, and F. Scholkmann, "False positives and false negatives in functional near-infrared spectroscopy: Issues, challenges, and the way forward," *Neurophotonics* **3**((2016).
85. J. Cao et al., "Directional changes in information flow between human brain cortical regions after application of anodal transcranial direct current stimulation (tDCS) over Broca's area," *Biomed Opt Express* **9**(11), 5296-5317 (2018).
86. E. C. Peterson, Z. Wang, and G. Britz, "Regulation of Cerebral Blood Flow," *International Journal of Vascular Medicine* **2011**(823525 (2011).
87. J. S. Querido, and A. W. Sheel, "Regulation of cerebral blood flow during exercise," *Sports Med* **37**(9), 765-782 (2007).
88. Y.-C. Tzeng, and P. N. Ainslie, "Blood pressure regulation IX: cerebral autoregulation under blood pressure challenges," *European journal of applied physiology* **114**(3), 545-559 (2014).
89. P. Peri-Okonny et al., "Exercise, the Brain, and Hypertension," *Curr Hypertens Rep* **17**(10), 82 (2015).
90. M. J. Cipolla, *The Cerebral Circulation*, Morgan and Claypool Life Sciences, San Rafael CA (2009).
91. Z. Li et al., "Spectral analysis of near-infrared spectroscopy signals measured from prefrontal lobe in subjects at risk for stroke," *Med Phys* **39**(4), 2179-2185 (2012).
92. C. Huo et al., "Effective Connectivity in Response to Posture Changes in Elderly Subjects as Assessed Using Functional Near-Infrared Spectroscopy," *Frontiers in Human Neuroscience* **12**(98), (2018).
93. J. Myers, "Exercise and Cardiovascular Health," *Circulation* **107**(1), e2-e5 (2003).
94. B. M. Bosch et al., "Effect of cerebral vasomotion during physical exercise on associative memory, a near-infrared spectroscopy study," *Neurophotonics* **4**(4), 041404-041404 (2017).
95. H. Zhang, L. Zhang, and Y. Zang, "Fluctuation amplitude and local synchronization of brain activity in the ultra-low frequency band: An fMRI investigation of continuous feedback of finger force," *Brain Res* **1629**(104-112 (2015).
96. A. V. Andersen et al., "Assessing low-frequency oscillations in cerebrovascular diseases and related conditions with near-infrared spectroscopy: a plausible method for evaluating cerebral autoregulation?," *Neurophotonics* **5**(3), 1-14, 14 (2018).
97. E. L. Urquhart et al., "Mapping cortical network effects of fatigue during a handgrip task by functional near-infrared spectroscopy in physically active and inactive subjects," *Neurophotonics* **6**(4), 045011 (2019).
98. A. Hillebrand et al., "Direction of information flow in large-scale resting-state networks is frequency-dependent," *Proceedings of the National Academy of Sciences* **113**(14), 3867 (2016).
99. A. R. Anwar et al., "Effective Connectivity of Cortical Sensorimotor Networks During Finger Movement Tasks: A Simultaneous fNIRS, fMRI, EEG Study," *Brain Topography* **29**(5), 645-660 (2016).
100. A. H. C. Fong et al., "Dynamic functional connectivity during task performance and rest predicts individual differences in attention across studies," *NeuroImage* **188**(14-25 (2019).
101. Z. Li et al., "Dynamic functional connectivity revealed by resting-state functional near-infrared spectroscopy," *Biomedical optics express* **6**(7), 2337-2352 (2015).
102. C. Aalkjaer, D. Boedtkjer, and V. Matchkov, "Vasomotion - what is currently thought?," *Acta Physiol (Oxf)* **202**(3), 253-269 (2011).
103. A. Oldag et al., "Assessment of Cortical Hemodynamics by Multichannel Near-Infrared Spectroscopy in Steno-Occlusive Disease of the Middle Cerebral Artery," *Stroke* **43**(11), 2980-2985 (2012).
104. P. Smielewski et al., "Clinical Evaluation of Near-Infrared Spectroscopy for Testing Cerebrovascular Reactivity in Patients With Carotid Artery Disease," *Stroke* **28**(2), 331-338 (1997).

105. F. Siebenhuehner et al., "Phase transfer entropy: a novel measure for effective connectivity among neuronal oscillations," *BMC Neurosci* **14**(Suppl 1), P305-P305 (2013).
106. T. Schreiber, "Measuring Information Transfer," *Physical Review Letters* **85**(2), 461-464 (2000).
107. C. E. Shannon, "A Mathematical Theory of Communication," *Bell System Technical Journal* **27**(3), 379-423 (1948).
108. F. Faul et al., "G*Power 3: A flexible statistical power analysis program for the social, behavioral, and biomedical sciences," *Behavior Research Methods* **39**(2), 175-191 (2007).
109. E. A. Allen et al., "Tracking whole-brain connectivity dynamics in the resting state," *Cerebral cortex (New York, N.Y. : 1991)* **24**(3), 663-676 (2014).
110. R. M. Hutchison et al., "Dynamic functional connectivity: Promise, issues, and interpretations," *NeuroImage* **80**(360-378 (2013).
111. J. Cao, H. Liu, and G. Alexandrakis, "Modulating the resting-state functional connectivity patterns of language processing areas in the human brain with anodal transcranial direct current stimulation applied over the Broca's area," *Neurophotonics* **5**(2), 025002 (2018).
112. A. V. Nosarev et al., "Exercise and NO production: relevance and implications in the cardiopulmonary system," *Front Cell Dev Biol* **2**(73-73 (2015).
113. G. Doucet et al., "Brain activity at rest: a multiscale hierarchical functional organization," *Journal of Neurophysiology* **105**(6), 2753-2763 (2011).
114. M. P. van den Heuvel, and H. E. Hulshoff Pol, "Exploring the brain network: a review on resting-state fMRI functional connectivity," *Eur Neuropsychopharmacol* **20**(8), 519-534 (2010).
115. G. Doucet et al., "Patterns of hemodynamic low-frequency oscillations in the brain are modulated by the nature of free thought during rest," *NeuroImage* **59**(4), 3194-3200 (2012).
116. P. A. Bandettini, and E. Bullmore, "Endogenous oscillations and networks in functional magnetic resonance imaging," *Human brain mapping* **29**(7), 737-739 (2008).
117. S. Marek, and N. U. F. Dosenbach, "The frontoparietal network: function, electrophysiology, and importance of individual precision mapping," *Dialogues Clin Neurosci* **20**(2), 133-140 (2018).
118. K. Semendeferi et al., "Prefrontal cortex in humans and apes: A comparative study of area 10," *American Journal of Physical Anthropology* **114**(3), 224-241 (2001).
119. F. A. Mansouri et al., "Managing competing goals — a key role for the frontopolar cortex," *Nature Reviews Neuroscience* **18**(645 (2017).
120. P. A. Boyle et al., "Processing resources reduce the effect of Alzheimer pathology on other cognitive systems," *Neurology* **70**(17), 1534 (2008).
121. S. Bajaj et al., "Oscillatory motor network activity during rest and movement: an fNIRS study," *Front Syst Neurosci* **8**(13-13 (2014).
122. J. Michely et al., "Network connectivity of motor control in the ageing brain," *NeuroImage: Clinical* **18**(443-455 (2018).
123. M. A. Yücel et al., "Mayer waves reduce the accuracy of estimated hemodynamic response functions in functional near-infrared spectroscopy," *Biomedical optics express* **7**(8), 3078-3088 (2016).
124. D. J. Green et al., "Vascular adaptation in athletes: is there an 'athlete's artery'?," *Experimental Physiology* **97**(3), 295-304 (2012).
125. F. Klein, and C. Kranczioch, "Signal Processing in fNIRS: A Case for the Removal of Systemic Activity for Single Trial Data," *Frontiers in Human Neuroscience* **13**(331), (2019).
126. L. Duan et al., "Wavelet-based method for removing global physiological noise in functional near-infrared spectroscopy," *Biomedical Optics Express* **9**(8), 3805-3820 (2018).
127. K.-E. Jang et al., "Wavelet minimum description length detrending for near-infrared spectroscopy," *Journal of Biomedical Optics* **14**(3), 034004 (2009).

128. M. T. T. Wong-Riley et al., "Brain cytochrome oxidase: functional significance and bigenomic regulation in the CNS," in *Cytochrome Oxidase in Neuronal Metabolism and Alzheimer's Disease* F. Gonzalez-Lima, Ed., pp. 1-53, Plenum Press, New York (1998).
129. J. Eells et al., "Mitochondrial signal transduction in accelerated wound and retinal healing by near-infrared light therapy," *Mitochondrion* **4**(559-567 (2004).
130. D. W. Barrett, and F. Gonzalez-Lima, "Transcranial infrared laser stimulation produces beneficial cognitive and emotional effects in humans," *Neuroscience* **230**(13-23 (2013).
131. P. Cassano et al., "Review of transcranial photobiomodulation for major depressive disorder: targeting brain metabolism, inflammation, oxidative stress, and neurogenesis," *Neurophotonics* **3**(3), 031404-031404 (2016).
132. X. Wang et al., "Up-regulation of cerebral cytochrome-c-oxidase and hemodynamics by transcranial infrared laser stimulation: A broadband near-infrared spectroscopy study," *J Cereb Blood Flow Metab* **37**(12), 3789-3802 (2017).
133. M. R. Hamblin, and Y. Y. Huang, Eds., *Photobiomodulation in the Brain*, Acamemic press, San Diago, CA (2019).
134. J. Hwang, D. Castelli, and F. Gonzalez-Lima, "Cognitive enhancement by transcranial laser stimulation and acute aerobic exercise," *Lasers in Medical Science* **31**((2016).
135. S. G. Hipskind et al., "Pulsed Transcranial Red/Near-Infrared Light Therapy Using Light-Emitting Diodes Improves Cerebral Blood Flow and Cognitive Function in Veterans with Chronic Traumatic Brain Injury: A Case Series," *Photobiomodulation, Photomedicine, and Laser Surgery* **37**(2), 77-84 (2019).
136. L. Li et al., "Whole-cortical graphical networks at wakeful rest in young and older adults revealed by functional near-infrared spectroscopy," *Neurophotonics* **5**(3), 035004 (2018).
137. S. H. Jin, P. Lin, and M. Hallett, "Reorganization of brain functional small-world networks during finger movements," *Human brain mapping* **33**(861-872 (2012).
138. M. A. Yaqub, S.-W. Woo, and K.-S. Hong, "Effects of HD-tDCS on Resting-State Functional Connectivity in the Prefrontal Cortex: An fNIRS Study," *Complexity* **2018**(1613402 (2018).
139. E. Bullmore, and O. Sporns, "Complex brain networks: graph theoretical analysis of structural and functional systems," *Nature Reviews Neuroscience* **10**(3), 186-198 (2009).
140. V. Latora, and M. Marchiori, "Efficient Behavior of Small-World Networks," *Physical Review Letters* **87**(19), 198701 (2001).
141. V. Latora, and M. Marchiori, "Economic Small-World Behavior in Weighted Networks," *Physics of Condensed Matter* **32**((2002).
142. D. J. Watts, and S. H. Strogatz, "Collective dynamics of 'small-world' networks," *Nature* **393**(6684), 440-442 (1998).
143. H. Niu et al., "Revealing Topological Organization of Human Brain Functional Networks with Resting-State Functional near Infrared Spectroscopy," *PLOS ONE* **7**(9), e45771 (2012).
144. J. Peters et al., "Brain functional networks in syndromic and non-syndromic autism: A graph theoretical study of EEG connectivity," *BMC medicine* **11**(54 (2013).
145. H. Niu et al., "Test-Retest Reliability of Graph Metrics in Functional Brain Networks: A Resting-State fNIRS Study," *PLOS ONE* **8**(9), e72425 (2013).
146. M. Rubinov, and O. Sporns, "Complex network measures of brain connectivity: Uses and interpretations," *NeuroImage* **52**(3), 1059-1069 (2010).
147. S. Maslov, and K. Sneppen, "Specificity and Stability in Topology of Protein Networks," *Science* **296**(910-913 (2002).
148. J. Wang et al., "GRETNA: a graph theoretical network analysis toolbox for imaging connectomics," *Frontiers in Human Neuroscience* **9**(386), (2015).

149. T. Pruitt et al., "Transcranial Photobiomodulation (tPBM) With 1,064-nm Laser to Improve Cerebral Metabolism of the Human Brain In Vivo," *Lasers Surg Med* (2020).
150. Y. Uozumi et al., "Targeted increase in cerebral blood flow by transcranial near-infrared laser irradiation," *Lasers Surg Med* **42**(566-576 (2010).
151. R. O. Poyton, and M. D. Hendrickson, "Molecular basis for photobiomodulation: Light-induced nitric oxide synthesis by cytochrome c oxidase in low-level laser therapy," in *Handbook of Low Level Laser Therapy* M. R. Hamblin, M. d. Sousa, and T. Agrawal, Eds., pp. 165-184, Pan Stanford Publishing (2017).
152. D. Keeser et al., "Prefrontal transcranial direct current stimulation changes connectivity of resting-state networks during fMRI," *The Journal of neuroscience : the official journal of the Society for Neuroscience* **31**(43), 15284-15293 (2011).
153. A. Sierakowiak et al., "Default mode network, motor network, dorsal and ventral basal ganglia networks in the rat brain: comparison to human networks using resting state-fMRI," *PloS one* **10**(3), e0120345-e0120345 (2015).
154. J. S. Damoiseaux et al., "Consistent resting-state networks across healthy subjects," *Proceedings of the National Academy of Sciences* **103**(37), 13848 (2006).
155. M. Corbetta, and G. L. Shulman, "Control of goal-directed and stimulus-driven attention in the brain," *Nature Reviews Neuroscience* **3**(3), 201-215 (2002).
156. Q. Li et al., "Core language brain network for fMRI language task used in clinical applications," *Netw Neurosci* **4**(1), 134-154 (2020).
157. S. L. Bressler, and V. Menon, "Large-scale brain networks in cognition: emerging methods and principles," *Trends in Cognitive Sciences* **14**(6), 277-290 (2010).
158. N. Blanco, W. Maddox, and F. Gonzalez-Lima, "Improving executive function using transcranial infrared laser stimulation," *J Neuropsychol* **11**((2015).
159. K. Wu et al., "Topological Organization of Functional Brain Networks in Healthy Children: Differences in Relation to Age, Sex, and Intelligence," *PLOS ONE* **8**(2), e55347 (2013).
160. O. Sporns, and J. Zwi, "The Small World of the Cerebral Cortex," *Neuroinformatics* **2**(145-162 (2004).
161. F. Vecchio et al., "Transcranial direct current stimulation generates a transient increase of small-world in brain connectivity: an EEG graph theoretical analysis," *Experimental Brain Research* **236**(1117+ (2018).
162. R. M. Birn et al., "The effect of scan length on the reliability of resting-state fMRI connectivity estimates," *NeuroImage* **83**(550-558 (2013).
163. S. Geng et al., "Effect of Resting-State fNIRS Scanning Duration on Functional Brain Connectivity and Graph Theory Metrics of Brain Network," *Front Neurosci* **11**(392 (2017).
164. S. Sagar et al., "Diffuse correlation spectroscopy (DCS) study of blood flow changes during low level laser therapy (LLLT): a preliminary report," *Proc.SPIE* (2017).
165. F. Gonzalez-Lima, and D. W. Barrett, "Augmentation of cognitive brain functions with transcranial lasers," *Front Syst Neurosci* **8**(36-36 (2014).
166. I. S. Glover, and S. N. Baker, "Cortical, corticospinal and reticulospinal contributions to strength training," *The Journal of Neuroscience* JN-RM-1923-1919 (2020).
167. A. M. Horowitz et al., "Blood factors transfer beneficial effects of exercise on neurogenesis and cognition to the aged brain," *Science* **369**(6500), 167 (2020).
168. F. Cogiamanian et al., "Improved isometric force endurance after transcranial direct current stimulation over the human motor cortical areas," *The European journal of neuroscience* **26**(242-249 (2007).
169. A. P. Pinto et al., "Sensory-motor and cardiorespiratory sensory rehabilitation associated with transcranial photobiomodulation in patients with central nervous system injury: Trial protocol

for a single-center, randomized, double-blind, and controlled clinical trial," *Medicine (Baltimore)* **98**(25), e15851-e15851 (2019).